Development of an Integrated Timing System for the HartRAO Lunar Laser Ranging Station

by

Cilence Munghemezulu

Submitted in partial fulfilment of the requirements for the degree

DOCTOR OF PHILOSOPHY

in the

Faculty of Natural and Agricultural Sciences

University of Pretoria

2018

Declaration of originality

This is to declare that the research work presented here is entirely my own work, unless or otherwise explicitly acknowledged by citation of published and unpublished sources. This research has not been submitted previously for assessment in any form to the University of Pretoria or to any other institutions for any other purposes.

Signature: Date:

Development of an Integrated Timing System for the HartRAO Lunar Laser Ranging Station

Author	Cilence Munghemezulu
Supervisor	[1,3]Prof. Ludwig Combrinck
Co-supervisor	[2,3]Dr. Joel O. Botai
	[1]Hartebeesthoek Radio Astronomy Observatory, P.O. Box 443, Krugersdorp 1740, South Africa
	[2]South African Weather Service, Pretoria, South Africa
	[3]Department of Geography, Geoinformatics and Meteorology
Degree	Doctor of Philosophy

Abstract

The Hartebeesthoek Radio Astronomy Observatory is currently developing a Lunar Laser Ranger (LLR) station based on a 1 m classical Cassegrain telescope that was donated to the project by the Observatoire de la Côte d' Azur (OCA) of France. The LLR project at HartRAO currently consists of different subsystems that will be integrated to form a complete functioning system. This integrated system will produce sub-centimetre accuracy ranging data, allowing the distance from the Earth to the Moon to be determined with high accuracy and be used for a number of scientific investigations. Such subsystems include the laser systems (one suitable for Satellite Laser Ranging (SLR), the other for LLR) timing and photon detection systems, data analysis software, steering and control hardware, and integrated software modules such as the pointing model for the telescope. This research project focused on the development of the timing subsystem for this new LLR station. In particular, it involved the determination and evaluation of the oscillator error budget, development of MATLAB scripts for analysis of the rubidium oscillator drift and ageing characteristics as well as GPS analysis of possible multi-path effects.

The technique of the LLR involves ranging to the Moon by transmitting short laser pulses (about 0.03 m) from the ranging station to the retro-reflectors that are located on the surface of the Moon. Different models exist that are used to correct for these errors. However, the stability of the local clock forms the basis of ensuring that accurate Time of Flight (ToF) is measured accurately and precisely. This requires picosecond (10^{-12}) level or better accuracy to minimise systematic errors in the ToF measurement. Hence, the aim of this study was to

develop an integrated timing system for this new station that will meet this stringent requirement.

A 4380A rubidium timing reference system was acquired for the LLR station at HartRAO. This reference timing system has a timing accuracy of less than 10 ns Root Mean Square (RMS), a frequency accuracy of better than 1×10^{-13} over a 1 day period. An Allan deviation (locked to the Global Positioning System – (GPS)) of 6×10^{-13} at 1 second and a phase noise of -110 dBc/Hz at 1 Hz. It has temperature stability of $\sim1\times10^{-12}$/℃. This timing system is locked to GPS time and updated accordingly to ensure that it is aligned with Universal Coordinated Time (UTC). The installation site for the GPS antenna was preliminary investigated for the extent of multipath from the surrounding features. The GPS antenna requires a stable platform and the location of the antenna must be chosen to minimise the effects of multi-path, which can affect the measured position and as a result affect the consistency of GPS time that is used to update the rubidium clock. Results from this experiment indicate that a cut-off angle of 10º-20º in GPS observations can minimise reflections from the ground and nearby objects.

The rubidium 4380A proved to be a stable timing system with predictable clock behaviour over short time intervals. However, to achieve 1 mm ranging precision, a high photon return rate ought to be achieved. The estimated return rate of 5 photons per minute implies that the LLR must range for longer than 30 minutes in order to collect an adequate number of photons to statistically achieve sub-centimetre ranging precision during calculation of the normal points.

The new LLR station once completed will be the only station in Africa to be capable of ranging to the retro-reflectors located on the surface of the Moon. It will also improve the current ILRS network by providing data that are important in improving the accuracy of the Moon's orbit parameters and reduce network dependent biases. This new LLR station will contribute to both local and global communities to meet the scientific objectives of the currently growing space science endeavours by many countries as well as supporting socio-economic developments.

Keywords: lunar laser ranging, rubidium, hydrogen maser, global positioning system

Acknowledgements

I am grateful to the following people and organizations:

- Prof Combrinck. L: for supervising the project and support throughout my studies.
- Dr Botai. O.J: for supervising the project and encouragement during my studies.
- HartRAO: all the wonderful people that keep the observatory working and the support. My colleagues at space geodesy lab at HartRAO for fruitful discussions over the years.
- The department of Geography, Geoinformatics and Meteorology: I would like to thank my colleagues for their support.
- Family and Friends: my mother and siblings for their support for many years. My wife Zinhle Olga Mashaba for her love and continuous support.
- Funding: from the University of Pretoria, Inkaba yeAfrica, National Research Foundation (NRF) and HartRAO is acknowledged.

Publications and proceedings

Peer-reviewed:

- Munghemezulu, C., Combrinck, L. and Botai, O. 2018. A case study of the application of GPS to lunar laser ranging timing systems. *Journal of Applied Geodesy*, Ahead of Print, doi:10.1515/jag-2018-0006

- Munghemezulu, C., Combrinck, L. and Botai, J.O., 2016. A review of the lunar laser ranging technique and contribution of timing systems. *South African Journal of Science*, *112*(3-4), pp.1-9.

- Munghemezulu, C., Combrinck, L., Botai, J. and Mashaba, Z., 2016. Mapping GPS multipath: a case study for the lunar laser ranger-timing antenna at HartRAO. *South African Journal of Geomatics*, *5*(2), pp.142-155.

- Munghemezulu, C., Combrinck, W.L., Botai, J.O. and Botha, R.C., 2016. Design of the timing system for the new Lunar Laser Ranger proposed for the Matjiesfontein Space Geodetic Observatory in the Great Karoo, South Africa: preliminary results. *South African Journal of Geology*, *119*(1), pp.91-98.

- Munghemezulu, C., Combrinck, L., Botai, O.J. and Quick, J., 2016. Analysis of the performance of hydrogen maser clocks at the Hartebeesthoek Radio Astronomy Observatory. *South African Journal of Geomatics*, *5*(3), pp.325-339.

Conferences:

- Munghemezulu, C., Combrinck W. L., Botai, O.J and Botha, R., 2016. Timing system for the Lunar Laser Ranging station at HartRAO, South Africa: Preliminary results. 20th International Workshop on Laser Ranging GFZ, Potsdam, Germany, 4-9 October 2016.

- Munghemezulu, C., Combrinck. L and Botai, O.J., 2014. Timing and single-photon detection subsystems for the satellite/lunar laser ranging system, South Africa. 4th Combined Science & Technology Train and Space Geodesy Observatory Workshop, Matjiesfontein, South Africa, 7-11 April 2014.

- Munghemezulu, C., Combrinck. L and Botai. O.J., 2014. Development of an integrated timing and photon detection system for the HartRAO Lunar Laser Ranger. Presented at the 10th Inkaba yeAfrica/!Khure Africa (AEON) Conference, Matjiesfontein, South Africa, 29 September – 3 October 2014.

Table of Contents

List of Figures

List of Tables

Acronyms

APD	Avalanche Photodiode
APOLLO	Apache Point Observatory Lunar Laser-ranging Operation
CEI	Connected Element Interferometer
DDE	Dynamic Data Exchange
DMS	Data Management Systems
DORIS	Doppler Orbitography and Radiopositioning Integrated by Satellite
DOP	Dilution of Precision
DSAC	Deep Space Atomic Clock
EOP	Earth Orientation Parameters
GGOS	Global Geodetic Observing System
GMF	Global Mapping Function
GNSS	Global Navigation Satellite System
GPS	Global Positioning Systems
GSFC	Goddard Space Flight Center
GTR	General Theory of Relativity
HartRAO	Hartebeesthoek Radio Astronomy Observatory
IAG	International Association of Geodesy
IGS	International GNSS Service
ICRF	International Celestial Reference Frame
IERS	International Earth Rotation and Reference Systems Services
ILRS	International Laser Ranging Services
ITRF	International Terrestrial Reference Frames
IUGG	International Union of Geodesy and Geophysics
IPWV	Integrated Precipitable Water Vapour
LAGEOS	LAser Geodynamics Satellite
LLR	Lunar Laser Ranging
MOBLAS	MOBile LAser Ranging System
MLRS	McDonald Laser Ranging Station
NASA	National Aeronautics and Space Administration
Nd:YAG	Neodymium-doped Yttrium Aluminium Garnet
NIST	National Institute of Standards and Technology
NWM	Nell Mapping Function
OCA	Observatoire de la Côte d’ Azur
O-C	Observed – Computed
OCXO	Oven-Controlled Crystal Oscillator
PTP	Precision Time Protocol
PPN	Parameterized Post-Newtonian
RINEX	Receiver Independent Exchange
RMS	Root Mean Square
S/LLR	Satellite/Lunar Laser Ranging

SNR	Signal-to-Noise Ratio
Si-APD	Silicon Avalanche Photodiode
SLR	Satellite Laser Ranging
TCXO	Temperature-Compensated Crystal Oscillator
TEC	Total Electron Content
TEQC	Translation Editing and Quality Check
TCG	Time-Code-Generator
TIC	Time-Interval-Counter
TPS	Topcon Positioning System
ToF	Time-of-Flight
TWSTFT	Two Way Satellite Time and Frequency Transfer
USNO	US Naval Observatory
UTC	Coordinated Universal Time
VCXO	Voltage Controlled Crystal Oscillator
VMF	Vienna Mapping Functions
VLBI	Very Long Baseline Interferometry
WRMS	Weighted Root Mean Square
ZHD	Zenith Hydrostatic Delay
ZTD	Zenith Total Delay
ZWD	Zenith Wet Delay

Chapter 1

General Introduction

1.1. Introduction

Space geodetic techniques such as the Global Navigation Satellite Systems (GNSS), Satellite Laser Ranging (SLR), Very Long Baseline Interferometry (VLBI), Lunar Laser Ranging (LLR) and Doppler Orbitography and Radiopositioning Integrated by Satellite (DORIS), provide data for scientific research ranging from fundamental physics, geophysics, geodynamics to implementation and maintenance of the International Terrestrial Reference Frame (ITRF) and International Celestial Reference Frame (ICRF). The accuracies of these techniques have increased from metres (during the 1960's) to sub-centimetre level (1990's-present). With the increasing accuracies of these techniques, geophysical processes are better understood today, including interplanetary science such as the Earth-Moon system. These improvements have also benefited the public, for example, implementation and maintenance of reference frames such as ITRF.

Geodetic network capacity has been limited, in the Southern Hemisphere, but particularly in Africa, due to high costs involved in commissioning the geodetic instruments and lack of human capacity. However, the network geometry has been improving particularly for GNSS ground-based stations, while the VLBI and LLR stations are still limited. Many efforts have been made to extend the current networks of all the techniques, in particular the Hartebeesthoek Radio Astronomy Observatory (HartRAO) by installing GNSS equipment in Africa, Antarctica, Marion Island and Gough Island. Currently, HartRAO is working on improving the network of all the space geodetic techniques in the Southern Hemisphere. This includes adding an LLR station and a new geodetic VLBI antenna (historically termed VLBI2010, but is now called VGOS, where VGOS is the acronym for *VLBI Global Observing System* (GGOS) as well as a Russian Federation SLR system at the observatory.

Above all other space-based techniques, the LLR technique has the weaker geometrical network. At the moment, there are only three LLR active stations i.e. the Apache Point Observatory Lunar Laser-ranging Operation (APOLLO 3.5 m telescope), New Mexico, USA;

McDonald Laser Ranging Station (MLRS 0.75 m telescope) currently not supporting LLR due to lack of financial support, Texas, USA and Observatoire de la Côte d' Azur (OCA 1.54 m Cassegrain telescope), France. There are a few upcoming LLR stations that will increase the network volume i.e. Matera Laser Ranging Observatory (already providing some data), Italy; Geodetic Observatory Wettzell, Germany; Mount Stromlo Satellite Laser Ranging Observatory, Australia and HartRAO, South Africa (source: http://ilrs.gsfc.nasa.gov/).

In South Africa, HartRAO is currently developing and upgrading the LLR system based on the ex-OCA 1 m aperture telescope (see Figure 1) in collaboration with OCA and NASA (Combrinck, 2011a). This new LLR station at HartRAO will improve the network geometry in the Southern Hemisphere and form part of the International Laser Ranging Service (ILRS) network.

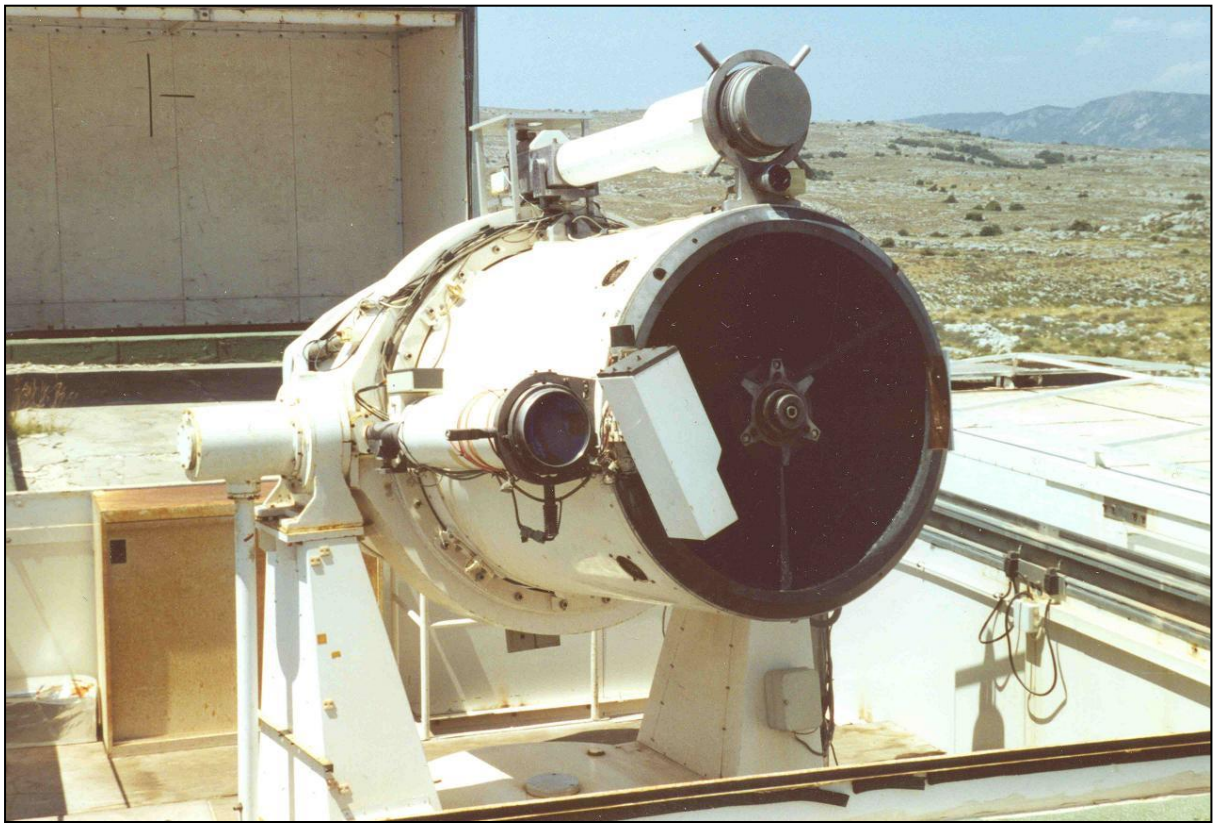

Figure 1. The 1 m classical Cassegrain telescope in operation (equipped for SLR) at OCA, France, before it was moved to HartRAO, South Africa (picture credit: Combrinck, L).

Space geodesy techniques currently face great challenges and these are in the improvement of the techniques' accuracy and precision, this involves improving the hardware

components, existing atmospheric models, analysis strategies and software stabilities to achieve sub-centimetre accuracy (Pearlman et al., 2002). The current LLR project at HartRAO faces similar challenges, e.g. a station to form part of the ILRS must have time stability of 1 picosecond (10^{-12}) or better. The ability to have high timing stability depends heavily on environmental conditions such as multipath (reflections of the GNSS signals off objects in the vicinity of the GNSS antenna, which create apparent signal path length increases, affecting the solved for position) if the timing system is driven by GNSS, and ambient temperature variations.

This particular project will contribute towards the LLR development at HartRAO by analysing the timing subsystem requirements, error budget, and factors affecting oscillator stability towards developing, integrating and commissioning a working solution. The solution towards a complete timing system is manifold, as the frequency generating subsystem (rubidium oscillator, steered by GNSS) is just a part of the hardware involved in measuring the Time of Flight (ToF) of the laser pulse from the LLR to the Moon and back. In addition to the Observed ToF, there is the Calculated ToF, based on a precise ephemeris and multiple models to account for various delays experienced by a photon traversing through the gravity field and atmosphere. During data analysis, the objective is to minimise the difference between the Observed – Computed (O – C) residuals, therefore both sides of the O-C Equation needs to be as accurate as possible. This implies highly accurate timing and frequency stability on the one side (O) and very accurate modelling on the other (C).

1.2. Problem outline

A timing subsystem forms part of the critical components in geodetic techniques. The accuracy of the measurements in geodesy relies on the timing subsystems embedded in the entire system. Highly accurate timing systems such as rubidium, Cesium or hydrogen microwave amplification by stimulated emission of radiation (hereafter maser) atomic clocks are utilised to provide signals that are used to measure the delay of the pulses accurately. Without a stable timing system, the measured ToF will be biased, therefore, resulting in less accurate measurements of the range parameters (e.g., to measure ToF with an accuracy of centimetre-level or better, a timing system with an accuracy of ~1 ps level is required).

The entire LLR system will need to be synchronised to an accurate time and frequency source such as a rubidium frequency standard, which is currently utilised by the SLR MOBile LAser Ranging System (MOBLAS-6) station at HartRAO. The rubidium frequency standard tends to drift over time (as all other clocks), creating inconsistencies in the time signature. A GNSS receiver is usually used to steer or correct the drift of the rubidium frequency standard by providing a 1 pulse per second (pps) signal and a certain frequency e.g., 10 MHz, which are phase-locked to an internal ovened crystal. This oscillator is steered by the GNSS constellation, whose clocks are in turn, updated by a network of atomic clocks on the ground. In practice, by using GNSS time, one can thus refer and adjust a local reference clock to the atomic standards on the ground (i.e. by doing a time transfer). Typically a certain frequency standard (5 MHz or 10 MHz) will achieve 1 picosecond accuracy and resolution, therefore, keeping the system and subsystems stable, and when compared to GPS, within a known offset (typically a couple of micro-seconds).

1.3. Research objectives

The subsystems relying on frequency and time of the LLR consist of subcomponents such as micro-controllers, GPS-timing system, system delay measurements, comparator delay, software time, photon detection package, telescope control systems, which must all be synchronized to the same time standard to achieve sub centimetre accuracy in the ranging measurements and a time accuracy of 1 picosecond. Not all subsystems require the same timing accuracy. As an example, a control circuit to enable a particular event might require a response time and enabling accuracy of a few milliseconds; whereas the timing of the laser pulses, ToF requires 1 picosecond precision.

Research objectives are to:

- Review the LLR technique and compare the observed and calculated ToF components in order to understand the O – C residuals and their error sources.
- Apply techniques to visualise and minimise the multipath effect on GPS timing antennas for the LLR station.
- Design an integrated time/frequency for the LLR station.
- Evaluate the performance of the integrated time/frequency system for the LLR station.

- Analyse the performance of the on-site hydrogen maser clocks as they act as a crucial backup source for the LLR station and as independent calibrators of fractional frequency stability.

1.4. Significance of the research

Geodesy is the discipline that deals with the measurement and representation of the Earth and other celestial bodies. It consists of three pillars, which are the time-varying Earth geometric shape, its gravitational field and rotational parameters. Geodetic techniques have the capabilities of observing geophysical parameters with high spatial and temporal resolution, and high precision. The Earth system, which includes but are not limited to crustal deformation, gravity variations, atmospheric science, etc., can be studied with high precision by making use of space geodetic techniques. These physical parameters are of utmost importance in understanding global change phenomena (Plag et al., 2009).

In order to deal with geodetic data in an integrated manner, the International Association of Geodesy (IAG) has established the Global Geodetic Observing System (GGOS) as an observing system during the International Union of Geodesy and Geophysics (IUGG) meeting in 2003 in Sapporo, Japan (Plag et al., 2009). The foundation of GGOS is space geodetic techniques that make geophysical observations about the Earth system (Figure 2). The challenge for GGOS is to integrate these systems and their data products in a way that helps society to better manage global change and to move from centimetre (cm) observational accuracy-level to millimetre (mm) accuracy-level in all the observational techniques and modelling thereafter (Rummel et al., 2009; Gross et al., 2009).

The ILRS network is very important to GGOS since it provides SLR and LLR ranging measurements (Rothacher et al., 2009). However, the current network geometry is poor in the Southern Hemisphere (Figure 3); the new LLR project at HartRAO will improve and strengthen the current network. The station will be able to switch between SLR i.e. ranging to the satellites (both low and high orbit satellites) that are equipped with retro-reflectors, and LLR mode that will allow the system to range to the Moon’s retro-reflectors. However, this thesis will focus on LLR requirements and integration.

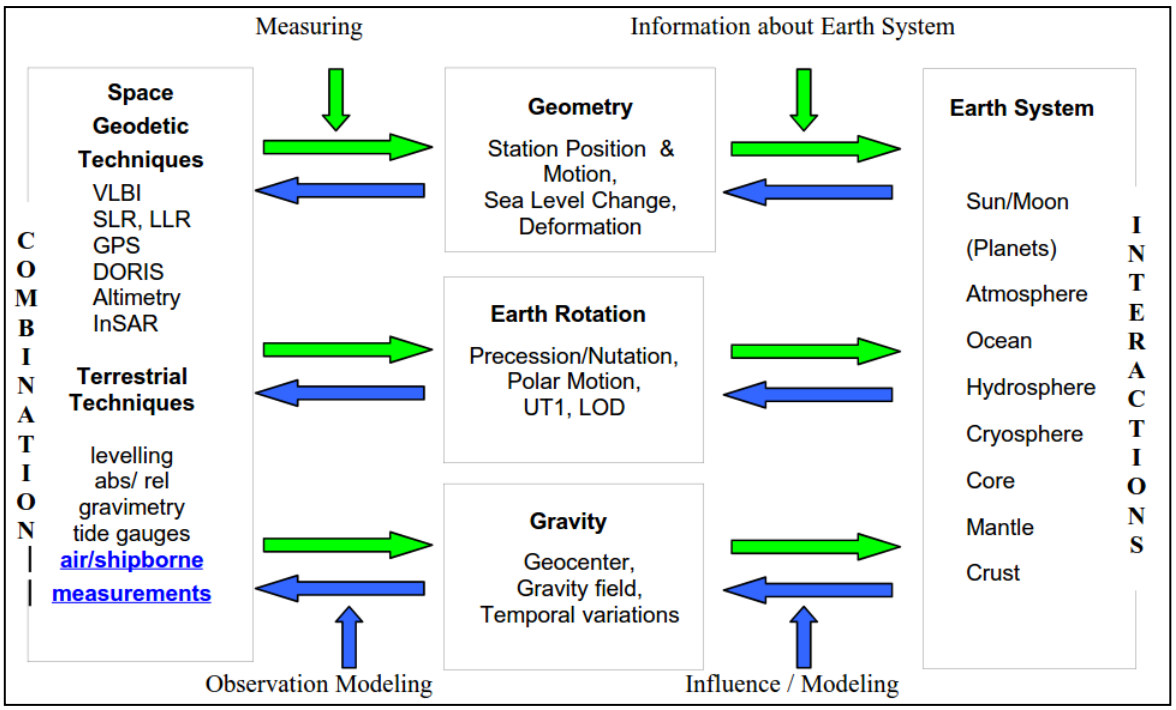

Figure 2. Contribution of geodetic techniques in measuring and monitoring the Earth system (Rummel et al., 2009).

There are many scientific contributions to be accomplished through the LLR project at HartRAO. For example, South Africa has entered the era of space science with a number of South African satellites being deployed to space such as CubeSat and SumbandilaSat. These satellites require precise orbital ephemerides, which are derived from SLR measurements. Especially, Earth observing satellites that monitor changing landscape e.g., ice, land cover change or sea level; they need calibration measurements from the SLR techniques to increase the accuracy of the observations. Hence, a better understanding of the geophysical processes. The geographical location of HartRAO station in the Southern Hemisphere provides an opportunity for scientific experiments that will allow us to range simultaneously with another observatory (e.g., OCA) to the Moon or satellites. This will constrain station dependent biases (Combrinck, 2011a).

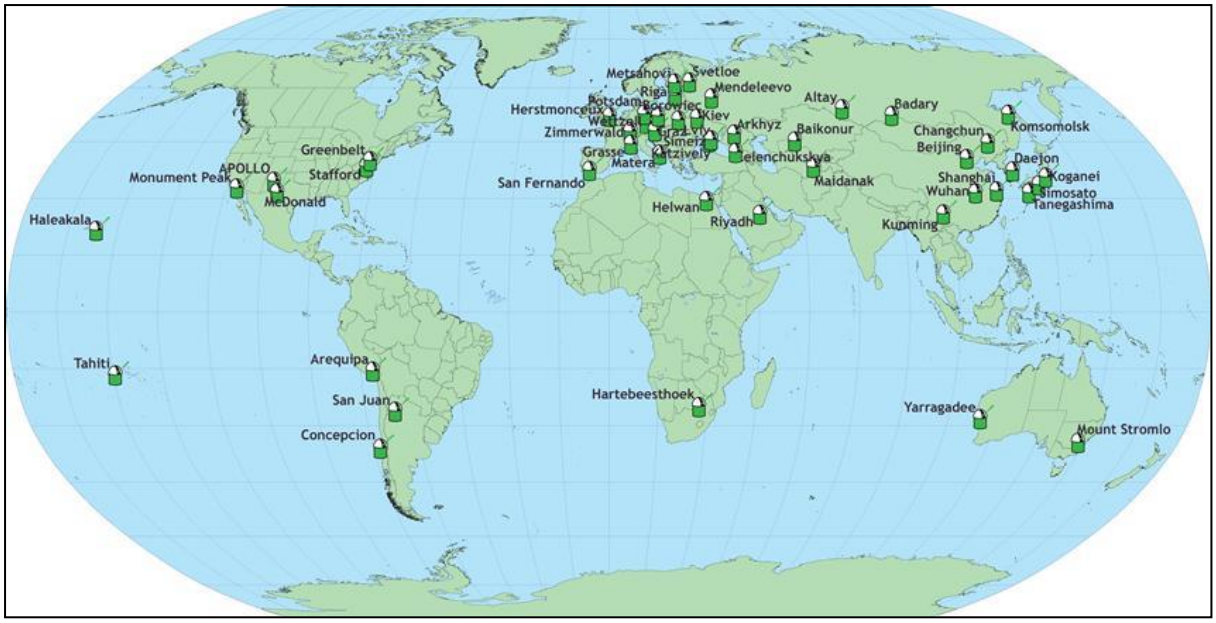

Figure 3. The current distribution of LLR and SLR stations in the ILRS network. Currently, there are only three active LLR stations that are capable of ranging to the Moon. The Southern Hemisphere has poor geometry, therefore the addition of the LLR at HartRAO will strengthen the current existing network (Source: http://ilrs.gsfc.nasa.gov/).

Given the current poor geometrical coverage of the LLR/SLR stations in the South Hemisphere, this means that many satellites are not being tracked as they pass through the Southern Hemisphere region. This project gives us an opportunity to improve the determination of the orbit parameters and the ranging geometry (Combrinck, 2011a). Other scientific contributions include a test for the General Relativity Theory (GRT) (Alley, 1983; Combrinck, 2013) and a contribution to the ITRF (Altamimi et al., 2011). Research on GRT has already started at HartRAO to estimate Parameterized Post-Newtonian (PPN) parameters γ and β directly as part of the least-squares solution of precise orbital determination from LAGEOS II SLR data (Combrinck, 2011b).

According to Vasilyev et al., (2015) the current lunar ephemerides are only derived from the LLR observations obtained from six LLR stations using data from 1969 to 2013. The accuracy of the lunar ephemeris (for example, JPL-DE 432 or IPA-EPM2013) are known to sub-meter level (Folkner et al., 2008). This accuracy can be improved by an addition of new LLR stations that are well distributed globally to increase the LLR observations and reduce geometric dependent biases. Vasilyev et al., (2015) have simulated the impact of adding a new station (the Altay Russian LLR station-3.12 m telescope) to the LLR network. They obtained an improvement of 2-16% in lunar ephemeris and corresponding geophysical parameters.

Based on these conclusions, the HartRAO LLR station can be expected to also make significant improvements on parameters that are derived from LLR data.

The quality of the ranging variables depends entirely on the accuracy of the timing and detection subsystems. All the subsystems are required to be operating using the same time and frequency signals; this includes the microprocessors, controller module, safety modules, and event timers etc., to achieve 1-picosecond time resolution for the entire system and millimetre ranging accuracy. The development and integration of optimum timing and detection systems for the LLR are necessary at all cost and this project contributes to the entire LLR system to ensure harmonious coordination of the subsystems and accurate measurements.

The LLR project also fits well within the social perspectives in South Africa, i.e. it will help to equip all the participating students with unique skills and will make a mark in Africa's history as the first project to range to the Moon on the African continent.

1.5. Challenges in lunar laser ranging technologies

The ILRS network has poor geometry as compared to the International GNSS Service (IGS) network. There are several reasons for this, which include high initial costs for commissioning SLR/LLR stations; operational costs for LLR are also high. In contrast, IGS network GNSS stations are relatively less expensive, requires very little maintenance, and can operate automatically for a long time. For purposes of network densification, GNSS is therefore more suitable.

The consistent demand of high accurate ranging data from ILRS community has led to further research on electronics that runs on the SLR and LLR systems as well as the data processing strategies and modelling of the geophysical processes. Some of the important electronic components include timing systems and photon detectors with the capability to detect single photons. A research group at Czech Technical University in Prague, Czech Republic have developed a timing measurement device with 4-femtosecond (10^{-15}) stability (Panek et al., 2010). The group also developed a variety of instruments that are applicable to time transfer experiments, SLR and LLR techniques, such as an optical trigger device with sub-picosecond timing jitter and stability (Kodet and Prochazka, 2012). These developments contribute towards ranging accuracy and improve the probability of detecting returning photons. It is clear that the availability of suitable electronics for SLR and LLR systems are no

longer limitations in developing highly accurate timing and detection subsystems at this stage. However, the atmosphere contributes large errors in ranging accuracy by introducing an atmospheric delay variable (at the level of several metres at low elevation), which is difficult to model at mm level, as it is variable and requires real-time meteorological observations during ranging.

Limitations pertaining to this particular project include those discussed above and especially the costs involved since this project is in the developmental stage. The LLR systems will be designed in an optimal way to minimise the cost involved, specifically on the timing subsystem.

1.6. Thesis outline

This thesis takes the format of published papers as chapters. Hence, there will be some repetition within the chapters.

Chapter 2

Current and historical literature on the LLR technique are reviewed in this chapter. The Equation of O-C residuals is described to better understand error sources. MATLAB scripts were developed to simulate selected parameters that influence measured time-of-flight (ToF); these are external system delay parameters. The status of the Matjiesfontein project (proposed final destination of the LLR) is outlined.

Chapter 3

In this chapter, the multipath effect on the on-site location selection for the timing antenna is investigated; techniques are developed in MATLAB to identify a suitable site for the installation of the timing antenna.

Chapter 4

The design and integration of the timing subsystem for the LLR are discussed and implemented in this chapter. Internal system delay parameters are discussed as they contribute towards total system error budget.

Chapter 5

The performance of the hydrogen maser clock at HartRAO is analysed in this chapter. These masers act as a backup system for the LLR station. In case of an emergency such as malfunctioning of GPS satellites, the 4380A can be locked to the maser to maintain accurate station time.

Chapter 6

The 4380A is tested on GNSS positioning and precipitable water vapour application. The test includes using a hydrogen maser and 4380A rubidium clock as frequency standard for a GNSS Leica receiver and investigating the influence of these timing systems on the GNSS applications. This experiment serves to illustrate the working system implemented in Chapter 4. Other LLR subsystems are currently not completed; hence, this experiment was not directly related to the LLR system.

Chapter 7

This chapter contains conclusions on the outcomes from the results obtained from previous chapters and implications thereof to the overall LLR system.

1.7. Concluding remarks

This research contains components of design, technical development and engineering (hardware and software), scientific analysis and interpretation. These are inseparable in a complex system where failure to consider all aspects of a critical subsystem of an advanced scientific instrument will lead to total failure of the complete experiment. As the LLR system will be the most recent and most modern of all LLR systems, optimal configuration, systems and scientific analysis and successful integration must be at the highest end of current technological development and scientific strategy. These aspects are critical to enable us to deliver on the target of sub-centimetre meter accuracy specified for the project.

Chapter 2

A review of the lunar laser ranging technique

Abstract

The lunar laser ranging (LLR) technique is based on the two-way ToF of laser pulses from an Earth station to the retro-reflectors that are located on the surface of the Moon. The LLR technique and contribution of the timing systems and its significance in light of the new LLR station currently under development by the Hartebeesthoek Radio Astronomy Observatory (HartRAO) are discussed. Firstly, developing the LLR station at HartRAO is an initiative that will improve the current geometry of global network of LLR stations; all active stations are presently located in the Northern Hemisphere. Secondly, data products derived from the LLR experiments – such as accurate lunar orbit, tests of the general relativity theory, Earth–Moon dynamics, the interior structure of the Moon, reference frames, and station position and velocities – are important in better understanding the Earth–Moon system. Factors affecting the range bias are highlighted such as the effect of Earth tides on station position and delays induced by timing systems, as these must be taken into account during the development of the LLR analysis software. HartRAO is collocated with other fundamental space geodetic techniques, which makes it a true fiducial geodetic site in the Southern Hemisphere and a central point for further development of space geodetic techniques and networks in Africa. Furthermore, the new LLR will complement the existing techniques by providing new niche areas of research both in Africa and internationally.

2.1. Introduction

The study of Earth's gravity, Earth's rotation, geo-kinematics and the inclusion of space-time currently completes the definition of space geodesy (Combrinck, 2012). This definition has evolved from the early days of F.R. Helmert, who firstly defined geodesy as the science of the measurement and mapping of the Earth's surface (Torge and Müller, 2012; Helmert, 1880). It is clear that geodesy as a discipline has two objectives that are closely related: (i) scientific objectives constitute the study of geodynamic phenomena, the gravity field of the Earth and other planets, the shape and size of the Earth and its orientation in space through Earth orientation parameters and (ii) practical objectives include cadastral surveying to determine points accurately (up to millimetre level) on the Earth's surface, accurate timing, terrestrial geodetic reference frames, and accurate positioning for civil engineering applications (Torge and Müller, 2012). These objectives are realised through space-based techniques: Global Navigation Satellite Systems (GNSS), Very Long Baseline Interferometry (VLBI), Satellite Laser Ranging (SLR), Lunar Laser Ranging (LLR) and Doppler Orbitography and Radiopositioning Integrated by Satellite (DORIS). Together these techniques are fundamental in defining and maintaining different reference systems and reference frames, and determining three-dimensional station positions, velocities, Earth orientation parameters and polar motion with high accuracy, spatial resolution and temporal stability (Altamimi et al., 2011; Lu et al., 2014).

The accuracy of geodetic products depends on a number of factors such as instrumental accuracies, analysis strategies, the accuracy of the models used during data processing (e.g. atmospheric models), third-body perturbation effects and relativistic effects. Among these factors, the stability of timing frequency standard systems plays a crucial role in the accuracy of the measurements. Development of highly stable clocks such as the hydrogen maser and Cesium clocks allows accurate timing and data correlation to be carried out with high levels of accuracy (Wynands and Weyers, 2005). The application of GNSS in metrology (i.e. time transfer techniques) has advanced the traditional time-keeping services (e.g. mobile reference clocks, terrestrial communication systems using Loran-C or direct radio broadcasts) and allowed comparison of clocks that are distributed around the world with high accuracy and the maintenance of Coordinated Universal Time (UTC) (Lombardi, 2005). These timing systems

contribute towards Earth and space observational techniques in support of accurate measurements.

Earth observation and space development technologies are very important for the development of a country and have socio-economic benefits such as climatology, land management and monitoring applications. South Africa, Nigeria, Egypt, Algeria, Kenya and, more recently, Ethiopia are African countries that are harnessing space-related technologies ranging from Earth observation satellites and space geodesy to radio and optical astronomy (Martinez, 2008; Ngcofe and Gottschalk, 2013).

The Hartebeesthoek Radio Astronomy Observatory (HartRAO) is located north of Krugersdorp in South Africa (Figure 4). It is collocated with a DORIS station, several GNSS stations, 26-m, 15-m and a 13.2-m VGOS (VLBI2010) VLBI telescopes, as well as two SLR stations (NASA MOBLAS-6 and a Russian system). Currently, HartRAO is building a new LLR system based on a 1-m aperture telescope donated to HartRAO by the Observatoire de la Côte d' Azur of France (Combrinck, 2011a). The observatory is a fundamental (fiducial) site in the Southern Hemisphere as it limits geometrical errors during computation of geodetic or astronomical parameters in the global network and provides high-quality scientific data with high temporal resolution (Combrinck, 2011a).

During data analysis of the Earth-Moon time delay, the objective is to minimise the difference between the observed (O– computed (C) residuals, therefore both sides of the O - C Equation needs to be as accurate as possible. This implies highly accurate timing and frequency stability on the one side (O) and very accurate modelling on the other (C). Both components are described in detail to understand their sources in Section 2.6.

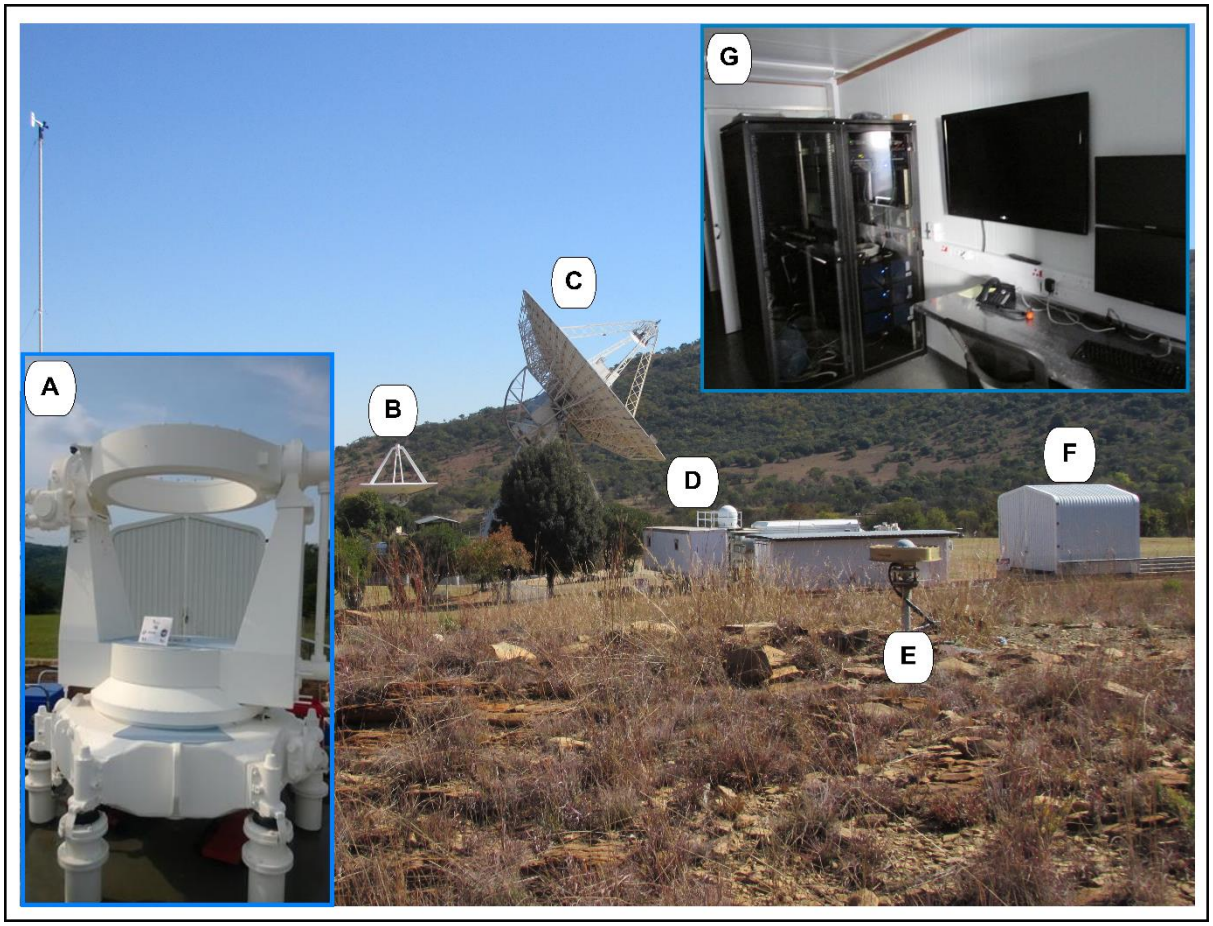

Figure 4.Some of the geodetic instruments collocated at HartRAO, South Africa. A: the LLR azimuth-elevation mount; the tube and other components were removed for upgrade and maintenance. B: 15 m VLBI telescope; C: 26 m VLBI telescope; D: MOBLAS-6 SLR station; E: HRAO GNSS station; F: LLR enclose; G: LLR control room.

2.2. Historical developments of lunar laser ranging

The US Apollo and the Soviet missions deployed arrays of corner-cube retro-reflectors on the surface of the Moon during the late 1960s and 1970s; the LLR technique has therefore been used to study the Earth–Moon system since 1969. On the Moon's surface, there are currently Apollo 11, 14 and 15 reflectors deployed by the Apollo missions and Lunokhod I and II reflectors deployed by the Soviet Union (Williams and Newhall, 1996; Figure 5). The McDonald Observatory was the first observatory to range to a retro-reflector on the Moon using a 2.7 m telescope (Barker et al., 1975).

Currently, there are four LLR stations in the world that range to the Moon's retro-reflectors on a regular basis. These active stations are: (i) the Apache Point Observatory Lunar

Laser-ranging Operation (APOLLO), New Mexico, USA; (ii) McDonald Laser Ranging Station (MLRS), Texas, USA; (iii) the Observatoire de la Côte d' Azur (OCA),France; and (iv) Matera, Italy (Hofmann et al., 2014). These stations are located in the Northern Hemisphere, which results in a weak geometry for the LLR network, as no stations are active in the Southern Hemisphere. However, the South African radio astronomy observatory (HartRAO), Mount Stromlo observatory in Australia (Greene and MckLuck, 2002), ESO La Silla Observatory IV in Chile (Fienga et al., 2014), National Astronomical Observatory of Japan (Noda et al., 2014) and the Russians (Vasilyev et al., 2014) are planning and developing LLR stations. These additional stations will improve and contribute to the current network of the International Laser Ranging Service (ILRS) and to lunar and Earth sciences as a whole.

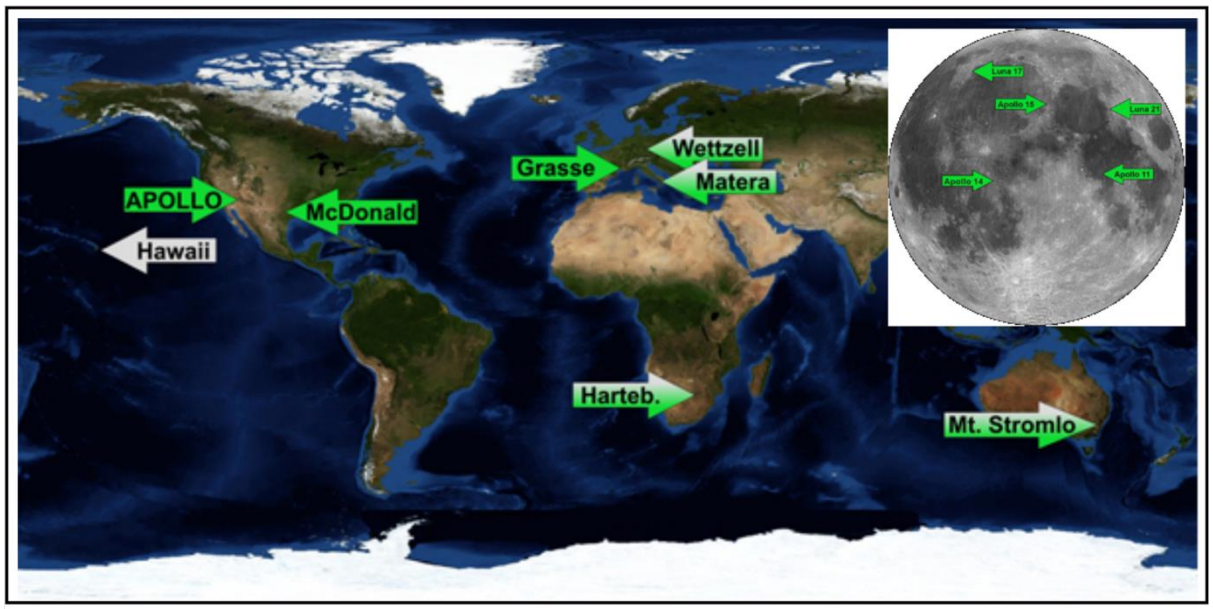

Figure 5. Distribution of the ILRS network of LLR stations. The insert map illustrates the location of the retro-reflectors on the surface of the Moon (International Laser Ranging Service, 2009).

Since the LLR technique was developed, range precision has increased from about 100–250 mm to less than 20 mm (Murphy, 2007). A similar increase in the range precision of the normal points in SLR applications has been reported in Botai et al., (2015) and this increase has been attributed to improvements in the internal system components as well as advanced models. System component improvements can be summarised as (i) replacement of the ruby laser with a neodymium-doped yttrium aluminium garnet (Nd:YAG) laser, (ii) higher emission frequency rates (5–20 Hz), (iii) faster and more sensitive detectors and (iv) improved timing systems (<20 ns) with lower jitter (<10 ps) resolutions.

The existing LLR stations have provided valuable data to date. In particular, the APOLLO LLR station seems to be the only station that is capable of receiving up to 1000 photons per session (one session typically lasts for 1 h with an expected 2–10 return photons per pulse) (Murphy et al., 2014). In comparison, the photon return rates of the McDonald MLRS2 and Grasse stations range from 1 to 105 per session and from 2 to 605 per session, respectively, when ranging to the Apollo 15 retro-reflector on the Moon (Figure 6). The data used were provided by the Paris Observatory Lunar Analysis Center (POLAC) and are available to the public (http://polac.obspm.fr/llrdatae.html). Furthermore, these stations indicate that the ToF to the Apollo 15 retro-reflector array can range from 2.3 s to 2.7 s.

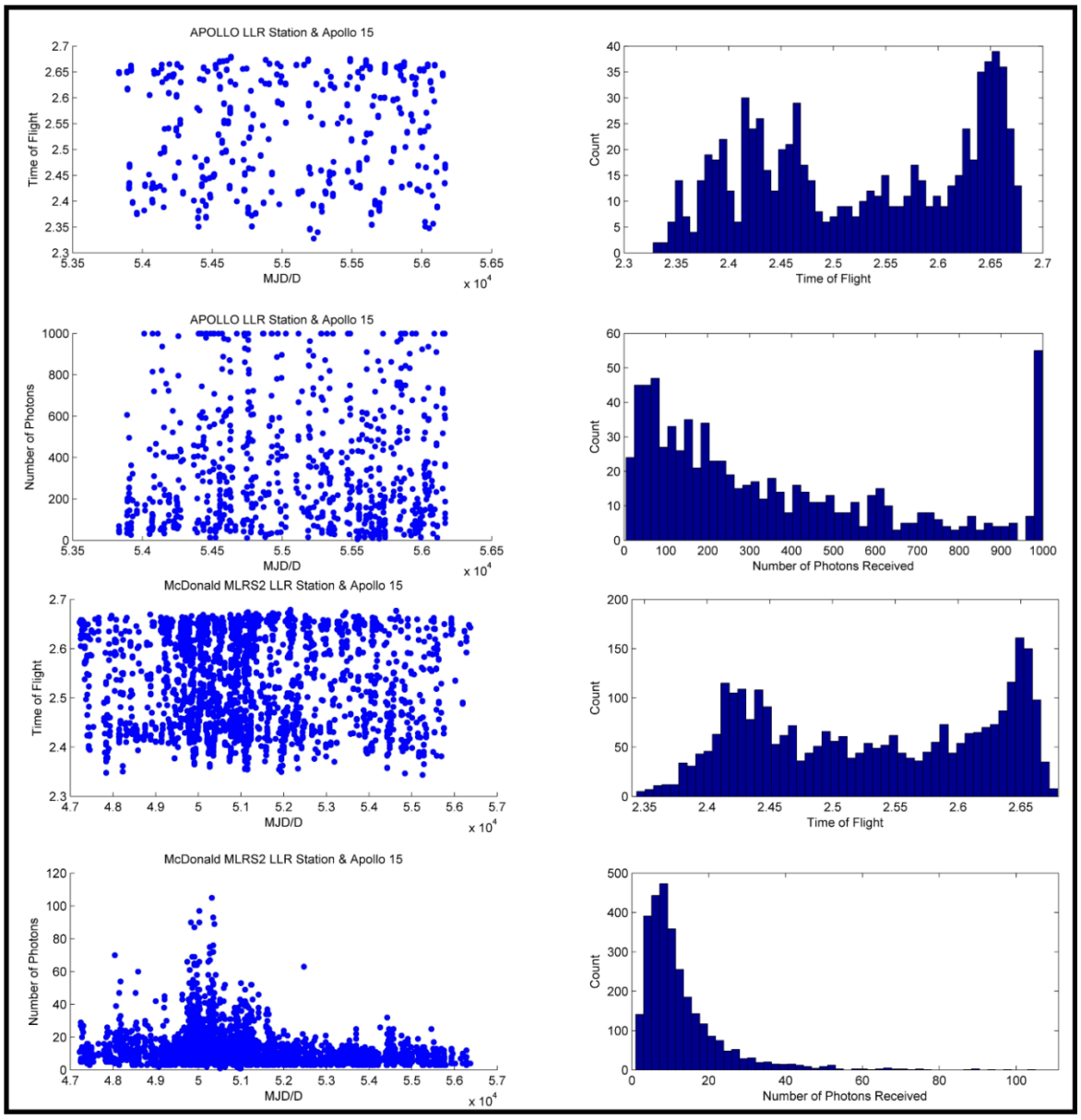

Figure 6.Time-of-flight and received a number of photons measured between Apollo 15 retro-reflector, APOLLO and McDonald MLRS2 stations.

2.3. Time measurement systems and timescales as applied to LLR

In the early days of civilisation, Earth was thought to be a perfect clock by counting the number of sunrises or sunsets and constructing a calendar as Earth rotates around its axis. Advancements were made to measure time and intervals more accurately by developing mechanical clocks. One such advancement is the pendulum clock that was built with an accuracy of about 10 seconds per day (Lombardi, 2011a). It is important to note that during this time, there was no method developed to synchronise individual clocks.

The development of timing systems led to developments of many technologies that have societal benefit, including GPS, the electric power grid, mobile phones (Lombardi, 2011b), and many other applications that are taken for granted. The reported accuracy of the first operational atomic clock was 0.1 ms/day (Henderson, 2005). The accuracy of the Cesium atomic clocks increased with the development of the laser cooling technologies, the National Institute of Standards and Technology (NIST) has so far developed the NIST-F1 and NIST-F2, with an accuracy of more than 10^{-15} at 1 s, which are the most accurate Cesium clocks (Heavner et al., 2014). Quartz and rubidium clocks are being used in scientific experiments such as LLR and SLR since they are relatively affordable and they offer a good accuracy of about 10^{-12} at 1 s.

Before continuing on, the terms: time and frequency should be clarify within the context of LLR measurements. According to Lambardi, (2002), a clock provides time (in the form of seconds, microseconds, days, months, etc.) and this information can be used to synchronize events. A clock can be used to measure time lapse between two events. In this case, a laser photon leaving the telescope, reflected by the retro-reflector on the surface of the Moon and back to the telescope. The form T = 1/F relates frequency (F) and time (T), and frequency is a measure of the rate of a repetitive event (e.g., 1 KHz equals 10^3 events per second) as produced by an oscillator (Lambardi, 2002). Crystal oscillators such as quartz or rubidium are used to produce precise frequencies that drives measurement devices such as event timer (normally runs on 5-10 MHz) an example is the ultra-stable event timer presented in Samain et al., (2010).

It is important to note that the time available at the LLR station is Coordinated Universal Time (UTC), which is derived from the International Atomic Time (TAI) to be within 0.9 s of Universal Time (UT1). The TAI is derived from the network of hydrogen masers and ceasium clocks. UTC time is broadcasted using time transfer techniques such as WWV (National

Institute of standards and Technology Time and Frequency shortwave radio ststion) and GNSS. Due to irregularities in Earth's rotation, leap seconds are introduced to keep the difference between UTC and UT1 less than 0.9 seconds.

$$|\text{UTC-UT1}| < 0.9\ s. \tag{2.1}$$

According to Mulholland, (1977), measurements made at the station will be in UTC, however for computational purposes; this time must be converted to ephemeris time (ET) as

$$t_t(ET) = \text{UTC} + (\text{IAT-UTC}) + \delta_c + \Delta T. \tag{2.2}$$

In Equation (2.2), (IAT-UTC) is an integer number in seconds defined by international conversion, δ_c is a constant value of ~32.184317 s and is used to account for the difference in the origins of IAT and ET at the initial epoch of IAT, ΔT is a relativistic correction to account for the behaviour of the clock as it moves through gravitational potential field. In Newtonian computation, this term will equal to zero. In Einsteinian general relativity, ΔT can be approximated by

$$\Delta T = 1658(\sin E + 0.04) + 2\cos\phi(\sin[UT1 - \lambda] - \sin\lambda). \tag{2.3}$$

In Equation(2.3), E is the eccentric anomaly of the Earth clock, λ and ϕ are the longitude and latitude of the clock (Mulholland, 1972; Pavlov et al., 2016; IERS, 2003).

2.4. Basic principles of lunar laser ranging

Ranging to the Moon involves transmitting short laser pulses (about 0.03 m) from the ranging station to the retro-reflectors located on the surface of the Moon. The two-way ToF of the laser pulses is measured on the ground using highly accurate timing systems. Most SLR stations utilise Nd:YAG lasers at 532 nm wavelength with a repetition rate ranging from 5 Hz to 2 kHz. In SLR applications, laser energy ranging from ~1 to 100 mJ are used to range to artificial satellites such as LAGEOS. Higher laser energies (100 to 200 mJ) and lower laser pulse frequencies (~20 Hz) as well as larger telescopes are used for LLR applications. This is mainly due to the greater Earth-Moon distance (~384 400 km) compared to shorter distances between the satellites that are orbiting the Earth (~5900 km for LAGEOS satellites).

A detailed description of the Earth-Moon distance is described in Mulholland, (1977) and Larden, (1982). Here, a summary is given. In Figure 7, a simplified geometry of the Earth-Moon system is presented. The vector $\vec{r}$ represents the telescope position in the earth-fixed system, $\vec{k}$ vector presents the selenocentric position of the retro-reflector on the Moon in the lunar-fixed system, $\vec{R}$ and $\vec{M}$ represents the Earth and the Moon orbits respectively. Computation of the Earth-Moon distance is done in the Barycentric Celestial Reference Frame (BCRF).

Ephemeris coordinates for the telescope are determined by modelling sidereal, polar, nutation and precession motions of the vector $\vec{r}$ at the time of the laser transmission ($t_{\vec{r}1}$). This is the UTC time detected by the start detector at the station. Earth tides and ground water variation will introduce small station displacement ($\delta\vec{r}$) that must be modelled to improve telescope coordinates. These factors might not be significant during the 2.5 s journey of the photon at the computation accuracy of about centimetre level because of their relatively long period (~days to months). However, HartRAO aims to achieve sub-centimetre computation accuracy. In this case, a gravimeter on site can aid in improving solid Earth tide modelling by comparing modelled with actual vertical displacement; this could lead to site dependent "tuned" Love numbers, which will improve solid Earth modelling.

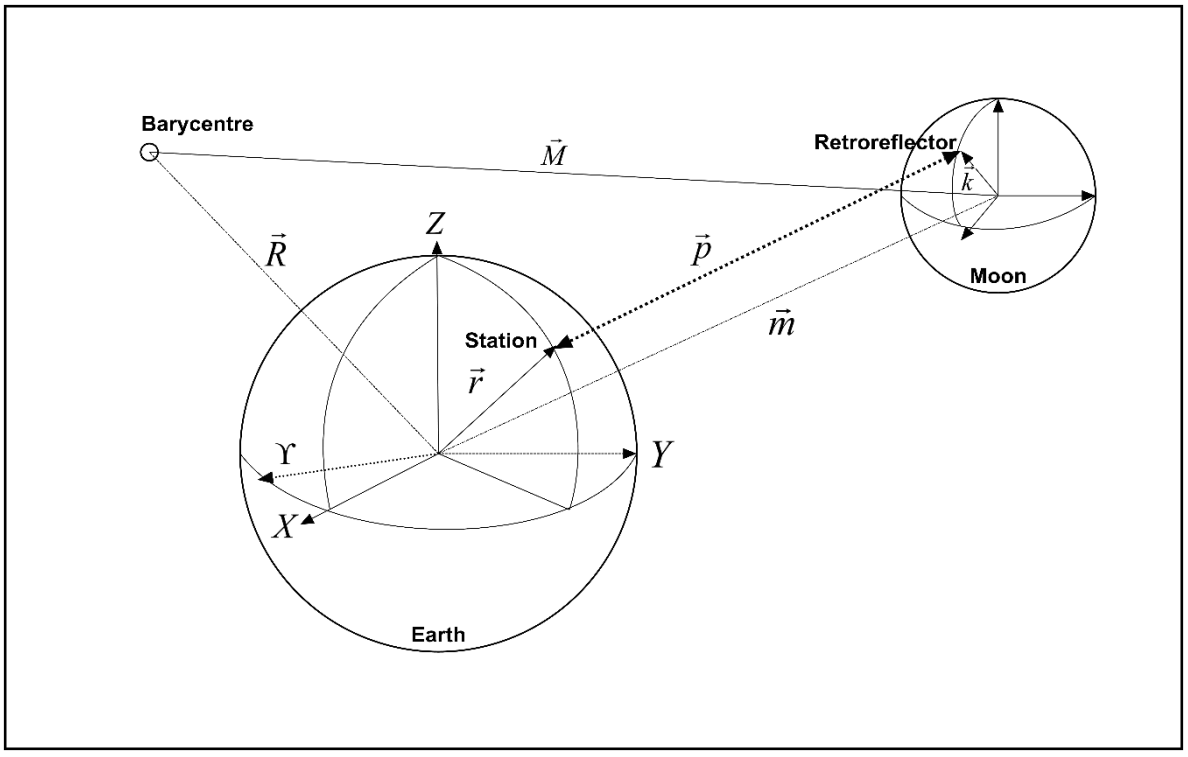

Figure 7. Simplified Earth-Moon system (After: Larden, 1982).

The time at which the photons are reflected by the lunar retro-reflector is not known but estimated by assuming that the atmospheric conditions remained relatively unchanged and it is estimated by

$$t_{\vec{k}1} = T_{ET} + \Delta T / 2. \tag{2.4}$$

The lunar reflector $\vec{k}$ position at the time $t_{\vec{k}1}$ is determined using a lunar ephemeris, where lunar librations are corrected. The Jet Propulsion Laboratory (JPL) ephemeris DE430 model is normally used. The results are transformed into the BCRF. The barycentric frame is assumed to be fixed in space and has its origin at the centre of mass of the solar system (Larden, 1982).

The basic observational equation is given in Müller et al. (2008) as

$$d = c\frac{\tau}{2} = |\vec{m} - \vec{r} + \vec{k}| + c\Delta\tau. \tag{2.5}$$

In Equation (2.5), d is the station-reflector distance, c is the speed of light in vacuum, τ is the ToF of the laser pulse, $\vec{m}$ describes a vector connecting the geocentre and the selenocentre. The laser pulse is delayed due to interaction with the non-linear atmospheric environment, which must be corrected as well as other factors such as relativistic effects. The term $\Delta\tau$ describes these corrections, which must be applied to obtain an accurate observed distance.

The Earth-Moon distance is approximately 385 000 km, this presents a challenge in LLR compared to SLR due to the fact that fewer photons are received per single laser shot containing about 10^{15} photons. To illustrate the impact of the Earth-Moon distance on the photon return rate, Degnan (1993) provided a radar link equation that estimates the success of receiving photoelectrons n_{pe} as detected by the receiving telescope as

$$n_{pe} = \eta_q \left(E_T \frac{\lambda}{hc} \right) \eta_T G_T \sigma \left(\frac{1}{4\pi R^2} \right)^2 A_t \eta_R T_a^2 T_c^2. \tag{2.6}$$

In Equation (2.6), η_q is the detector's quantum efficiency, E_T the laser pulse energy, λ the wavelength of the laser, h is Planck's constant, c the speed of light in vacuum, η_T the efficiency of the transmitter optics, G_T the transmitter gain, σ the reflector optical cross section and η_R is the efficiency of the receiver optics. The effective area of the telescope-

receiving aperture is given by A_t, T_a is the one-way atmospheric transmission if present, and T_c is the one-way transmissivity of cirrus cloud. The slant range R to the Moon can be calculated using

$$R = -(R_E + h_t)\cos\theta_{zen} + \sqrt{(R_E + h_t)^2 \cos^2\theta_{zen} + 2R_E(h_s - h_t) + h_s^2 - h_t^2}, \qquad (2.7)$$

where R_E is the Earth radius (6378 km), h_t is the station height above sea level, h_s is the Moon altitude above sea level, θ_{zen} is the zenith angle of the Moon as observed from the ranging station. Table 1 list estimated parameters for the LLR station at HartRAO, using Equation (2.6) and (2.7), 5 photons per minute are estimated to be received by the telescope.

The observed raw data (d_{oi}) are filtered to detect gross errors, evaluated to access the accuracy of the observations and compressed for further analysis in the form of a normal point (NP_i) dataset (see Equation (2.8)) (Sinclair, 1997). The residuals are computed from the predicted and observed ranges and the outliers are removed using a range window. A suitable trend function is usually fitted to the residuals, (polynomial fit or using a set of orbital parameters) to detect further outliers by analysing the deviations from the fit (f_{ri}). The data can then be divided into bins, different retro-reflectors/satellites have recommended a number of bins to be used e.g., for LAGEOS 1 and 2, a 120-second bin width is used to divide the data for the duration of the observation. For each interval of the bin, *i*, a mean value ($\bar{f}_{ri}$) of all deviations is formed and added to the trend function at the centre of the interval (Degnan, 1993). This point is referred to as a normal point and thus represents a single observation of the particular interval,

$$NP_i = d_{oi} - (f_{ri} - \bar{f}_{ri}). \qquad (2.8)$$

Table 1. Estimated parameters used to simulate radar link equation for the LLR station at HartRAO.

Radar Link Equation Parameters	Values
Detectors quantum efficiency	50%
Laser pulse energy	120 mJ
Wavelength of the laser	532 nm
Efficiency of the transmitter optics	80%
Transmitter gain	1.04E+23
Retro-reflector optical cross section	~0.0016 m^2
Efficiency of the receive optics	50%
Telescope receiving aperture	~1 m
One-way atmospheric transmission if present	1
Beam pointing error	45
One-way transmissivity of cirrus cloud	1
Far field divergence of half-angle between the beam center and the 1/e^2 intensity point	3

The systematic errors must still be modelled out during further processing, some of which are discussed later in this chapter. The internal system accuracy of the station can be evaluated using Equation (2.9) as given in Sinclair (1997), where n_i represents the number of observations within the bin.

$$RMS_i = \sqrt{\frac{1}{n_i}\sum_j (f_{ri} - \bar{f}_{ri})^2}. \tag{2.9}$$

2.5. External factors contributing to observed time delay

In light of the new LLR analysis software being developed at HartRAO, it is necessary to take into account all the factors that affect ranging to the Moon and satellites, and which eventually affects the accuracy of determining the Moon's orbit. In terms of SLR, these are listed in Combrinck and Suberlak (2007) and Combrinck (2010) as: Earth's geopotential (Botai and Combrinck, 2011a), solid Earth tides (Petrov, 2005), ocean tides, planetary third-body perturbation (Sun, Moon and planets), relativistic acceleration (Combrinck, 2013), atmospheric tide and atmospheric drag (Van Dam and Herring, 1994), solar radiation pressure (Ziebart, 2001), Earth radiation pressure, thermal radiation acceleration (Vokrouhlicky, 1997), lunar librations (Mulholland et al., 1972) (for LLR), Shapiro delay (Shapiro, 1964), tropospheric delay (Mendes and Pavlis, (2004) and Mendes et al., (2002)) and delay induced by electronic

systems. The delays due to electronic systems for the HartRAO station are discussed in Chapter 4.

Two separate software suites will be used for either SLR or LLR analysis, as although some of the corrections are similar (e.g. station displacement due to the solid Earth tides) the analysis problem is in fact quite different. Not all these factors are discussed, further information can be found in the references provided, and only corrections for a few factors are discussed to illustrate the importance of considering these factors in the LLR analysis package. In a simplified version, the ToF of the laser pulses can be described by

$$ToF = T_{sy} + D_{at} + G_{rt} + T_{td} + \varepsilon, \tag{2.10}$$

where,T_{sy} represent actual time interval measurement by the station (discussed in details in Chapter 4), D_{at} is the time delay due to the atmosphere, G_{rt} is the General Relativity correction, T_{td} is the time variation induced by tidal effects and ε includes all other corrections not listed above and unknowns. The ToF is the actual time interval measurement at the station which is composed of several components. The station timing system does not "know" about all those single contributions but measures just the gross sum as a time interval. T_{sy} is here rather the "true" Moon distance (expressed in a ToF). It is the main task of data processing to account for the true Moon distance by removing the other disturbing contributions. Practical examples are given from Section 2.5.1 to 2.5.4 for selected parameters.

2.5.1. Tidal correction on station position

The gravitational attractions of the Sun, Moon and planets on Earth, result in a force that deforms the Earth's gravitational field and induces solid Earth tides (Métivier et al., 2009). This is coupled with ocean and atmospheric loading effects as well as the mantle convection processes within the Earth. The Earth system responds to these effects through mass displacement, rotational acceleration and continuous deformation of the solid crust (Combrinck and Suberlak, 2007). Space geodetic instruments such as LLR are affected by these continuous deformation effects and they translate to an additional range bias during ranging. Hence, the LLR analysis software (currently under development at HartRAO) must be able to model these effects with high accuracy in order to improve the range bias. The Earth tide, pole tide and ocean tide effects are well described in McCarthy and Petit (2013) and readers are referred to this reference for more information.

The solid Earth tides can be conveniently modelled as variations in the standard geopotential coefficients C_{nn} and S_{nm} (Eanes et al., 1983) and can be described as

$$\Delta\bar{C}_{nm} - i\Delta\bar{S}_{nm} = \frac{k_{nm}}{2n-1}\sum_{j=2}^{3}\frac{GM_j}{GM_E}\left(\frac{R_e}{r_j}\right)^{n+1}\bar{P}_{nm}\left(\sin\Phi_j\right)e^{-im\lambda_j}\left\{with\ \bar{S}_{n0}=0\right\}. \qquad (2.11)$$

In Equation (2.11), k_{nm} is the nominal Love number for degree *n* and order *m*, R_e represents equatorial radius of the Earth, GM_E is the gravitational parameter for the Earth, gravitational parameter for the Moon (j=2) and Sun (j=3) is given by GM_j, the distance to the geocenter to the Moon or the Sun is represented by r_j, Φ_j is the body fixed geocentric latitude of Moon or Sun, λ_j represent body fixed east longitude (from Greenwich) of the Moon or Sun and $\bar{P}_{nm}$ represents the normalized associated Legendre function.

A library developed in FORTRAN to compute station displacement due to Earth tides was developed by Petrov (2005) and it is currently used by the Satellite Data Analysis Software (SDAS) developed at HartRAO (Combrinck and Suberlak, 2007). The same library was also used in this study to illustrate the effects of Earth tide on the Earth crust for the HartRAO site, where the LLR telescope is located. A continuous station displacement can be clearly seen with different magnitudes ranging from -16 cm to 30 cm in vertical displacement (Figure 8). Gravitational pull by the Sun, Moon and planets also result in ocean tides, an additional weight by ocean loading influences crustal displacement and results in temporal variations of telescope coordinates. Stations that are inland are often less prone to these perturbations compared to stations that are close to the coast. Currently, there are plans to move the new LLR station at HartRAO (once completed) to Matjiesfontein in the Great Karoo, Western Cape (Combrinck and Botha, 2014).

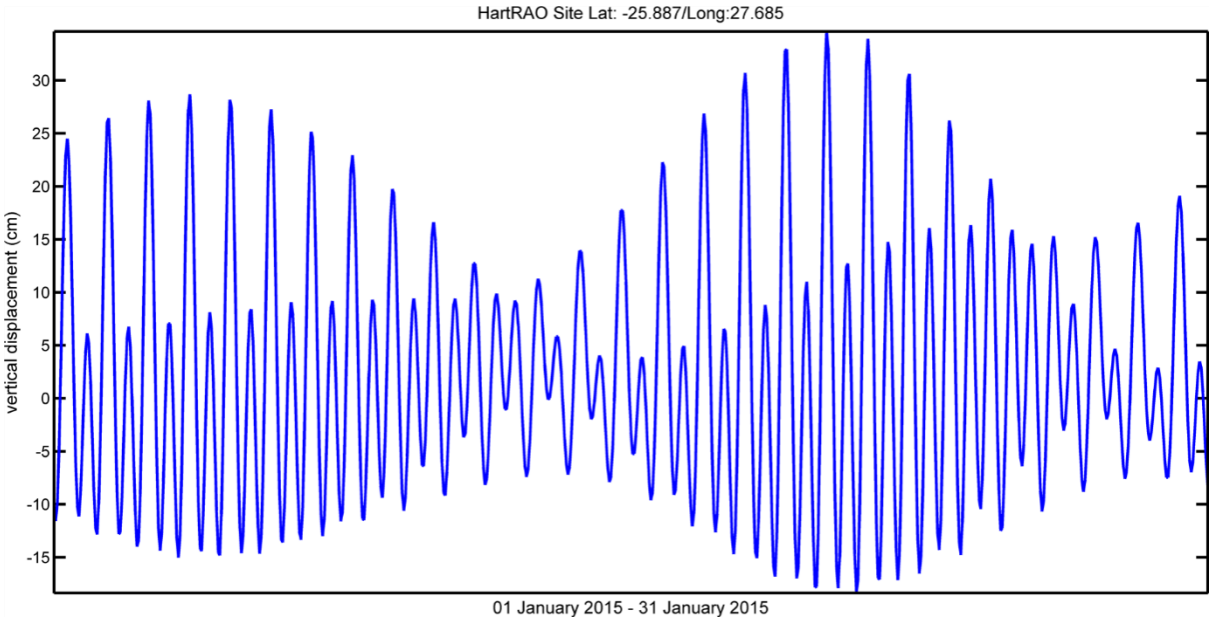

Figure 8. Station vertical displacement for HartRAO site, simulated for the month of January 2015.

This new site is about 240 km from the Southern Ocean, the effects of ocean tides are expected to have more influence on the station position as compared to the current location (HartRAO, Krugersdorp). To better understand and model the effects of ocean and Earth tides, atmospheric loading and local hydrological cycles requires instruments such as a superconducting gravimeter, which ought to be mounted as close as possible to the ranging telescope to measure small displacements. A typical example is the APOLLO station at Apache Point, Texas, their gravimeter has a noise level of 1 nm s^{-2} and this is very sensitive to model these effects to millimetre accuracy or better (Sinclair, 1997). HartRAO has installed a gravimeter to compensate for these effects and to improve the existing models.

2.5.2. Tropospheric delay correction

The troposphere introduces a significant delay (up to several metres) both in the radio and optical wavelengths. Different models have been developed to account for this delay; the recommended models for laser ranging observations across the full optical spectrum are described in Mendes and Pavlis, (2004) and Mendes et al., (2002). The delay increases with decreasing pointing elevation angles. Data from a network of radiosondes and ray tracing distributed worldwide are used to create and validate tropospheric models. The routines to

perform atmospheric corrections described in Mendes and Pavlis, (2004) and Mendes et al., (2002) are available at (ftp://tai.bipm.org/iers/conv2010/chapter9/). I convert the routines from FORTRAN to MATLAB for easy simulation.

To illustrate the amount of delay introduced by the atmosphere at different elevation angles for 0.532 µm wavelength, daily average values measured by MET4 unit at the HartRAO site: 24.5 ºC, 859.6 mb and 58.7% relative humidity were used. Figure 9 illustrates range delay at different elevation angles. A step of 0.1 in elevation angle change will require ~6 mm correction for the HartRAO site Combrinck, (2010).

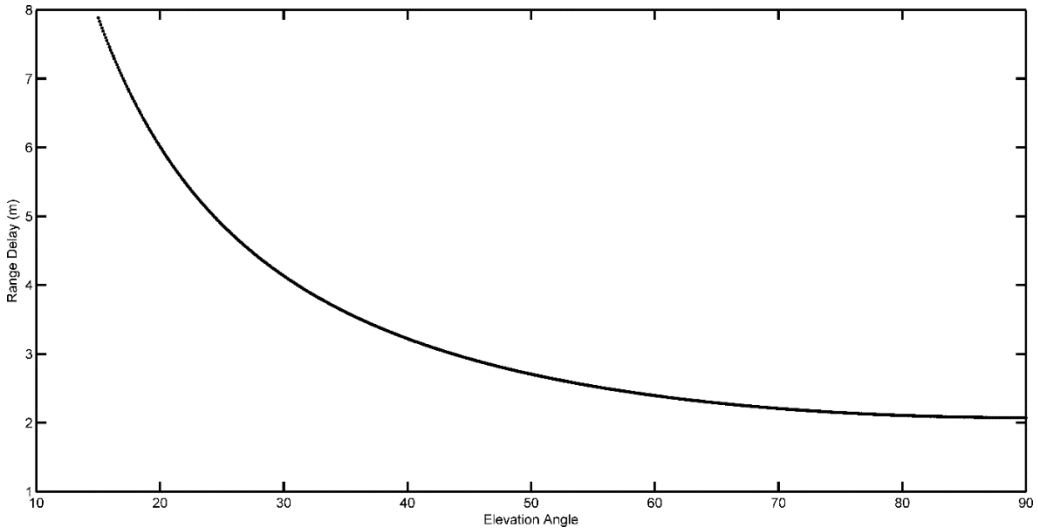

Figure 9. Range delay due to the atmospheric effects at 0.532 µm wavelength. The model is based on Mendes et al., (2002) and Mendes and Pavlis (2004). The models were applied to the HartRAO site.

2.5.3. Degradation of lunar retro-reflectors

As reported in Murphy et al., (2010), the lunar retro-reflectors have depicted a decrease in efficiency over the years. This is mainly attributed to dust caused by the descending and ascending stages of the lunar modules. Temperature variation on the lunar surface can vary from 115ºC to -180ºC during noon and midnight respectively (Cremers et al., 1971). These extreme temperature variations will also degrade the performance of the retro-reflectors and thus limit the capability to improve the precision of LLR measurements. The next generation of lunar retro-reflectors are being developed with an increase in size and better thermal stability (e.g., Preston and Merkowitz, 2013).

2.5.4. Timing systems

Timing systems are crucial in space geodetic and astronomical instrumentation. In particular, the accuracy of measurements depends on the accuracy of the reference timing systems. Most reference timing stations for SLR and LLR are at the level of 10^{-12} Allan deviation at 1 s using rubidium/quartz crystal oscillators (ILRS, 2009), while the hydrogen maser clocks used in VLBI techniques are better than 10^{-14} at 1 s (ILRS, 2015). Most stations are limited in utilising highly accurate timing systems such as maser clocks due their high cost. The noise levels within event timers and photon detection systems also play a crucial role in the accuracy of the normal data points and range bias. It is envisaged that the new LLR station will utilise the newly developed 4380A-GPS disciplined master timing reference by Microsemi Corporation. This unit has an Allan deviation of 10^{-13} at 1 s and less than 10 ns Root Mean Square (RMS) timing accuracy. A low jitter event timer of 3 ps RMS and a solid state photon detector (Single Photon Avalanche Diode) with Quantum Efficiency (QE) of 50 % will be integrated to allow for sub-centimetre ranging precision.

The impact of timing systems on the observed range measurements can be seen in Figure 10, where the normal point data quality of the Potsdam SLR station between 2003 and 2011 indicates high variation ranging from 10 to 25 mm (ILRS, 2009). During the 2011 period, an old timing system of the Potsdam SLR station was replaced with a more modern timing system with better specifications (Table 2). Noticeably, the Single Photon Avalanche Diode (SPAD) with QE of 28 % was replaced with the SPAD that has QE of 40 % and low jitter. As a result, the normal point data are characterised by low variations, which can be directly linked to the improvement of the timing systems (among other improvements) post 2011.

Table 2. Historical improvement of the Potsdam SLR station timing system (ILRS, 2009).

Date installed:	**2001/07/20**	**2001-2004**	**2011/05/01**
Timing Equipment			
Detection type	SPAD (AD230)		SPAD (MPD-ICTC)
Quantum efficiency (%)	28		40
Jitter (ps)	75		20
Signal processor	CFC (TC4S4)		
Time measurement	Interval	Event	Event
Model	SR620	A031-ET	A032-ET
Resolution (ps)	4	1	1
Precision (ps)	20	10	7

SPAD, single-photon avalanche diode; CFD, constant fraction discriminator

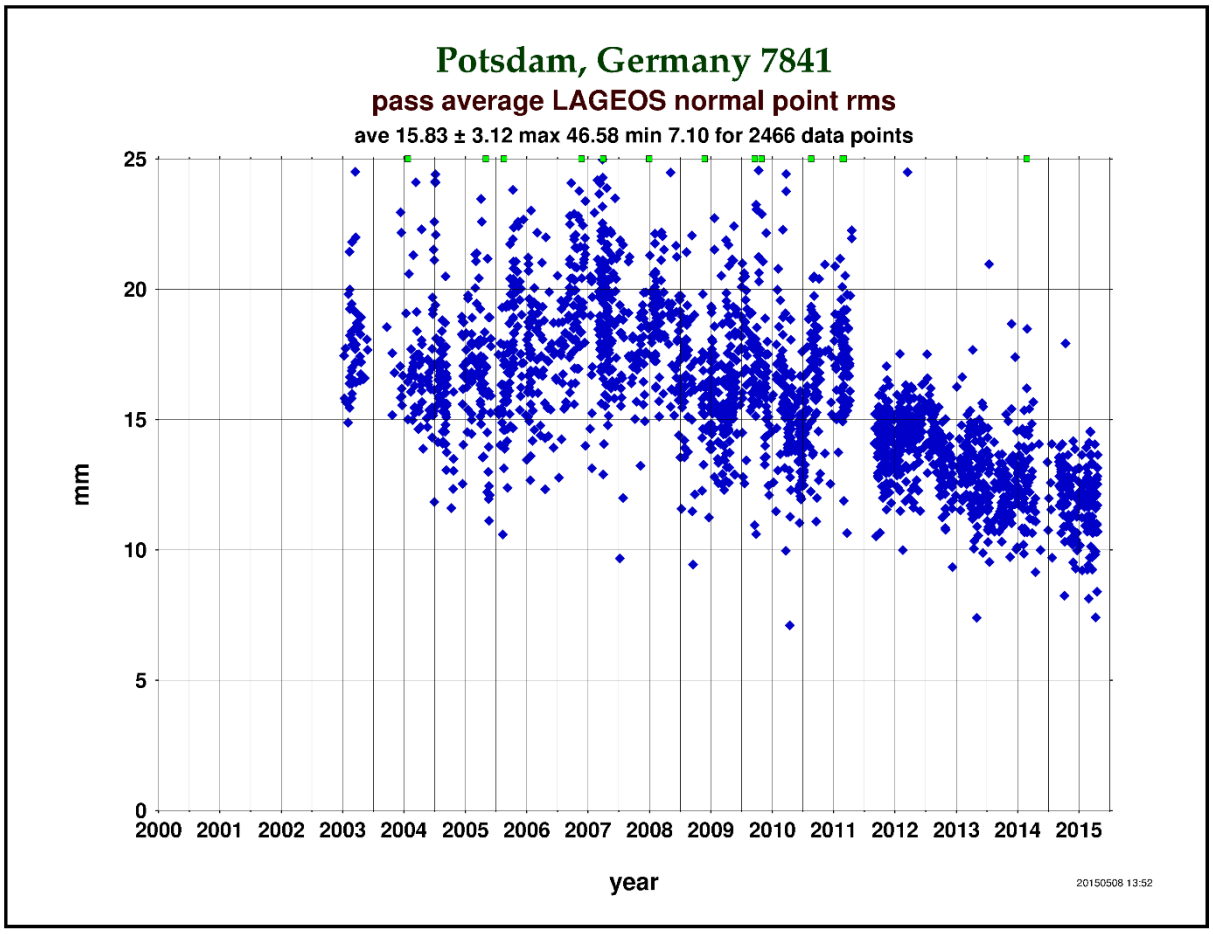

Figure 10. Potsdam SLR station performance measured based on normal point RMS for LAGEOS ranging data (ILRS, 2009).

2.6. Towards understanding O – C parameters and their sources

The goal of LLR data analysis software at HartRAO is to minimise the residuals (Δt_r) computed between the observed (t_o) and computed time delay (t_c) as

$$\Delta t_r = t_c - t_o. \tag{2.12}$$

To achieve this goal, Mulholland, (1972) and Larden, (1983) can be used to understand the O-C parameters. Each term in Equation (2.12) contains many parameters that must be understood. The first term to be explored is the computed time delay (t_c),

$$t_c = t_d^{'}(ET) - t_t(ET) + \frac{2}{c}\vec{p}\cdot\delta\vec{r} + \Delta t(t_t) - \Delta t(t_d). \tag{2.13}$$

In Equation(2.13), $\delta\vec{r}$ is the Earth-tide deformation vector for the telescope position, $\vec{p}$ is the vector between the telescope and the retro-reflector (see Figure 7). The dot product is calculated between $\delta\vec{r}$ and $\vec{p}$ and divided by *c*, the velocity of light to convert the results to time. The term $t_t(ET)$ describes the time at which laser photons are transmitted by the telescope (see Equation (2.2)). The term $\delta\vec{r}$ can be modelled as described in Section 2.5.1. The relativistic corrections $\Delta t(t_t)$ and $\Delta t(t_d)$ are approximated using Equation (2.3).

The time at which a photon is detected at the telescope is given by

$$t_d^{'}(ET) = t_d(ET) + \Delta_1 + \Delta_2. \tag{2.14}$$

The atmospheric contribution Δ_2 and gravitational effect Δ_1 on the photon during the average travel time of the photon (~2.5 seconds) remains relatively the same i.e., $\Delta_1 = \Delta_2$. Modelling atmospheric effects can be achieved as described in Section 2.5.2. In this case, it was assumed that the telescope coordinates from the time of transmission to reception of photon would not change significantly during the round trip journey of the photon. The observed component (t_o) involves measuring internal system delay, calibrating the system by way of ranging to onsite stable pier, ranging to the Moon's retro-reflector and using a photon detection system to measure the returns. Photons interact with the atmosphere and they are affected by gravity, all these effects must be taken into account during data analysis. It is important to note that parameters such as internal system delay can only be determined if the telescope is in working condition.

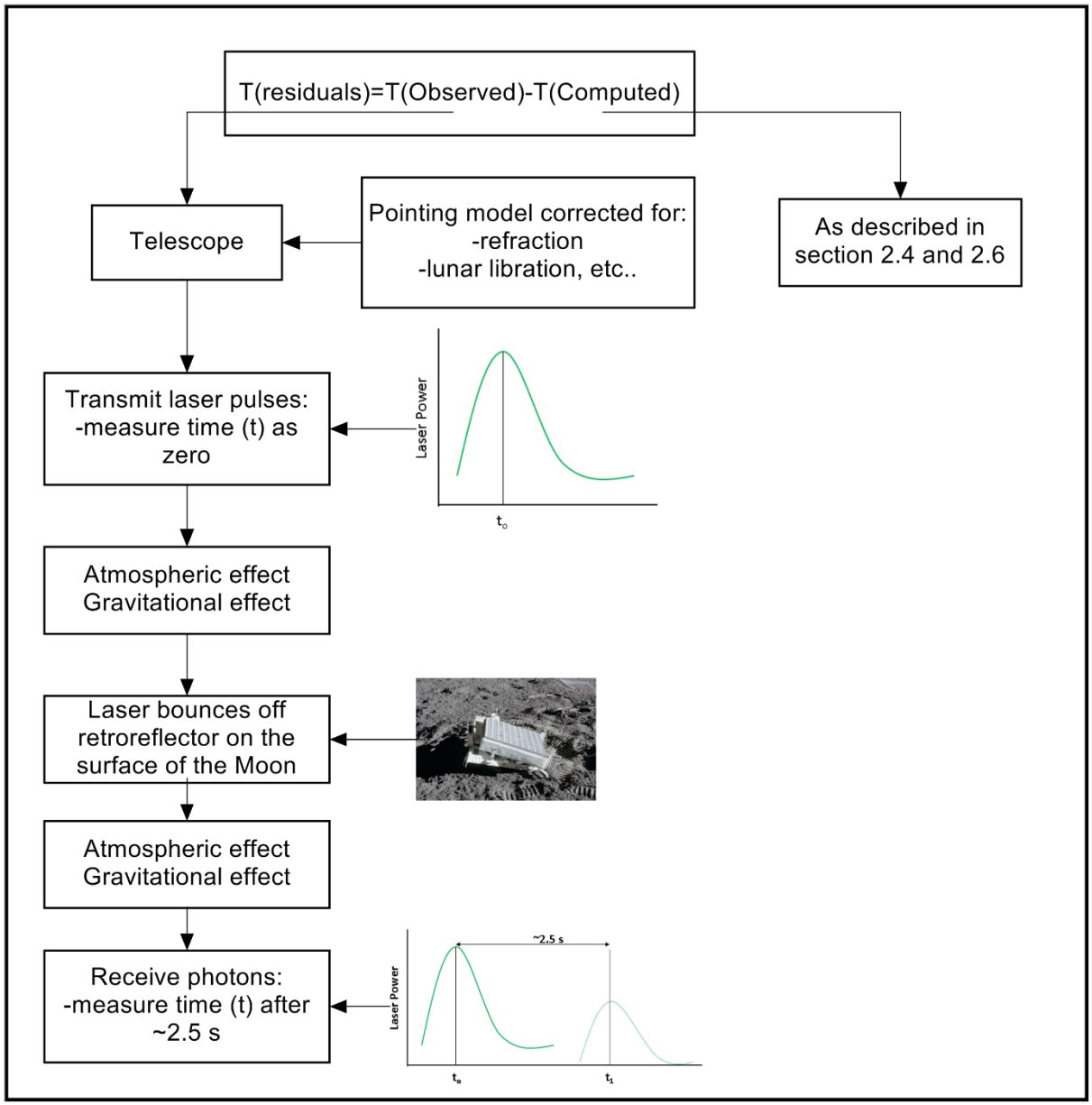

Figure 11. Summary of the processes involved in computation of O-C residuals.

In Figure 12, improvement in the precision of LLR data since the first observations were made in the 1970's can be seen. The improvements can be linked to the improvements in the observed component (t_o) of Equation (2.12). The hardware improvements in ranging stations (see Section 2.5.4) and model improvements play a crucial part in improving the accuracy of LLR estimated parameters. The LLR station at HartRAO needs both good hardware and software to fully operate at sub-centimetre accuracy regime, an example of this is the APOLLO station (see Section 2.7.1 for more details).

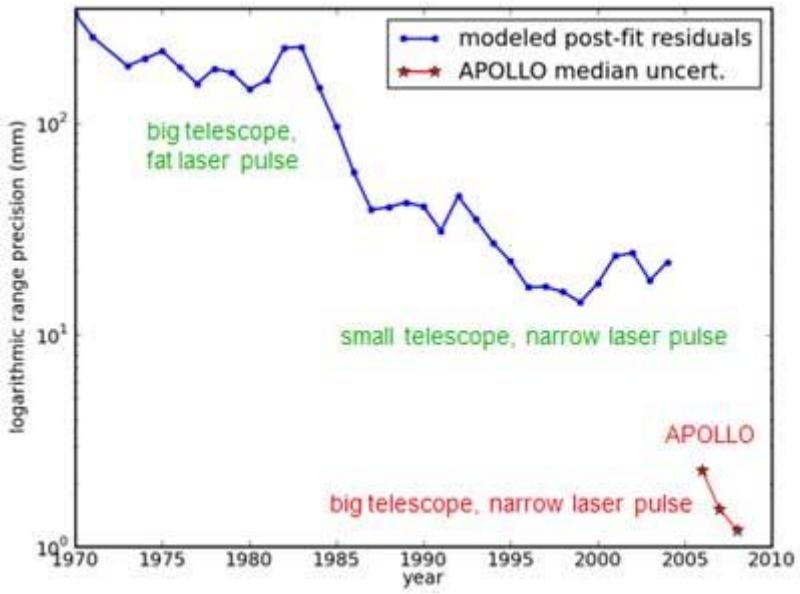

Figure 12. Analysis of the results from LLR data indicate an increase in range accuracy. Currently, the APOLLO station can achieve sub-centimetre accuracy (Source: Crawford, 2009).

2.7. Examples of lunar laser ranging systems

2.7.1. Apache Point Observatory Lunar Laser-ranging Operation (APOLLO)

The APOLLO timing system is based on the 16-channel Time-to-Digital Converter (TDC, model 7186H) developed by Phillips Scientific (www.phillipsscientific.com). The TDC has 12-bit (25 ps) resolution and operates together with a GPS-slaved clock, which provides a 100 MHz frequency reference signal to UTC. The precise time interval between the 4x4 Avalanche Photodiode (APD) detection events and the next clock pulses is maintained by the TDC. This configuration was designed to cope with multiple photon returns given that, the APOLLO system was expected to detect 2-10 lunar return photons per pulse. In contrast, the HartRAO LLR system is expected to receive only 3-5 photons per minute due to its smaller telescope (1-m versus 3.5 m). The timing system at APOLLO performs at ~20 ps resolution, for more detail description of the APOLLO system refer to Murphy *et al*., (2000) and Murphy *et al*., (2002). The APOLLO station is depicted in Figure 13.

Figure 13. APOLLO station (photo credit: Tom Zagwodzki/Goddard Space Flight Center).

2.7.2. Observatoire de la Côte d' Azur (OCA)

The OCA LLR station (depicted in Figure 14) timing system is based on the HP 5071A commercial Cesium atomic clock; GPS provides the system with a 200 MHz reference frequency signal. The frequency accuracy of the clock is lower than 10^{-12}, with Allan variance root square of $5x10^{-12}$ in a time interval of $0.2 < t > 3$ s. The time precision of the OCA station is 5 ps and the resolution is 1.2 ps (Samain et al., 1998).

The timing system configuration for this station is simple compared to the APOLLO timing system configuration. At a rate of 10 Hz, the Nd:YAG laser emits four short pulses with an interval of 1.6 ns, 4.1 ns and 5.7 ns respectively. The infrared light generated by the laser is detected by an InGaAs photodiode detector, which is coupled to a fast comparator to send out the start signal to the start timer (precision of less than 5 ps). The return photons are detected by the APD (SSOAD230H) operating under Geiger mode. The signal is then sent to the event timer and the ToF is determined. This approach minimises the problem of multiple return lunar photons mixing in the detection system as experienced by APOLLO.

Figure 14. Grasse station (photo credit: Jean-Marie Torre/OCA).

2.8. Lunar laser ranging contribution to science and society

Earth observation techniques have a direct impact on the social lives of people. Imagery from remote sensing techniques are widely applied in areas such as agriculture (Bastiaanssen et al., 2000), ecosystem management (Kerr and Ostrovsky, 2003; Cohen et al., 2004), water management (Jackson et al., 1996), disaster management (Madry, 2015) and weather applications (Lazzara et al., 2011). These applications provide examples of the use of Earth observation techniques to assist in planning, early warning for natural disasters and management of Earth resources. More advanced remote sensing techniques such as VLBI, GNSS, LLR and SLR contribute in the same way as satellite remote sensing to the society. The derived data products such as the International Terrestrial Reference Frame (ITRF), Celestial Reference Frame, Earth Orientation Parameters, gravity field, atmosphere and ionosphere parameters form part of the foundation of Earth observation technologies (Rothacher, 2002). A set of station coordinates and velocities derived from the geodetic techniques are used to construct a reference frame that allows connection and comparison between different geodetic datasets over varying space and time. This is done through a combination of the datasets using scientific software such as CATREF (Altamimi, 2006) and taking into account the local site ties. The latest ITRF2008 has an accuracy of sub-centimetre (Altamimi et al., 2008). This system provides a basis for local reference frame systems, which are realised based on the ITRF, this includes, for example, the unified African geodetic reference frame (AFREF), which can be used for cadastral surveys, mapping and Civil engineering applications (Drewes and Hornik, 2013).

The LLR technique, in particular, contributes towards the advancement of the field of space geodesy, lunar science, the Earth-Moon system dynamics and gravitational physics. The increased accuracies in range measurements from 20-30 cm in early development stages to about 2-3 cm in recent developments, has provided ways to test and evaluate General Relativity Theory (Drewes and Hornik, 2013), and the gravitational constant with ranging accuracy at picosecond level. Williams et al. (2013) derived geophysical and orbit parameters of the Moon; the gravitational constant was evaluated to be $\dot{G}/G = 4 \pm 9 \times 10^{-13}$ yr^{-1} by Williams et al. (2004) and a more recent value of $-0.7 \pm 3.8 \times 10^{-13}$ yr^{-1} is reported in Hofmann et al. (2010). The LLR system at HartRAO is being developed by HartRAO staff as well as the PhD and MSc students registered at various South African Universities, hence capacity building and skills transfer are at a high level. This project will support society through contribution to

environment monitoring through proxy parameters, these parameters measure including the state of the atmosphere, gravity fields (for groundwater storage monitoring), seismic activities, which are important to society.

2.9. Proposed geodetic site at Matjiesfontein

2.9.1. Introduction

Matjiesfontein is set to host the S/LLR system that is currently in development at HartRAO site. The proposed site is located 5 km south of Matjiesfontein in the Great Karoo. The proposed site resides in a small depression to protect the instruments from human-induced noise interferences (see Figure 15). The site underwent extensive investigations, which include geophysical surveys by utilising magnetic, electromagnetic and seismic refraction surveys. The site was declared suitable and stable to host geodetic instruments. Preliminary results obtained from investigating atmospheric and astronomical seeing conditions by using a small astronomical refractor (10.8 cm aperture) indicated good seeing conditions ranging between 1-2 arc seconds (Combrinck et al., 2007).

The GPS station MATJ (Figure 16) on the site indicates velocities of 19.36 ± 0.26 mm/yr, 15.86 ± 0.28 mm/yr and -0.7 ± 1.07 mm/yr in North, East and Up components, respectively (Munghemezulu, 2013). Figure 17 illustrates snapshots of the proposed site and current developments in Matjiesfontein.

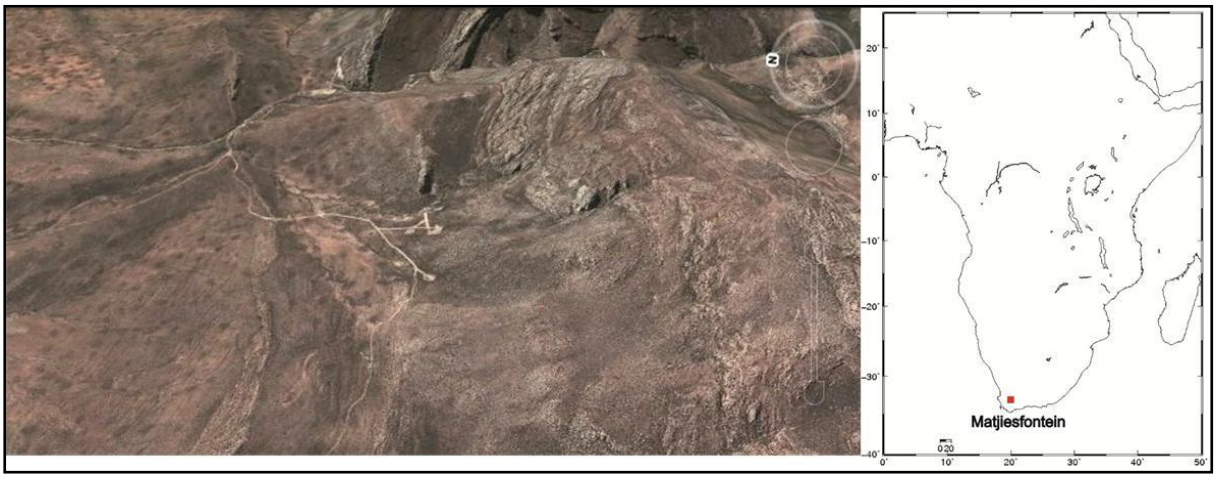

Figure 15.Left: Google map of the proposed site. Right: an insert map depicting the location of Matjiesfontein in the Western Cape of South Africa.

Figure 16. The panorama of the proposed site in Matjiesfontein village. The GPS station (MATJ) and the meteorological unit are already installed on the site. The site is located in a valley, this allows the instruments to be protected from radio signals.

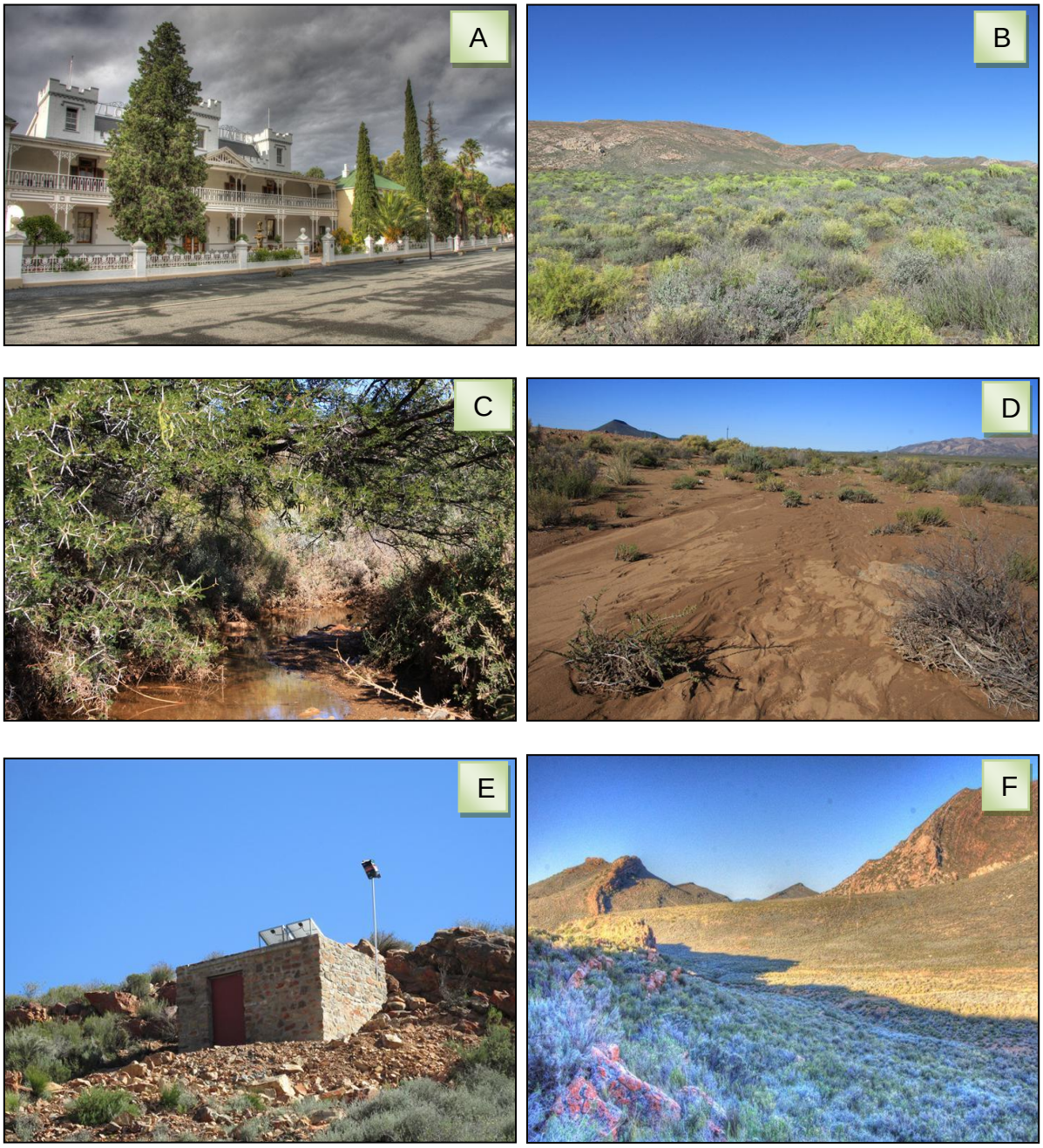

Figure 17. A: Lord Milner hotel in Matjiesfontein village. B: Indigenous plants found on the site. C & D: Natural streams that cross-cut the road to the site, bridges will be constructed to

allow easy access to the valley. E: A vault was constructed on site and it contains a seismometer, gravimeter and accelerometer. F: View of the proposed site facing the NE direction.

2.9.2. Progress made on the ex-OCA 1 m telescope

The ex-OCA 1 m telescope is being utilised by HartRAO to develop the system that will support both SLR and LLR techniques. The current developments and history on the ex-OCA telescope are detailed in Combrinck, (2011a); Figure 18 illustrates the current infrastructure of the system at HartRAO. A massive steel foundation was built to support the ~ 4.1 metric tonnes telescope. Such a foundation is necessary to allow sensitive pointing; the telescope must be stable enough to allow smooth tracking of the satellite or the Moon. If the telescope is not stable in both axis i.e., azimuth and elevation, this might result in a less accurate pointing model and fewer photon returns.

The run-off enclosure or housing for the telescope was designed and constructed at HartRAO (Figure 18: B). It is moved by electric motors and it takes approximately 2 minutes to move to its parking position, while MOBLAS-6 station takes about 8 minutes to close the telescope. The reaction time is very important in the case where there is rain, storm etc., to close-up the telescope as fast as possible and protect sensitive equipment. Figure 18:C depicts the refurbished telescope, the tube was removed for refurbishment and a 1-ton crane (overhead gantry) is used to move heavy equipment. The telescope is painted with a special paint (i.e., Ceratec and Supa Seal) to minimise thermal distortions.

Figure 18. A: Massive steel foundation for the telescope. B: construction of the mobile housing for the telescope. C: ex-OCA telescope has been refurbished and painted, the housing has been moved as seen behind the telescope (picture credit: Combrinck, L).

2.10. Concluding remarks

In this chapter, a reviewed of the LLR technique and the timing systems in light of the new LLR station at HartRAO. The difficulties associated with ranging to the Moon were highlighted and the emphasis was on factors that contribute to range bias, as these must be incorporated in the LLR analysis software. This new LLR station will contribute to both local and global communities to meet the scientific objectives of the currently growing space science endeavours by many countries as well as supporting socio-economic developments. Existing LLR stations are sparsely distributed globally and the station at HartRAO (currently in development) together with Mount Stromlo SLR observatory in Australia have the opportunity to expand the existing global network to the Southern Hemisphere.

Data products derived from highly technical space geodetic techniques such as LLR have indirect or direct benefits to the society; hence, the LLR project at HartRAO has received local and international support from organisations such as NASA (USA) and OCA (France). There are a number of factors that must be taken into considerations during the implementation of the LLR analysis software. The first step is to ensure that highly accurate timing subsystems are implemented (sub-picosecond level) to minimise local systematic errors. The delay induced by the environment can be modelled with current existing algorithms to a high level of confidence. This new LLR station will open many opportunities for current and future space programs both in Africa and internationally with societal benefits.

Chapter 3

Site selection for the lunar laser ranger timing antenna

Abstract

Accounting for multipath in Global Navigation Satellite Systems (GNSS) is a difficult task and an important one, especially during the pre-investigation phase for the installation of a permanent GNSS station for positioning or timing applications. Sites with a high level of multipath can cause positioning errors or timing errors resulting in the quality of GNSS products (position or timing) becoming degraded by several meters or nanoseconds. Investigation and attempt to map multipath as part of the site investigation for the installation of the timing antenna for lunar laser ranging applications at the Hartebeesthoek Radio Astronomy Observatory (HartRAO) were undertaken. A high-resolution wavelet power spectrum and a standard deviation parameter are used to map multipath in both the time and frequency domain as well as spatial variations on the sky plot. The high standard deviation values on the sky map are attributed to reflections due to shrubs or trees on the site, while less standard deviation areas are attributed to bare soil or less vegetated ground as this would give constant reflection over time provided the ground has constant moisture. I conclude that the site is suitable for installation of the timing antenna and that a mask of 15°-20° elevation angle will be applied to the timing antenna to minimise multipath at lower elevations.

3.1. Introduction

Multipath signals in most Global Navigation Satellite Systems (GNSS) applications are considered noise. Multipath occurs when an electromagnetic signal arrives at an antenna, not along a direct path, but via an indirect path due to the reflection of the signal by an object or surface near the antenna (Larson et al., 2008). Multipath signals are caused by surrounding features such as trees or soil reflecting transmitted signals from the satellites to the antenna. The errors caused by multipath on GNSS data products include positioning (Closas et al., 2009), timing (Ray and Senior, 2003) and Integrated Precipitable Water Vapour (IPWV) (Tregoning et al., 1998). However, recent studies have shown that multipath can be used in the GNSS-Reflectometry (GNSS-R) technique to study soil moisture content around GNSS antennas (Larson et al., 2010; Mironov and Muzalecsjiy, 2012), snow depth estimation (Botteron et al., 2013), and estimation of height and moisture content of the vegetation around GNSS antennas (Wan et al., 2015). Application of GNSS-R is also important in characterising sites for geodetic applications, where accuracy is of high priority such as time transfer techniques using GNSS (Ray and Senior, 2003). In this chapter, I present an experimental study, which aims to map multipath around the new site for the timing antenna for the new LLR station.

Radio signals transmitted by the GNSS satellites are also affected by the ionosphere. The ionosphere is the upper layer of the atmosphere about 60 km from the Earth's surface and it contains free ions and electrons that are produced by the solar radiation (Ratcliffe, 1972). The ionosphere causes a delay of radio signals ionospheric effect can result in a delay of up to 30 ns (Giffard, 1999). However, the error introduced by the ionospheric effect can be minimised by using dual-frequency receivers and applying double differencing method (Pullen et al., 2009). The troposphere also introduces a delay of up to meters in the radio frequency. The delay introduced by water vapour in the troposphere increases with a decrease in elevation angle. This delay is usually corrected by applying tropospheric delay models such as the GPT2w developed by Böhm et al., (2015).

The Hartebeesthoek Radio Astronomy Observatory (HartRAO) is currently building the Lunar Laser Ranging (LLR) station. The LLR station requires an accurate timing system, which must be steered by Global Positioning System (GPS). The GPS satellites broadcast position and time information to the end-user. Satellites are constantly updated with accurate timing information from the ground-based network of Cesium and Hydrogen maser clocks (Allan, 1980), which is referred to as time transfer and GPS plays an integral part in this regard.

One application of geodesy that requires precise timing is station time. Station time is required in order to be accurate enough (within nanoseconds of UTC) to be able to track Earth-orbiting satellites or retro-reflectors located on the surface of the Moon with high accuracy.

The technique of LLR involves transmitting short laser pulses to the retro-reflectors that are located on the surface of the Moon. The round-trip ToF of the laser pulses is measured using an event timer. The event timer requires stable frequency (which can range from 5 to 100 MHz) from the local timing system (e.g. rubidium clock). The local timing system drifts over time and this requires accurate time from the GPS to be updated and monitored. The measurement data are used to support and maintain International Terrestrial Reference Frame (ITRF), determination of the Moon orbit, study geodynamics and Earth-Moon dynamics. HartRAO aims to achieve millimetre-ranging accuracy. This will require all subsystems (these include pointing model, timing, laser, transmit and receive path efficiencies, etc.) to be accurate, for the minimisation of station error budget to better than centimetre level. A detailed review of the LLR technique is given in Munghemezulu et al., (2016) and the references therein.

3.2. Material and methodology

3.2.1. Study area and data

HartRAO is located in valley of Magaliesberg mountain ranges, 50 km north-west of Johannesburg. HartRAO is collocated with four instruments that are fundamental for space geodetic techniques, namely: Very Long Baseline Interferometry (VLBI), Satellite Laser Ranging (SLR), Global Navigation Satellite System (GNSS) antenna and Doppler Orbitography and Radio-positioning Integrated by Satellite (DORIS). Currently, the observatory is building a Lunar Laser Ranging system and a new 15 m VLBI2010 Global Observing System (VGOS) antenna (Figure 19).

The site for the timing antenna was chosen according to the following considerations: (i) the site must be close to the control room to minimise signal delay due to cable length, as this reduces the systematic errors introduced by the cable and variations of the ambient air temperature, (ii) the site must have minimal objects that can introduce multipath such as trees and reflective objects such as the LLR enclosure and the 26 m VLBI antenna. However, since some of the objects cannot be removed, an observational strategy of observing above certain

elevation angle has to be established to minimise the effects of multipath. Figure 20 illustrates the visibility of the satellites at the HartRAO site; the centre point represents the location of the proposed site for the timing antenna.

An experiment was carried out using a Topcon antenna and a Topcon receiver, GB1000 models for the period of 10 days. Observations were scheduled for days when there was a clear sky as clouds often introduce random multipath errors (Rao et al., 2013). The raw observations files were converted from Topcon Positioning System (TPS) format to the Receiver Independent Exchange (RINEX) format as recommended by Gurtner (2007).

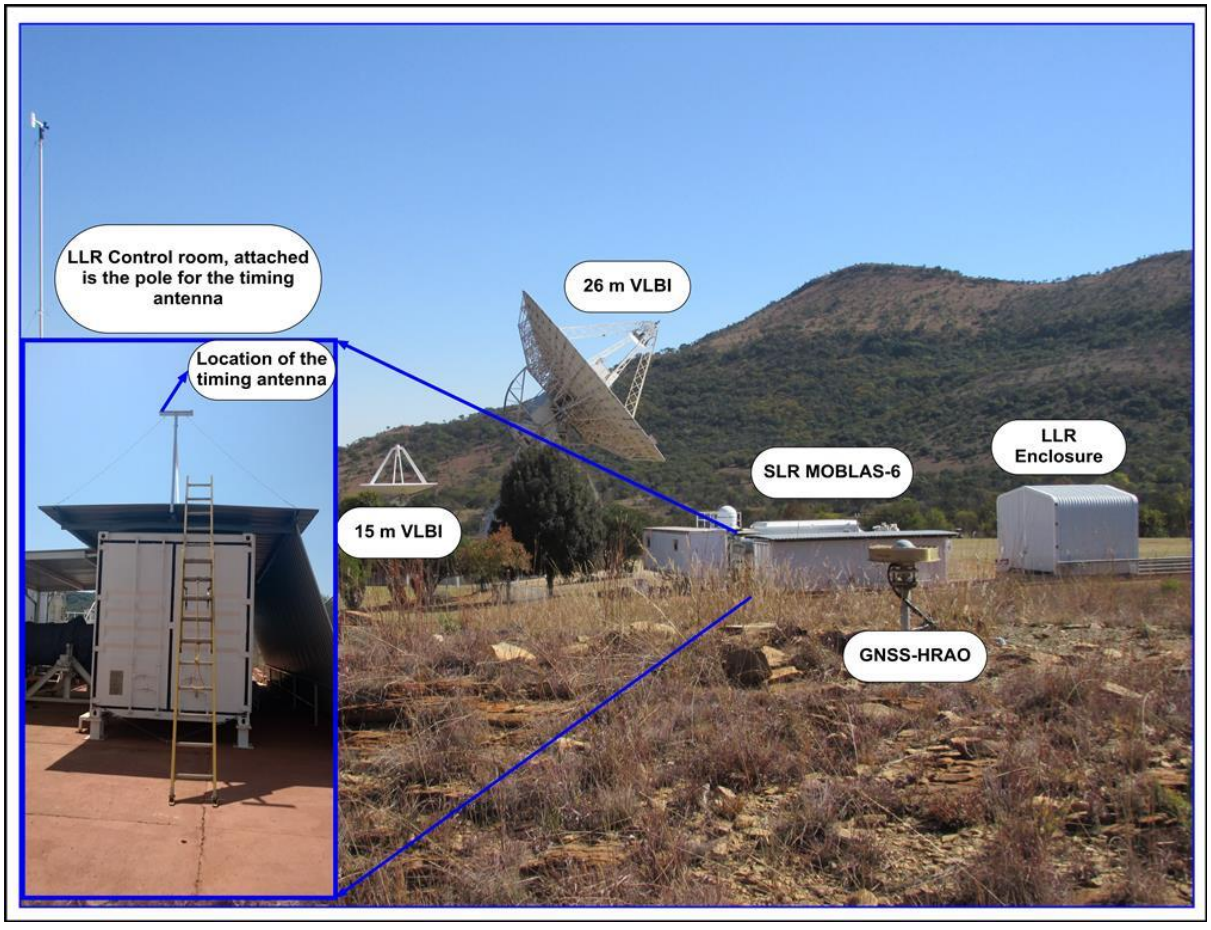

Figure 19. Space geodetic techniques collocated at HartRAO. The timing antenna will be mounted on top of the control room. The continuous operating GNSS station (HRAO) is important as it acts as a based/control station in solving positions of other points.

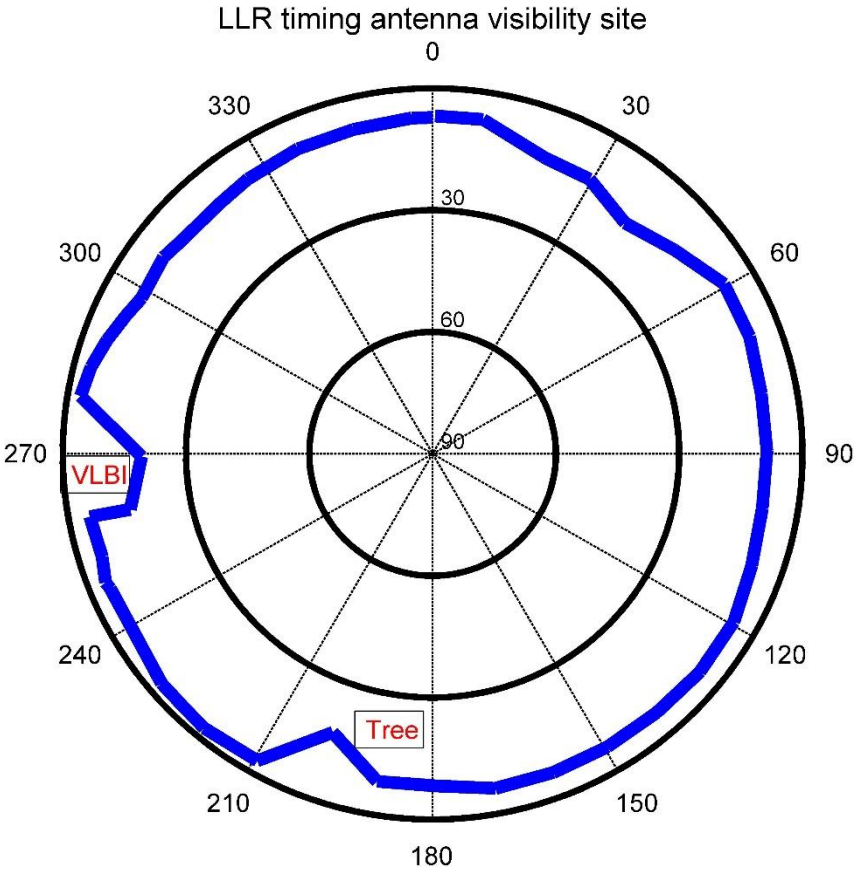

Figure 20. Horizon profile of the proposed timing antenna at HartRAO.

3.2.2. Methodology

A method for computing pseudo-range multipath errors (MP1 and MP2) was devised to assess the level of multipath in the vicinity of GNSS antenna by making use of the Translation Editing and Quality Check (TEQC) software (Estey and Meertens, 1999). Bilich and Larson (2007) indicated certain limitations associated with MP1 and MP2 derived from TEQC software to map multipath environment. One limitation is the use of RMS error values to represent multipath. In the current work, the RMS values that resulted are shown in Table 3. The RMS error values lack spatial component and as a result, multipath around the GPS station cannot be visualised. The second limitation involves MP1 and MP2 being a measure of pseudo-range precision and highly dependent on smoothing algorithms, firmware changes of the antenna or the receiver (Ray and Senior, 2003).

Table 3. Averaged Root Mean Square (RMS) calculated for all the satellites in view during specific days of the experiment. Each observation lasted for 24 hours.

Pseudo-range multipath error		
Day Number	**MP1 (m)**	**MP2 (m)**
254	0.295173	0.298755
255	0.298189	0.298982
256	0.298902	0.300827
257	0.301725	0.294977
258	0.299806	0.301071
259	0.31159	0.303643
260	0.300505	0.300962
261	0.300956	0.296886
262	0.290297	0.294945
263	0.290814	0.288795
264	0.292615	0.292331

Bilich and Larson (2007) introduced a method of extracting multipath from Signal to Noise Ratio (SNR) data that is reported in the standard RINEX file format, where SN1 and SN2 SNR data represents raw signal strength values as given by the receiver for the L1 and L2 phase observations. In the multipath environment, the SNR values measured by the tracking algorithm are a composite of direct and indirect signals. Equation (3.1) gives SNR (in an environment where only one indirect signal is introduced) as a function of multipath amplitude A_m, direct amplitude A_d and multipath relative phase ψ. Refer to Bilich and Larson (2007) for the derivation of Equation (3.1). However, this method works well when high data rates (1 s sampling interval) are available.

$$SNR^2 \equiv A_c^2 = A_d^2 + A_m^2 + 2A_d A_m \cos\psi. \tag{3.1}$$

TEQC software was used to derive MP1 and MP2 values. To further enhance multipath mapping by creating a gridded sky plot from the derived multipath values using linear

interpolation method and computing the wavelet power spectrum of the multipath time-series data to understand the magnitude in relation to the spatial location of the objects inducing multipath.

Multipath signals from GNSS are non-stationary signals since the frequency of the signals varies in space and time. This makes Wavelet Analysis (WA) suitable for studying multipath behaviour over time as compared to traditional Fourier Transform (FT) method. Morlet wavelet was used as given by

$$\psi_o(\eta) = \pi^{-1/4} \exp(i\omega_o \eta) \exp(-\eta^2 / 2). \tag{3.2}$$

Where η is the time and ω_o is the wavenumber (Torrence and Compo, 1998). To construct a picture depicting the amplitude of any feature with its variations over time and scale, a continuous wavelet transform (W_n) defined as the convolution of $x_{n'}$ (MP1 and MP2) time series with a scaled and translated version of ψ is used to derive the wavelet power spectrum, which is given in Equation (3.1),

$$W_n(s) = \sum_{n'=0}^{N-1} x_{n'} \psi * \left[\frac{(n'-n)\delta t}{s} \right]. \tag{3.3}$$

Where N is the length of the data at sampling time interval δt (30 seconds) and $(*)$ represents the complex conjugate (Torrence and Compo, 1998).

The standard deviation is calculated for each pixel of the linear interpolated multipath matrix as given by Equation (3.4),

$$\sigma = \sqrt{\frac{1}{n} \sum_{i=1}^{n} (x_i - \overline{x})^2}. \tag{3.4}$$

Where x_i is the linear interpolated MP1 or MP2 values and $\overline{x}$ is the mean value of MP1 or MP2. This data is projected to azimuth (φ) and elevation (θ) as a function of time i.e. $t \rightarrow \varphi(t), \theta(t)$. A higher value of σ will indicate areas that have high noise (e.g. trees, variation in moisture content) and low values indicate a uniform medium over time (e.g. clear sky or dry bare soil or less vegetated areas). However, it must be noted that this method is limited to the time span of the data since σ will change depending on the number of observations available. Therefore, multipath analysis using this method requires long time-series (e.g. more than a month) to capture all the seasonal variations due to changes in seasons, which will affect e.g. growth patterns of the trees and this will affect reflected patterns of the L1 and L2 signals.

3.3. Results and discussion

The GPS satellites provide many data points, but these points are only concentrated at specific satellite tracks and some parts of the sky are not fully covered (e.g. areas between $90°$ and $270°$ azimuths have a poor coverage in Figure 21). The gridded plots in Figure 21 (C, B and D) provide a complete picture of the distribution of multipath as well as signal-to-noise ratio (SNR) around GPS station. As illustrated in Figure 21, most multipath errors occur below $30°$ elevation angle and this is associated with low SNR ratio values. Radio signals from satellites at low elevation angles travel longer in the atmosphere (i.e. troposphere) than when the satellites are at high elevations (Degnan, 1993). Hence, the observations below $30°$ elevations are noisier compared to those at a higher elevation. The "spaghetti" features in MP1 and MP2 plots of Figure 21 at both low and high elevations indicate a variable atmosphere and these features could be attributed to clouds or cirrus clouds that vary in space and time. Infrared satellite cloud cover data indicated variable cloud cover during the time of the experiment. The data for the cloud cover can be retrieved from (http://www2.sat24.com/) for the given dates of the experiment.

The satellite number 17 was selected for the wavelet analysis since the satellite tracks at both low and high elevation angles. Figure 22 and Figure 23 illustrate wavelet power spectrum for MP1 and MP2 signals respectively. Two different clusters of peaks are evident at 0.001 and 0.005 frequencies for MP1 in Figure 22, which corresponds to 21 min and 4 min cycles, respectively. The MP1 signal has a strong cycle at 4 min compared to MP1 signal in Figure 23, which reveals a strong cycle at 21 min and a weaker cycle at 4 min. The two signals appear to respond differently when reflected by the same features and this is largely due to the fact that MP1 and MP2 are derived from different radio wavelengths where L1= 19 cm and L2= 24.4 cm, respectively.

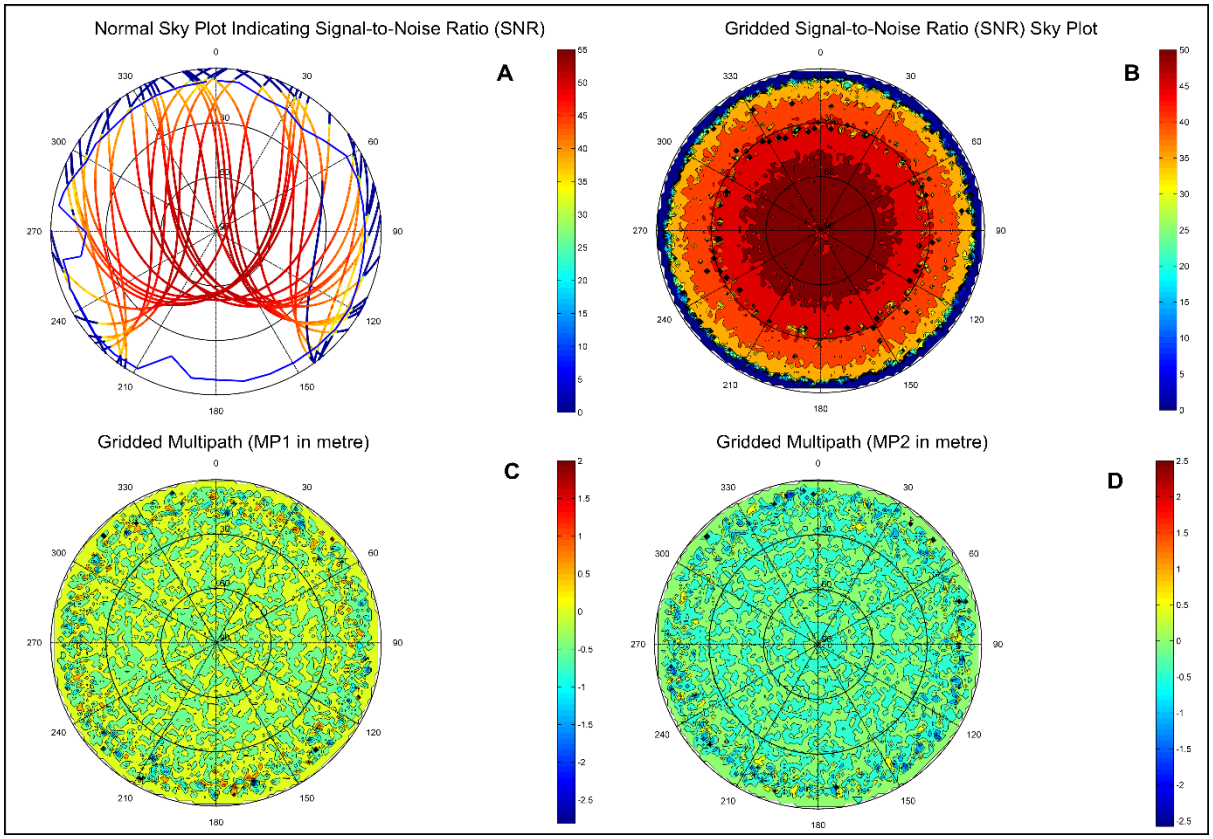

Figure 21. Enhanced visualisation of multipath and SNR data, the normal sky plot indicate satellite tracks across the sky while gridded plots indicate a complete picture distribution of multipath around GPS station.

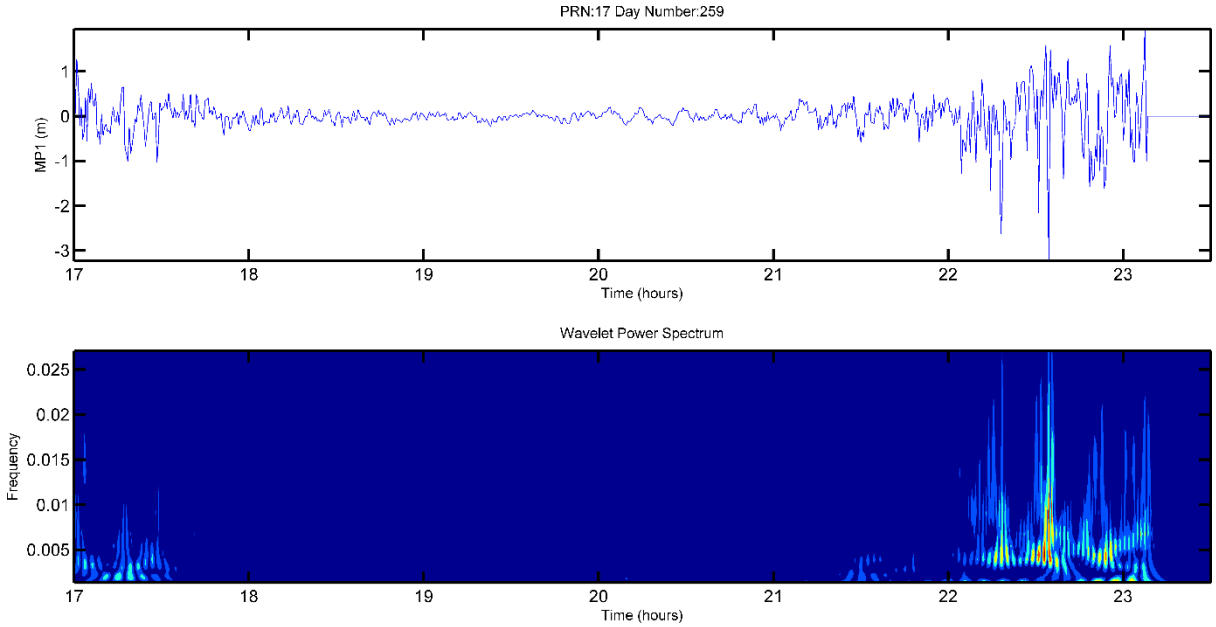

Figure 22. The multipath signal derived from the L1 band and its associated wavelet power spectrum.

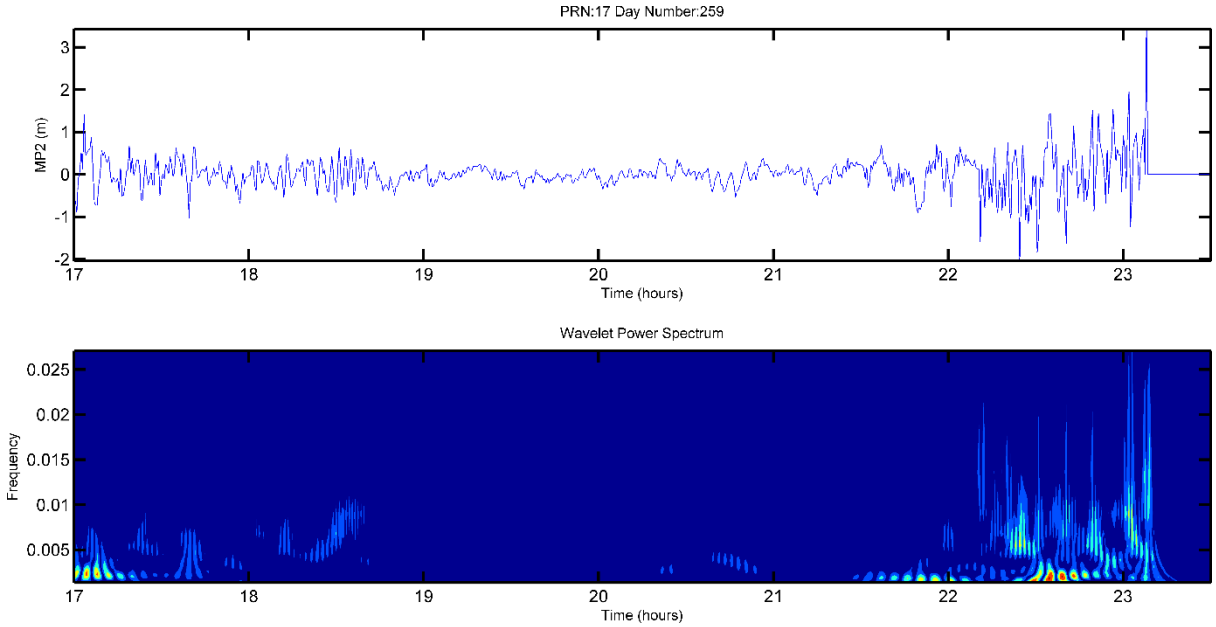

Figure 23. The multipath signal derived from the L2 band and its associated wavelet power spectrum.

The standard deviation maps in Figure 24 depict variations of the multipath over the 10 days observation period. Areas on the sky plot with low standard deviation indicate either stationary reflective objects like ground reflections at low elevation angles ($<30°$) or atmosphere, which is expected to have very little variations at high elevation angles ($>30°$). Areas with high standard deviation will only occur at lower elevation angles, objects such as shrubs/trees will introduce multipath with different magnitudes resulting in high standard deviation values on the map. Both MP1 and MP2 maps indicate areas of high standard deviations and low standard deviations, low standard deviation areas are therefore attributed to reflections due to bare soil and less vegetated areas and those of high standard deviation are attributed to reflection due to shrubs as they can be seen from the image mosaic of $360°$ view of the area.

There is very little that can be done in terms of physically removing shrubs to minimise multipath. Most applications such as positioning depend on receivers that can filter GPS noise "multipath" at low elevations such as adaptive filters (Yedukondalu et al., 2011). However, this approach is limited to visualisation and the spatial distribution of the source of the multipath. In other applications such as GNSS-Reflectometry, visualisation of multipath is important to understand the source of signals that might be related to e.g., vegetation monitoring using GPS (Chew et al., 2015). In the case of positioning applications where time

accuracy received from the GPS antenna depends on the position stability of the antenna, an observational strategy will be employed i.e., observing only satellites above 15°-20° elevation angles to minimise multipath.

More improvements still need to be made in this approach of mapping multipath to allow for mapping the distance of reflecting features on the sky-plot. The current approach does not provide exact distances from the GPS station to the reflection points on the ground. This is important in preliminary site survey using GPS as objects that can result in significant multipath can be mapped and removed before full installation of the GPS for different purposes.

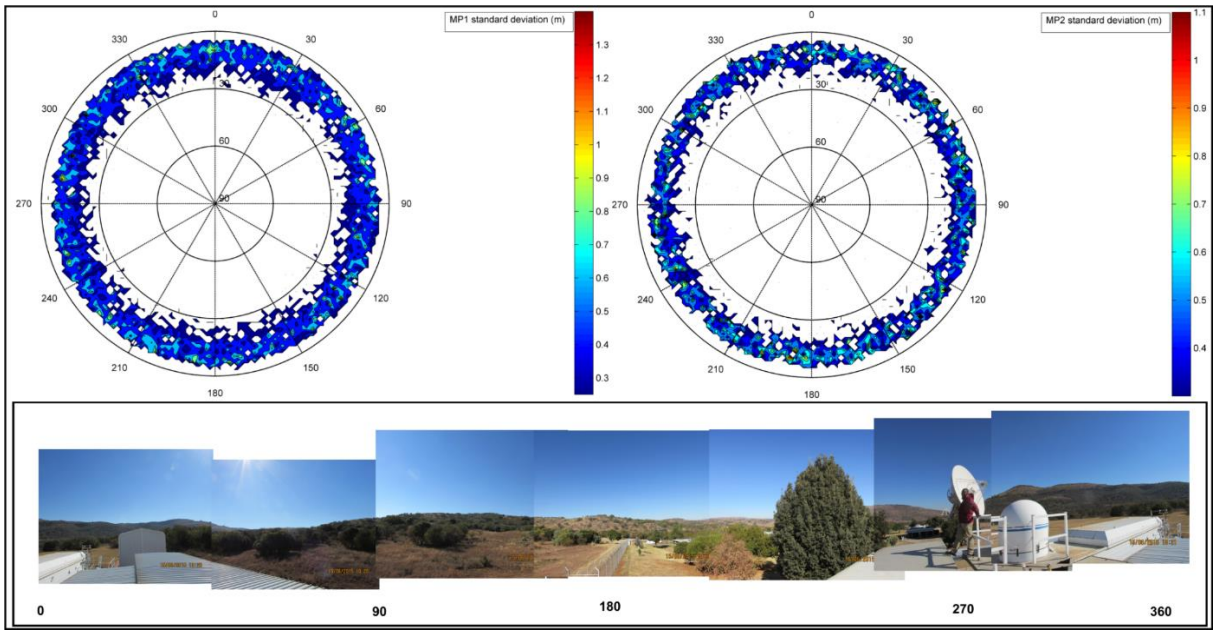

Figure 24. Standard deviation maps of MP1 and MP2 as viewed from the GPS timing antenna derived from 10 days of observations. The mosaics of pictures depict the actual site in 360° view.

3.4. Concluding remarks

Mapping multipath from GNSS signals is a difficult task given the many variables that change over a short and long period of time. These variables include moisture content of the soil or vegetation, canopy structure and clouds. The technique of multipath mapping can be very useful in preliminary site investigation for geodetic applications such as the installation of the new GNSS base station for timing or positional applications. RINEX observations for 10 days to map spatial location of multipath and its variation over time to aid in understanding the distribution of multipath before an installation for the timing antenna at HartRAO for LLR timing reference.

High-resolution time-frequency wavelet analysis demonstrates that the MP1 and MP2 signals peak at different frequencies with different intensities when reflected by the same feature. This analysis allows for extraction of information such as what time will the GNSS station receives maximum multipath and for how long and an observational strategy can be implemented. Through standard deviation maps, I conclude that the multipath on the site is mainly due to reflections from the mountains surrounding the geodetic site and that the site offers clear sky view of the satellites with minimal multipath from as from $30°$ and above in elevation. The high standard deviation is attributed to reflections due to shrubs, vegetation and bare soil around the site. An observational strategy at 15° to 20° will be implemented as these areas offer minimal multipath and a good environment for the timing antenna to operate at maximum efficiency

.

Chapter 4

Integration of the lunar laser ranging timing subsystem

Abstract

The Hartebeesthoek Radio Astronomy Observatory (HartRAO) in South Africa is developing an observational system capable of ranging picosecond laser pulses to the retro-reflectors located on the Moon, a technique called Lunar Laser Ranger (LLR). The new LLR station in the Southern Hemisphere to be installed at Matjiesfontein in the Karoo will contribute towards a better understanding of the dynamics of the Earth-Moon system. One of the most fundamental applications of the LLR system is to determine the Earth-Moon orbit parameters at high accuracy levels. As the observable of the LLR technique is the ToF of the laser photons to and from the Moon, a picosecond level (1 picosecond = 10^{-12} second) accuracy timing system is one of the key design considerations required for the new LLR system. Here I present results of an integrated design of the timing subsystem for the HartRAO LLR station. All subsystems that directly affect the timing system performance are described, including operational and environmental conditions. Based on the specifications of the equipment under consideration, results indicate that the timing subsystem will achieve a sub-picosecond Allan deviation at 1 s, a phase noise of -110 dBc at 1 Hz, and a drift rate of 5×10^{-11} per month (on free run). Furthermore, the cumulative RMS noise from the proposed system is estimated to be 43 mm per pulse. This noise level will require the station to range to the Moon for a longer period (at a rate of 5 photons per minute) in order to collect adequate photons to statistically achieve millimetre precision for normal point calculation. The current design specifications present a promising future for millimetre ranging at HartRAO.

4.1. Introduction

The Hartebeesthoek Radio Astronomy Observatory (HartRAO) in South Africa is currently developing a Lunar Laser Ranger (LLR) to range to retro-reflectors that are located on the Moon (Figure 25). This observatory is the only geodetic and radio astronomical site in Africa and has collocated all fundamental space geodetic techniques, including geophysical equipment such as a seismometer, gravimeter and accelerometer. In particular, the site hosts several Global Navigation Satellite Systems (GNSS) receivers, a NASA Satellite Laser Ranging (SLR) system (MOBLAS-6), two Very Long Baseline Interferometry (VLBI) telescopes (of sizes 26 m and 15 m) and a Doppler Orbitography and Radiopositioning Integrated by Satellite (DORIS) system. These techniques contribute towards the determination of geophysical parameters such as Earth Orientation Parameters (EOP), station positions and velocities, definition and maintenance of the International Terrestrial Reference Frame (ITRF) and the International Celestial Reference Frame (ICRF) (Plag et al., 2009). Overall, these parameters contribute towards improving geodetic parameters of the Earth-Moon system.

Space geodetic techniques require very accurate timing systems in order to make accurate measurements during observations. Timing components are an integral part of geodetic instruments as the stability of the timing systems determines the accuracy at which measurements can be made (Poultney, 1972). For instance, an accurate and stable clock such as a hydrogen maser, Cesium, rubidium or Oven-Controlled Crystal Oscillator (OCXO) is often used as a timing reference system depending on the application requirement and the budget of the experiment.

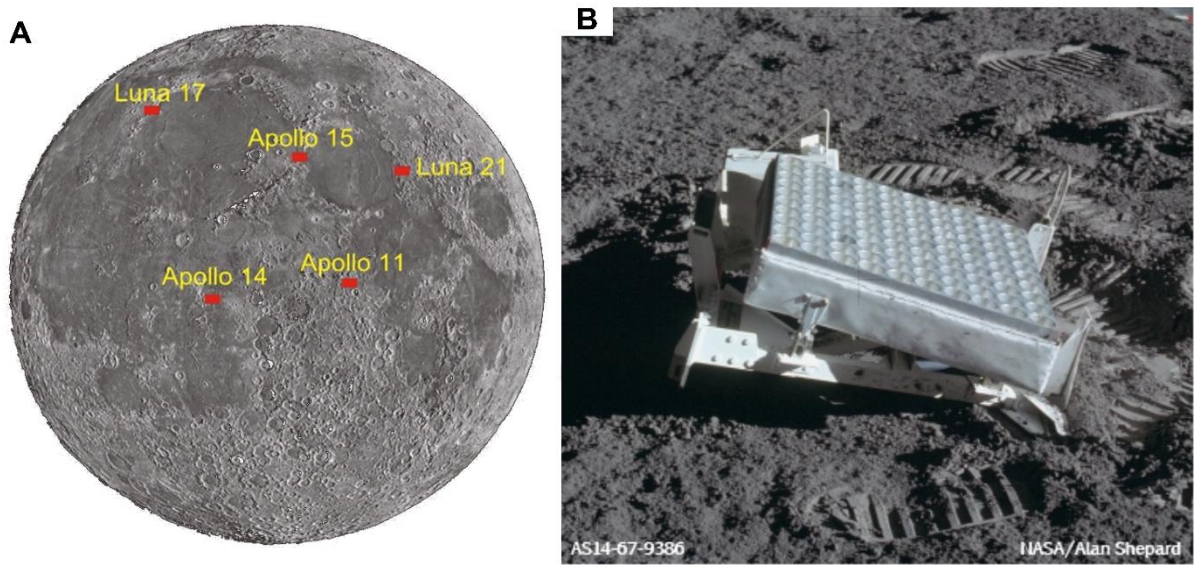

Figure 25. A: Location of the retro-reflectors on the Moon deployed by the APOLLO and the Soviet missions. B: An array of retro-reflectors from Apollo 14 on the Moon (Source: NASA).

These clocks are characterised by good short and long-term stabilities, drift rates over time as well as phase noise (Niell et al., 2007). In terms of the LLR, it is essential to consider these parameters for sub-centimetre ranging accuracy.

The new LLR system being constructed at HartRAO has to meet minimum requirements set by the International Laser Ranging Service and the Global Geodetic Observing System (GGOS). Part of the LLR requirements are that space geodetic techniques should make observations with millimetre accuracy and precision. This is a very stringent requirement that is yet to be attained in practice (Rothacher et al., 2009). In this regard, the main objective of the HartRAO LLR system is to have sub-centimetre level accuracy in measurements and normal point (i.e., the statistical average of a set of ranges) range data. These stringent requirements necessitate that all other subsystems being developed at HartRAO function in harmony, such as the pointing model for the telescope, compensation of structural deformation due to thermal effects, etc., to achieve these requirements (Combrinck and Botha, 2014). The emphasis of this chapter is placed on the design of a timing reference subsystem and a photon detection subsystem for the new LLR station based at HartRAO.

4.2. A brief history on time and frequency standards

The development of time keeping technologies have enabled and advanced most of our day-to-day living experiences. For example, in positioning applications, timing accuracy of 10 ns yields a corresponding position accuracy of about 3 m (Hellwig, 2003). However, by combining modern algorithms to mitigate delays due to atmosphere, a millimetre positioning accuracy can be attained. Table 4 lists the time and frequency standards, their evolution and accuracies. A laser cooled Cesium fountain currently provide the most accurate timing systems (Meekhof et al., 2001). However, these are very expensive for general public to use and most satellite/lunar laser ranging stations are still using ultra-stable Quartz and Rubidium oscillators with an accuracy of about 1×10^{-12} or better.

Rubidium oscillators are usually better than quartz, Oven-Controlled Crystal Oscillator (OCXO) or Temperature-Compensated Crystal Oscillator (TCXO) due to their long-term stability and reliability. The OCXO and TCXO are adversely affected by environmental changes (i.e. temperature, pressure, humidity and vibrations). Their aging characteristics can be in the order of about less than 5×10^{-9} per day (Lombardi, 2005). Lombardi, (2005) described the operations of Rubidium frequency standard as follows (Figure 26): they operate at 6,834,682,608 Hz, which is the frequency resonance of Rubidium atom (^{87}Rb); a quartz oscillator is controlled by the frequency of the Rubidium; a crystal oscillator generates a microwave signal that is applied to the ^{87}Rb vapour within a cell; this process forces the atoms into a particular energy state. An optical beam is then pumped into the cell and is absorbed by the atoms as it forces them into a separate energy states (Nez et al., 1993). According to Berquist and Collins, (2004), this process produces two isotopes, which results in two resonances and a filter cell is used to filter out one resonance.

The photocell detector is used to measure how much of the beam is absorbed and its output is used to tune a quartz oscillator. This oscillator is then locked to the Rubidium resonance frequency and standard frequencies (usually 5 MHz and 10 MHz) as well as 1 pps are derived from the quartz oscillator and provided as output signals (Lombardi, 2005). The Rubidium frequency standards are affected by environmental changes. For instance, different components operate optimally at different temperatures (e.g. gas cell and quartz oscillator). Recent developments to minimise these effects include voltage controlled crystal oscillator (VCXO), which provides temperature compensated signal output and microcontroller. This

uses the temperature signal to look-up a frequency error in a memory to offset the synthesizer and adjust the VCXO to compensate for temperature (Nez et al., 1993).

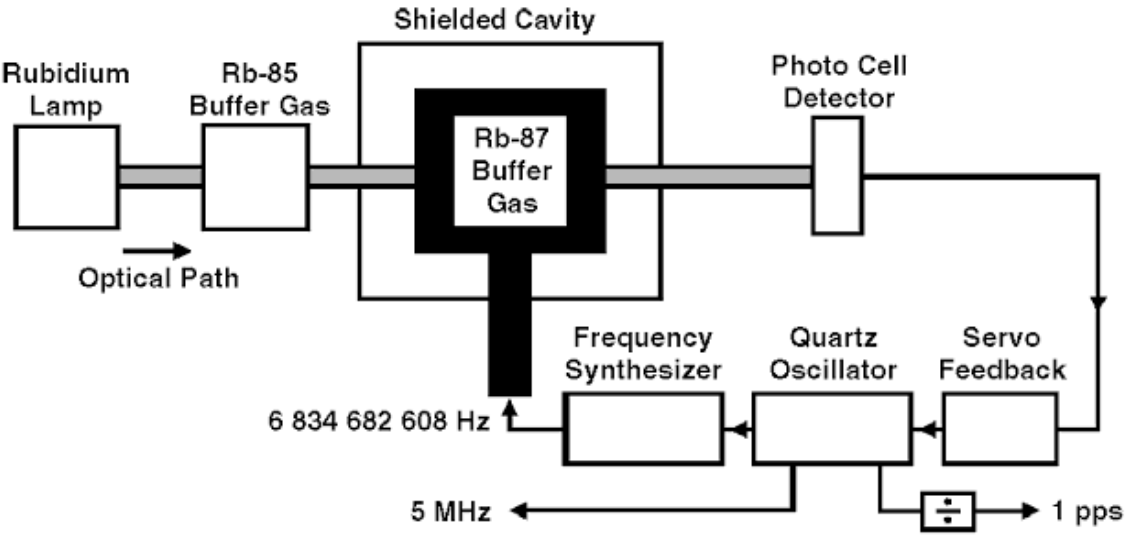

Figure 26. An example of a rubidium oscillator (Source: Lambardi, 2005).

Time transfer techniques play a crucial role in geodetic applications such as Very Long Baseline Interferometry (VLBI) and SLR/LLR to ensure accurate time is kept at a local station and corrections are applied that may results from clock drift or clock wonder. There are different methods that are used to distribute time and frequency signals such as using the optical fibre over short distances. This method can reach stability of up to 10 ps (e.g. Jefferts et al., 1997), two way satellite time and frequency transfer (TWSTFT) using laser (e.g. Kunimori et al., 1993; Prochazka et al., 2010) or GNSS (e.g. Lewandowski et al., 1993.

Table 4. The evolution of time and frequency standards (Source: Lombardi, 2005).

Standard	**Resonator**	**Date of Origin**	**Timing Uncertainty (24h)**	**Frequency Uncertainty (24 h)**
Sundail	Apparent motion of the Sun	3500 BC	NA	NA
Verge escapement	Verge and foliet mechanism	14th century	15 min	1×10^{-2}
Pendulum	Pendulum	1656	10 s	1×10^{-4}
Harrison Chronometer (H4)	Spring and Balance wheel	1979	350 ns	4×10^{-6}
Short pendulum	Two pendulums, slave and master	1921	10 ms	1×10^{-7}
Quartz crystal	Quartz crystal	1927	10 μs	1×10^{-10}
Rubidium gas cell	^{87}Rb resonance (6,834,682,608 Hz)	1958	100 ns	1×10^{-12}
Cesium beam	^{133}Cs resonance (9,192,631,770 Hz)	1952	1 ns	1×10^{-14}
Hydrogen maser	Hydrogen resonance (1,420,405,752 Hz)	1960	1 ns	1×10^{-14}
Cesium fountain	^{133}Cs resonance (9,192,631,770 Hz)	1991	100 ps	1×10^{-15}

Table 5. Summary of time and frequency transfer signal and methods (Source: Lombardi, 2005).

Signal or Link	Receiving Equipment	Time Uncertainty (24 h)	Frequency Uncertainty (24 h)
Dial-Up Computer Time Service	Computer, client software, modem and phone line	<15 ms	Not recommended for frequency measurement
Internet Time Service	Computer, client software, modem and phone line	< 1s	Not recommended for frequency measurement
HF Radio (3 to 30 MHz)	HF receiver and antenna	1 to 20 ms	10^{-6} to 10^{-9}
LF Radio (30 to 300 KHz)	LF receiver and antenna	1 to 100 us	10^{-10} to 10^{-12}
Global Navigation Satellite Systems (GNSS)	GNSS receiver antenna	<20 ns	$<2\times10^{-13}$

4.3. Lunar Laser Ranging at HartRAO

The LLR technique was developed during the 1960's when the Apollo and the Soviet missions deployed retro-reflectors on the surface of the Moon. The McDonald Observatory was the first observatory to detect photons reflected by the Apollo 11 reflector using a 2.7 m telescope (Williams et al., 1996). Lunar laser ranging involves sending short laser pulses to the Moon; the pulses are reflected by retro-reflectors back to the receiving telescope on the ground. The ToF is then measured using an event timer or interval counter. Therefore, given the speed of light plus a number of corrections (e.g., relativistic effects, atmospheric effects and solid Earth tides displacing the station position), the distance to-and-from the Moon can be calculated. Among other factors (atmospheric effects, lunar librations, etc.) that affect the accuracy of the measurements, timing systems have a significant contribution as well. The resulting distance from the lunar measurements contains a wealth of information about the Earth-Moon system (Dickey et al., 1994). The current International Laser Ranging Service (ILRS) network geometry (see for Figure 5, Chapter 2) is poor in the Southern Hemisphere relative to the Northern Hemisphere. It has been reported that there are only four LLR stations that are regularly ranging to the Moon (Hofmann et al., 2010).

These stations are:

- The Apache Point Observatory Lunar Laser-ranging Operation (APOLLO 3.5 m telescope), New Mexico, USA, date installed 2000's.
- McDonald Laser Ranging Station (MLRS 0.75 m telescope), Texas, USA, date installed 1980's.
- The Observatoire de la Côte d' Azur (OCA 1.54 m Cassegrain telescope), France, date installed 1980's.
- Matera (1.5 m telescope), Italy. Some data have recently been obtained by the Matera Laser Ranging Observatory (Italy) and it is hoped that this station will become a regular contributor (Hofmann et al., 2010), date installed 2000's.

A number of planned LLR stations will support the network geometry in the future, i.e. future LLR activity from the Geodetic Observatory Wettzell (Germany) and the Mount Stromlo Satellite Laser Ranging Observatory (Australia). In particular, the HartRAO LLR station in the Southern Hemisphere will potentially improve and strengthen the current network and contribute to global LLR ranging observations.

The geographical location of the proposed HartRAO station in the Southern Hemisphere provides an opportunity to perform interesting scientific experiments with other stations, particularly ranging simultaneously with the OCA station to the Moon or satellites. Such experiments are expected to constrain station dependent biases, improve the determination of the orbit parameters and the ranging geometry (Combrinck, 2011a). Other scientific contributions include tests of the General Relativity Theory (GRT) (Alley, 1983; Combrinck, 2013) and contributions to the ITRF (Altamimi et al., 2011). Research on GRT has already started at HartRAO to estimate Parameterized Post-Newtonian (PPN) parameters γ and β directly as part of the least-squares solution of precise orbital determination from LAGEOS I and II SLR data (Combrinck, 2011b). The current test for gravitational constant variation is at the level $\dot{G}/G = -0.7 \pm 4 \times 10^{-13}$ yr^{-1} (Williams and Folkner, 2009; Hoffmann et al., 2010). To understand small variations of the physical and geophysical parameters, millimetre level measurements of the Moon's orbit are required.

The development of an LLR station at HartRAO is based on an ex-OCA 1 m aperture telescope obtained through collaboration with OCA and NASA (Combrinck, 2011a; Figure 27). The telescope was used for SLR applications at OCA and the laser beam was transmitted through a beam expander (~18 cm in diameter). At HartRAO, the telescope-ranging configuration is currently being modified such that the laser pulses will be transmitted through the main 1 m aperture to ensure maximum collimation of the laser beam.

Software packages developed internally for the telescope include LLRSteer, LLRServo Control and LLR Central Control, which will control and steer the telescope as well as control other subsystems. These programs share data via the Dynamic Data Exchange (DDE) protocol. Subsets of the C language are used to develop programs, which are loaded into microprocessors; these communicate via USB interfaces with the main programs. The alt-az mount and optical tube have already been disassembled to evaluate the condition of the components; all seals have been replaced and all painted surfaces cleaned and recoated (Combrinck, 2013). It is envisaged that the telescope will be moved to Matjiesfontien, Great Karoo, where the seeing conditions were observed to be ranging from 1 to 2 arc seconds by using a small astronomical refractor (10.8 cm aperture). This site is better than the current site (HartRAO) and higher return rate of photons can be expected (Combrinck et al., 2007).

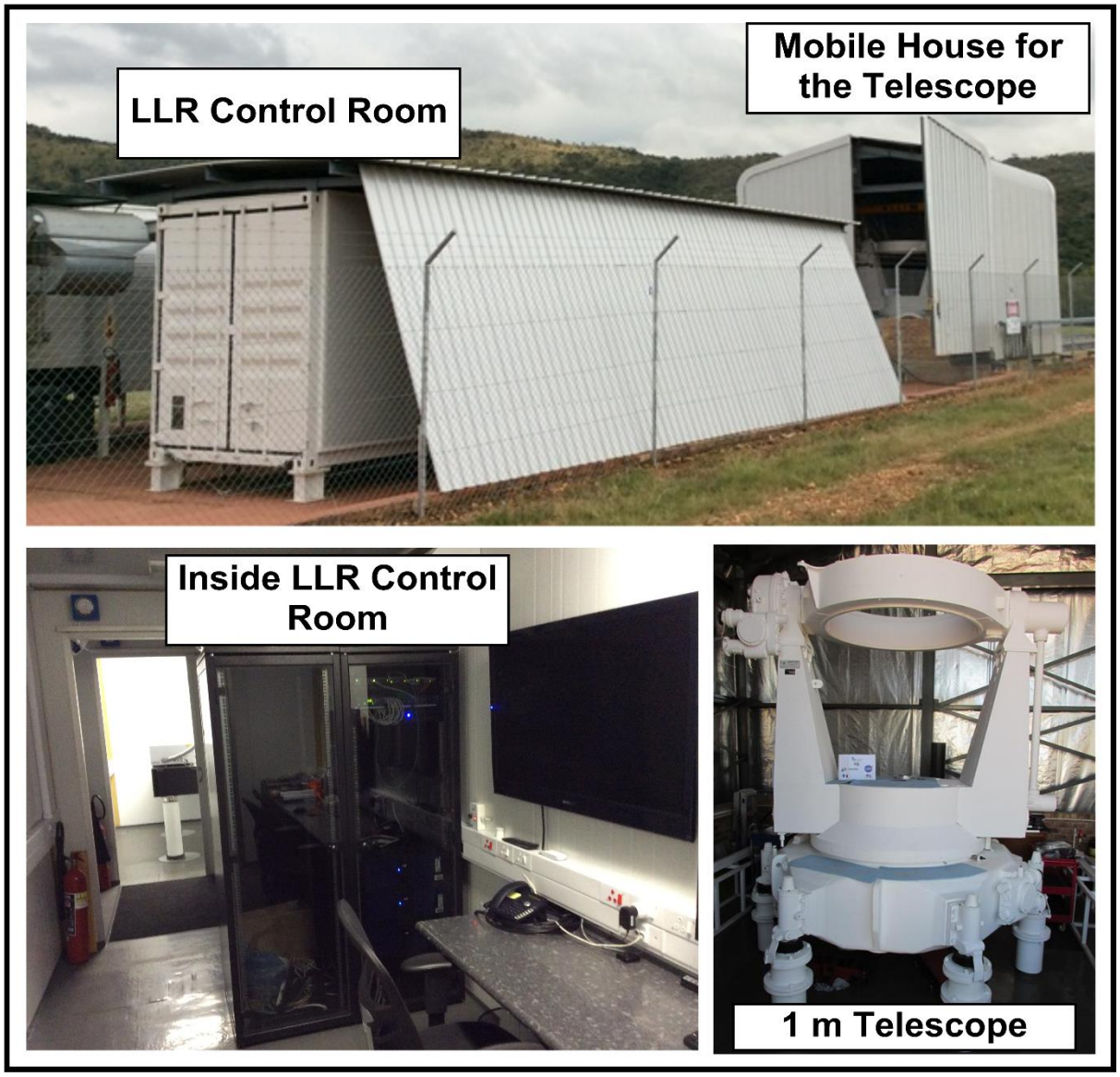

Figure 27. Subsystems of the Lunar Laser Ranger. The timing reference subsystem will be hosted inside the LLR control room and the measurement timing subsystems will be located at the telescope. The control room is kept at $20 \pm 3°C$.

4.4. Environmental factors affecting time and frequency transfer

Time transfer applications requires advanced algorithms to compute path delay (between the transmitter and the receiver). This is mainly because each specific delay applied to the receiver is site dependent. In the case of GNSS time transfer, ground based network of hydrogen masers and Cesium clocks are all steered to agree as closely as possible to the Coordinated Universal Time (UTC) (Lombardi, 2005). This time is used to steer on board GNSS satellite clocks, which is broadcasted together with positional information of the satellites to the receivers on

the ground. During this process, variable atmosphere introduces delay to the transmitted radio signals. For example, delay due to refraction at zenith can reach up to 6 ns and this value is worse at lower elevation angles (Levine, 2008). The ionosphere, troposphere and temperature variation are among the factors that limit the accuracy of time transfer in the radio frequency, these effects are discussed below.

4.4.1. Ionosphere

The Total Electron Content (TEC) can be defined as the amount of free electrons available along the path of the radio signal in the ionosphere, I TEC unit = 10^6 electrons/m^2 (Buonsanto, 1999; Moeketsi, 2007). An increase or decrease in TEC is directly proportional to the Sun's activity i.e., during day light or geomagnetic storms, TEC will increase in the ionosphere and decrease during night period (Olawepo et al., 2015). For more information on basic principles and computation of TEC from GNSS data refer to Hamzah, (2015) and Buonsanto, (1999).

To demonstrate the impact of TEC on GNSS timing applications, TEC was derived for GNSS station HRAO using GPS-TEC software developed at Boston College by Gopi, (2012) and it was converted to time delay (Figure 28). The results in Figure 28 clearly indicate variations in time delay ranging from 1.2 ns to 11 ns for this particular day of observation, with more variability during day time. A timing receiver for 4380A will need to be able to track TEC variations in real time and apply appropriate correction to minimise errors when updating the Rubidium clock. Therefore, it is important that observed TEC is used to correct for time delay due to ionospheric activities. Receiver and satellite biases play a crucial role in the accuracy of determining TEC.

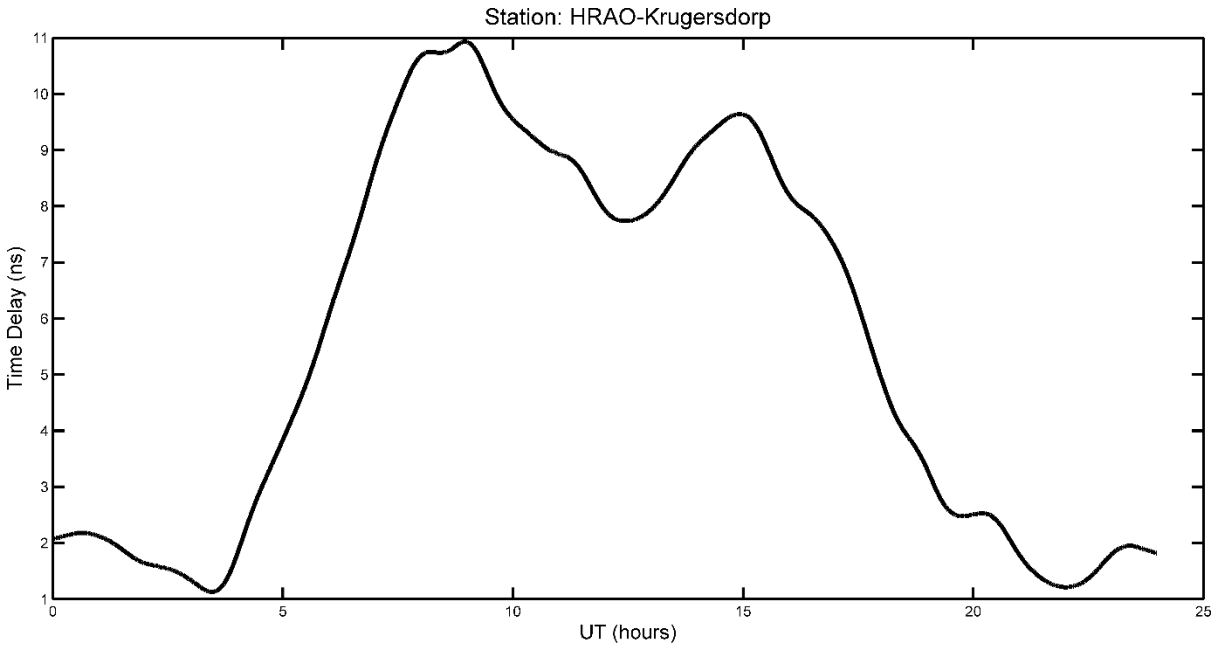

Figure 28. Estimated time delay due to TEC over HartRAO from the GNSS station HRAO, date: 2016/09/26.

4.4.2. Troposphere

The estimation of tropospheric parameters and observed parameters can lead to about 300 ps difference in clock solution in GNSS (Hackman and Levine, 2004). Weinbach and Schön (2010) reported that mapping functions such as Nell Mapping Function (NWM), Global Mapping function (GMF) and Vienna Mapping Functions (VMF1) fail to reduce noise level of the clock estimates, this was attributed to the low temporal and spatial resolution of the mapping functions. Clock estimates are directly related to the tropospheric parameters and this is site dependent.

The tropospheric slant delay as a function of elevation angle of the satellite can be modelled as the sum of a zenith hydrostatic delay (ZHD) and azenith wet delay (ZWD) components, with corresponding mapping functions (Weinbach and Schön, 2010). Meteorological observations at the GNSS site (pressure, humidity and temperature) can be used to estimate accurately ZHD component, however, the ZWD component cannot be accurately estimated from ground meteorological observations (e.g. Ohtani and Naito, 2000) to resolve small errors in GNSS clock solutions. A Raman Lidar sensing or Water Vapour Radiometer (WVR) is recommended to accurately estimate ZWD component. However, these instruments

are very expensive (Weinbach and Schön, 2010) and most software packages estimate ZWD component from least squares while solving for other parameters. Niell et al., (2010) found that ZWD estimated from VLBI technique gave better results compared to GNSS, Radiosonde and WVR techniques, this is mainly due to VLBI measurements are independent of minimum elevation angle. Figure 29 depicts Integrated Precipitable Water Vapor (IPWV) derived from GNSS station HRAO using locally observed meteorological parameters at the GNSS station. The observations indicate variable IPWV in the atmosphere that is characterized by the annual and inter-annual seasonal variations. Mashaba et al., (2016) proposed an automated computation of IPWV at HartRAO, this can be very useful during LLR observations as incorporating IPWV as suggested by Hackman and Levine (2004) can improve clock solution. Advanced dedicated PWV instrument such as WVR is required at the observatory to achieve better accuracies.

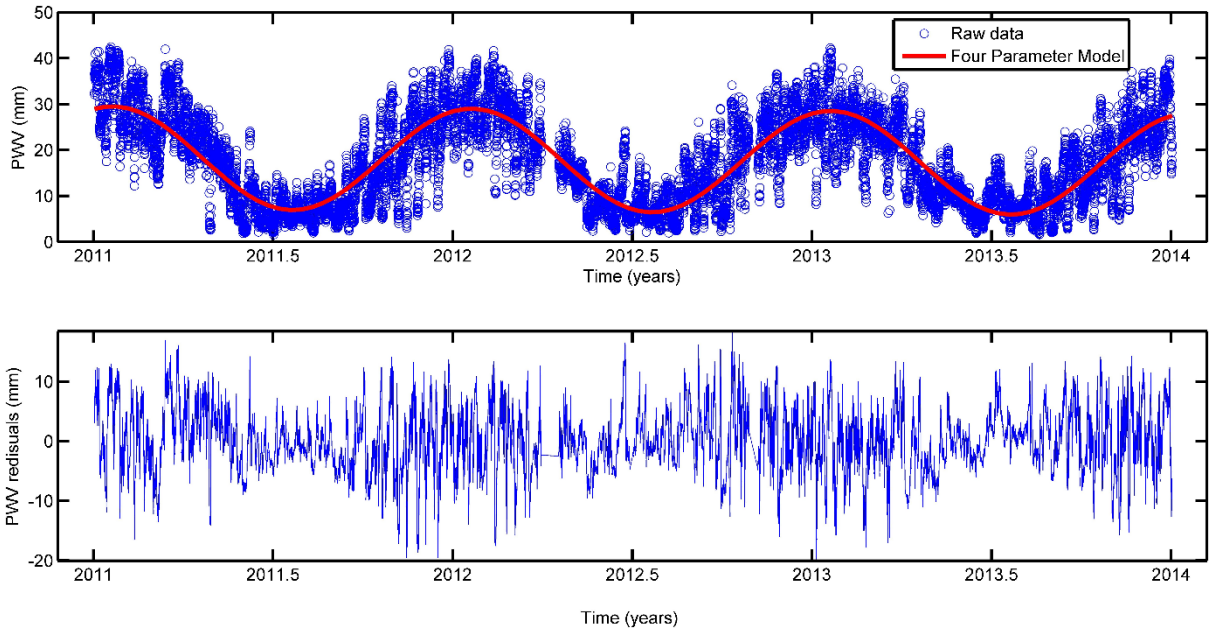

Figure 29. Time series of the IPWV derived from HRAO GNSS station (Source: Mashaba et al., 2016).

4.4.3. On site ambient air temperature

The telescope structure and electronic systems are very sensitive to changes in atmospheric parameters i.e., temperature, pressure and humidity. Temperature being the largest contributing

factor (Perry, 1943). Small degrees of variations in these atmospheric parameters can influence the pointing accuracy of the telescope or affect the stability of electronic systems.

Historical atmospheric data at the HartRAO site were considered to develop a better understanding of the conditions at which the various time and frequency systems will operate. Local atmospheric parameters are monitored using several meteorological units (MET3/4a) with a time resolution of 1 minute; data are publicly available from the SOPAC site: http://garner.ucsd.edu/pub. However, a more accurate MET4 unit will be used for the LLR station. Figure 30 depicts temperature and humidity variability at HartRAO for selected days, during summer in January and during the winter period in June. The data clearly indicates segments of linear trends, which can be considered separately to determine the rate at which temperature changes for a given linear segment using a linear fit model. Table 6 summarises the results of temperature stability for the selected time segments. As given in Table 6, the best ranging period would be described by the change in temperature per minute for the given period, if the values are between $-1°C$/min and $1°C$/min. This threshold indicates the time period in which the atmosphere is most stable and best performance of the electronic systems and the telescope can be achieved.

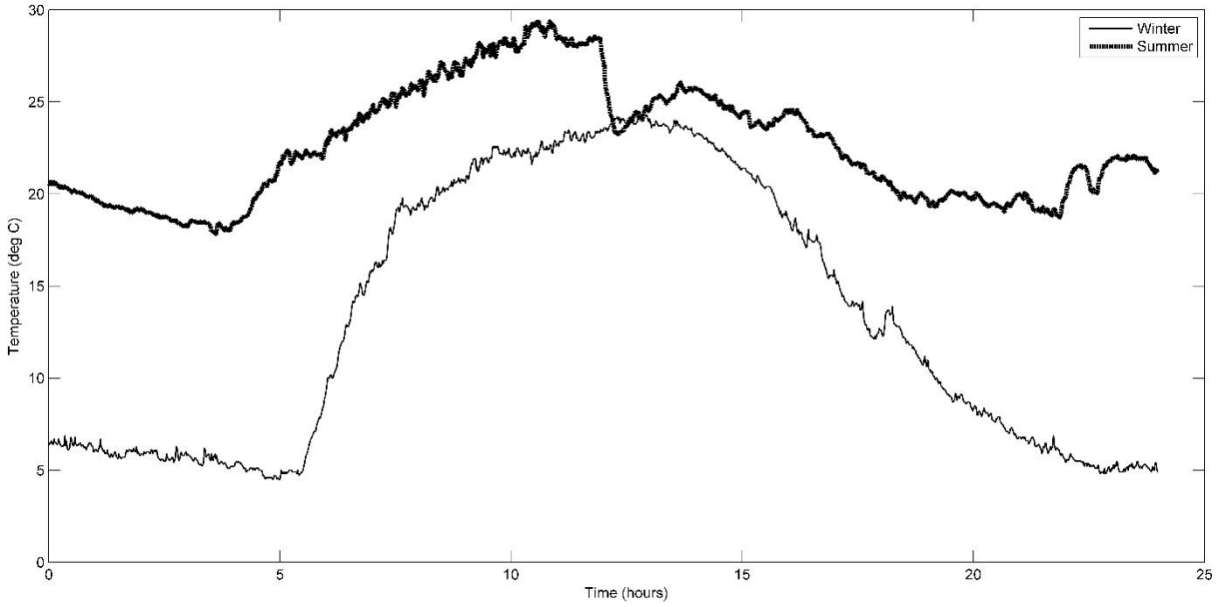

Figure 30. Variability of temperature at HartRAO for two different periods, during summer (2014/01/15) and winter (2014/06/15).

Table 6. Statistical results of the temperature stability at HartRAO for selected days.

Hours	Rates: °C/min	R^2 for linear fit
	2014-01-15 Summer	
0-4.2	-0.5929	0.9141
4.2-11.9	1.2452	0.9297
11.9-13.67	1.5398	0.842
13.67-23.9	-0.5009	0.5265
	2014-06-15 Winter	
0 -5.5	-0.3271	0.8504
5.5-7.8	6.2346	0.9773
7.8-13.78	0.7801	0.8717
13.78-23.9	-2.0465	0.955

The LLR station at HartRAO is located close to MOBLAS-6 SLR station from NASA, the SLR station was inaugurated on the 20th of November 2000 and it has been operating since then. The existence of this station provides an opportunity to study its performance in relation to environmental factors such as ambient temperature. This will provide valuable information during the construction phase of the LLR station and set out realistic expectations in term of its performance.

Prior to ranging to satellite/retro-reflectors on the surface of the Moon, the station must carry out pre-calibration i.e., the station must first range to a target with a well-known distance that is established through ground survey methods (e.g. http://itrf.ensg.ign.fr/local_surveys.php). After ranging to the satellite, the station must carry out post-calibration by ranging to the same calibration target (see Figure 31). The difference between pre and post calibration gives a range error/bias. This range error indicates a combination of factors that affect internal system delay over time, this include ambient air temperature, instabilities of mechanical system that drives the telescope and the frequency at which star calibrations are carried out at the station, the more often the star calibrations are carried out, the more accurate the telescope will be in pointing, etc. In particular, the ambient air temperature can easily affect the internal system delay. An increase/decrease in ambient temperature can affect thermal stability of the telescope structure and the mirrors, hence changing the internal system delay. Tsela et al., (2015) and Tsela et al., (2016) used ANSYS software to simulate the behaviour of the telescope structure when subjected to thermal load and they found that the telescope indicated structural deformation varying from 2.9 μm to 40.7 μm for ambient air temperature between 9℃ and 23℃. The 1-m telescope for the LLR station

was studied by Nkosi et al., (2016), based on their simulated results they reported that the mirror experiences deformations due to gravity at different positions up to 10 nm. All these factors contribute to range and time bias.

Figure 31. Google map depicting top view of HartRAO observatory.

Data from MOBLAS-6 SLR station was used to investigate the contribution of ambient air temperature to the range bias and the system delay. The data used spans for a period of 8 months for the year 2014. Figure 32 illustrates system delay variation as a result of ambient air temperature. The slope of the linear fit is 0.012 ns/℃, mean and standard deviation of the system delay are 107.224 ns and 0.2886 ns respectively. The range error obtained from ranging to calibration target "D" is depicted Figure 33, where seasonal variations can be seen. Figure 34 illustrate the relationship between the range bias and ambient air temperature, the range error seem to increase as the temperature increase at the rate of 0.00047 cm/℃. The data in Figure 33 also indicate contribution from local crustal stability, calibration target "D" has been installed on top of a stable building that has been in existence since 80's, time would allow the building to settle and be more stable, long term GNSS observations will be required to study the stability of the building in details. Nonetheless, based on these results, it is evident that ambient air temperature contributes to the stability of the SLR system (including LLR system)

and a dedicated temperature regulating system is required to minimise errors due to thermal fluctuations.

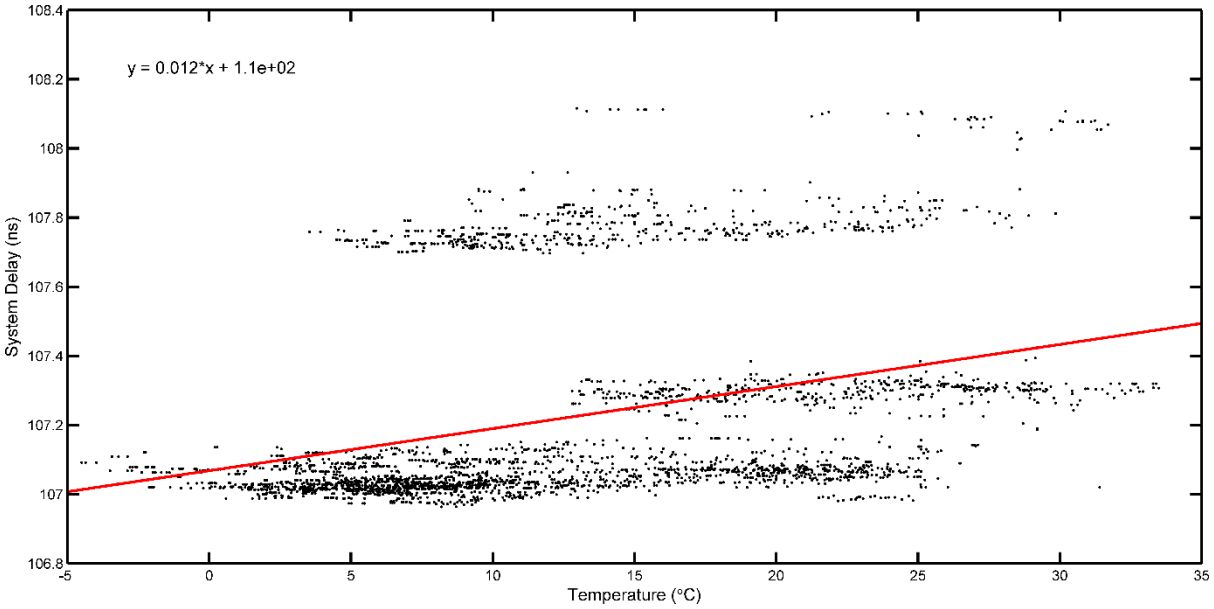

Figure 32. Effect of ambient temperature variation to system delay applied to MOBLAS-6 SLR station.

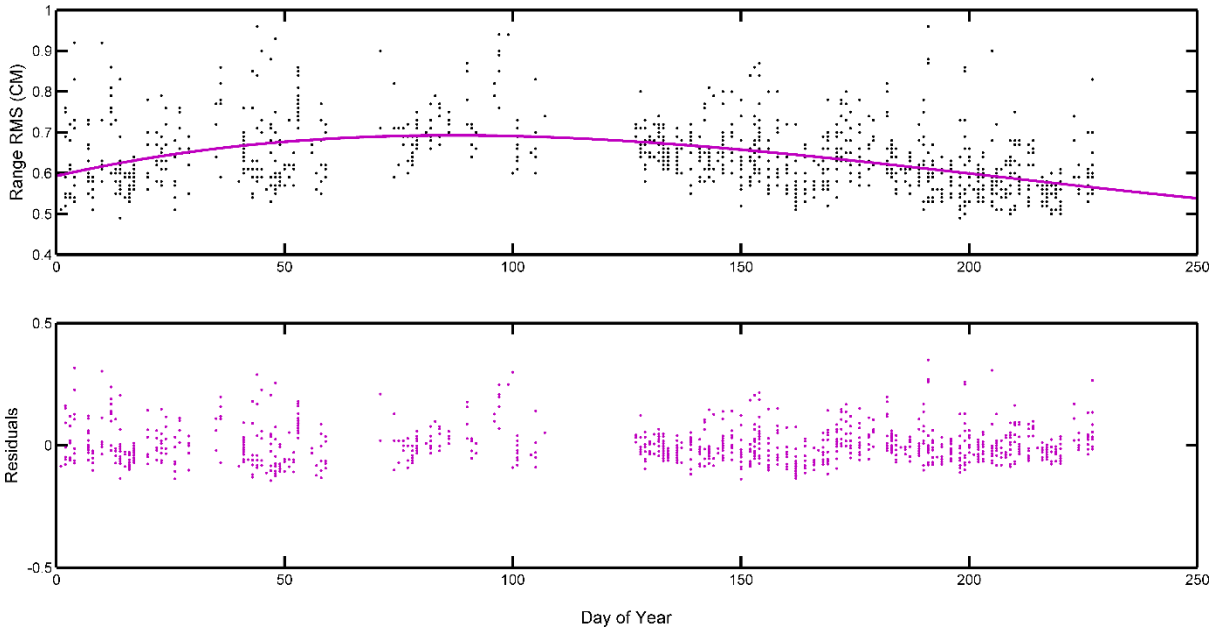

Figure 33. MOBLAS-6 calibration range bias, seasonal variation can be clearly seen. The 2nd polynomial was fitted to the data and the residual plot indicate that there are other factors contributing to the range error.

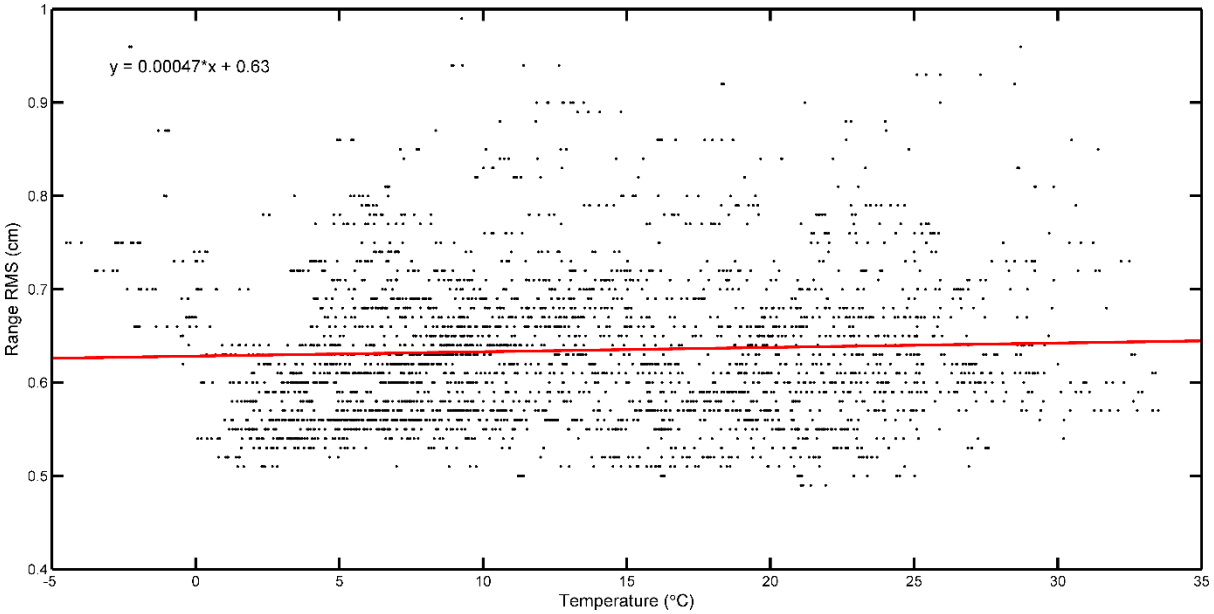

Figure 34. Influence of ambient temperature on range error for MOBLAS-6 SLR station.

4.4.4. Thermal monitoring system for the LLR control room

The LLR controlled room pictured in Figure 27 was designed to minimise thermal variations inside, an air-conditioning system is used to regulate the room temperature. Different components of the LLR such as the laser and timing subsystems are housed inside the LLR control room. These critical components require a stable environment to minimise errors or degradation of the output signals.

A thermal monitoring system was developed using Arduino Uno board and a digital temperature and humidity sensor (SEN0148) with an accuracy of ±0.5ºC and ±0.5% RH to monitor environmental conditions within the LLR control room. Data were sampled at 1 second interval for the period of one week. Figure 35 depicts results after one week, diurnal variations can be clearly seen with a maximum range of about 3.5℃. The sharp increase and decrease of the temperature is related to the rise and set of the Sun. The cooling system extract air with different temperature from outside during the period of one day and the diurnal pattern in Figure 35 is an indication of temperature variability of the ambient air. The minimum and maximum ambient air temperature during summer period is about 5℃ and 30℃ respectively within the period of 24 hours. The current cooling system can maintain temperature within the LLR control room to within 3.5℃ during the period of 24 hours. Our timing system frequency dependence on temperature is 3×10^{-10} over a temperature range from 0℃ to 50℃. This

current cooling system provides adequate environmental conditions necessary to operate the 4380A timing subsystem with minimum thermal noise as possible.

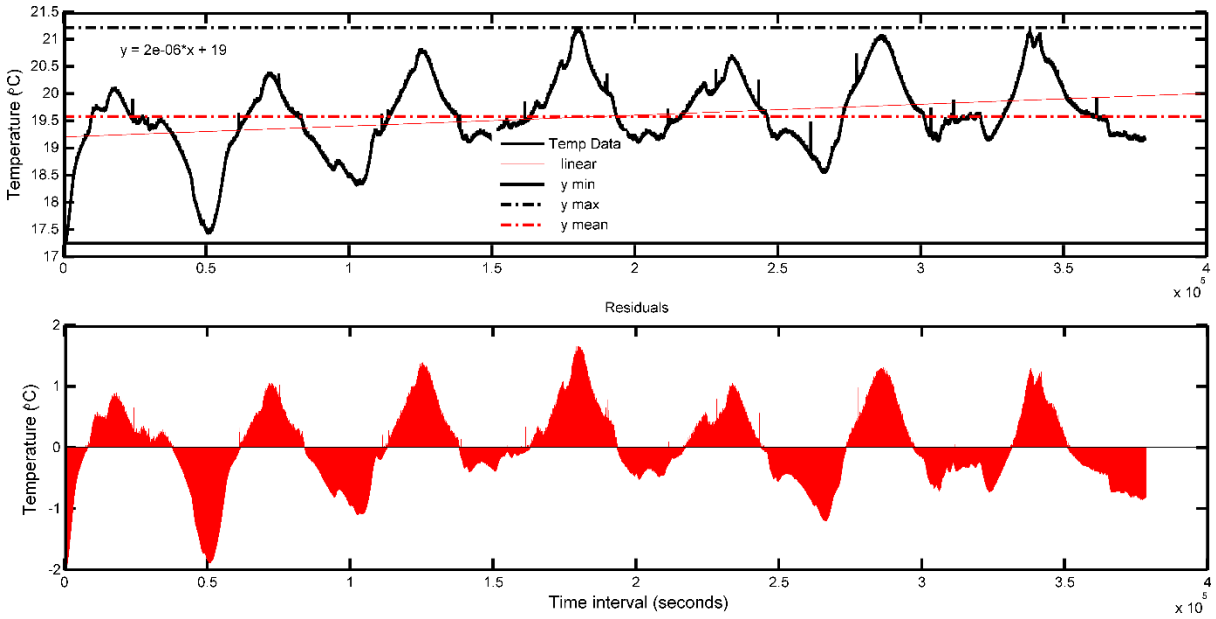

Figure 35. Temperature variability within the LLR control room. A linear fit indicate a slight increase in temperature during the period of one week.

4.5. Timing subsystem for the lunar laser ranger

The new sub-picosecond timing system for the LLR station is based on the newly developed 4393A rubidium clock developed by Microsemi. This reference timing system has timing accuracy of less than 10 ns Root Mean Square (RMS), frequency accuracy of less than 1×10^{-13} at 1 day, Allan Deviation (looked to GPS) of 6×10^{-13} at 1 second and a phase noise of -110 dBc/Hz at 1 Hz based on manual specifications. The 4380A has an excellent temperature stability of 3×10^{-10} over a temperature range from 0℃ to 50℃. The system has also a customized AC and DC power inputs to allow continuous power supply, Network Time Protocol (NTPv4), five of each: 1 pps, 5 MHz and 10 MHz output signals, and an option for external frequency reference input from highly stable clocks like hydrogen maser clocks.

Geodetic antennas are usually installed on a stable platforms such as bedrocks. Piers are constructed and anchored onto bedrock to ensure highly stable measurements are achieved (Ray and Senior, 2005). However, for timing applications, buildings that have stable foundation can also be used. Guidelines and recommendations on monumentation designs are

available at https://igscb.jpl.nasa.gov/network/monumentation.html. The GPS-702-GG Novatel dual-frequency antenna was installed on top of the LLR control room (Figure 36). The LLR control room is anchored on a stable concrete platform and the antenna is extended by 1-metre mount pole from the top of the LLR control room. This installation ensures that the antenna is not obstructed by nearby objects or introduction of multipath signals due to reflective surfaces (a discussion on site selection for this antenna is available at Munghemezulu et al., 2016b). The GPS-702-GG Novatel antenna is designed to observe both L1 and L2 frequencies from GPS satellites. The dual frequency capabilities of this antenna allow for ionospheric effects mitigation and it offers redundancy and flexibility for timing applications. The 4380A timing system incorporates OEM6 series as its GNSS receiver (for more information on Novatel antennas and OEM6 receivers refer to: http://www.novatel.com).

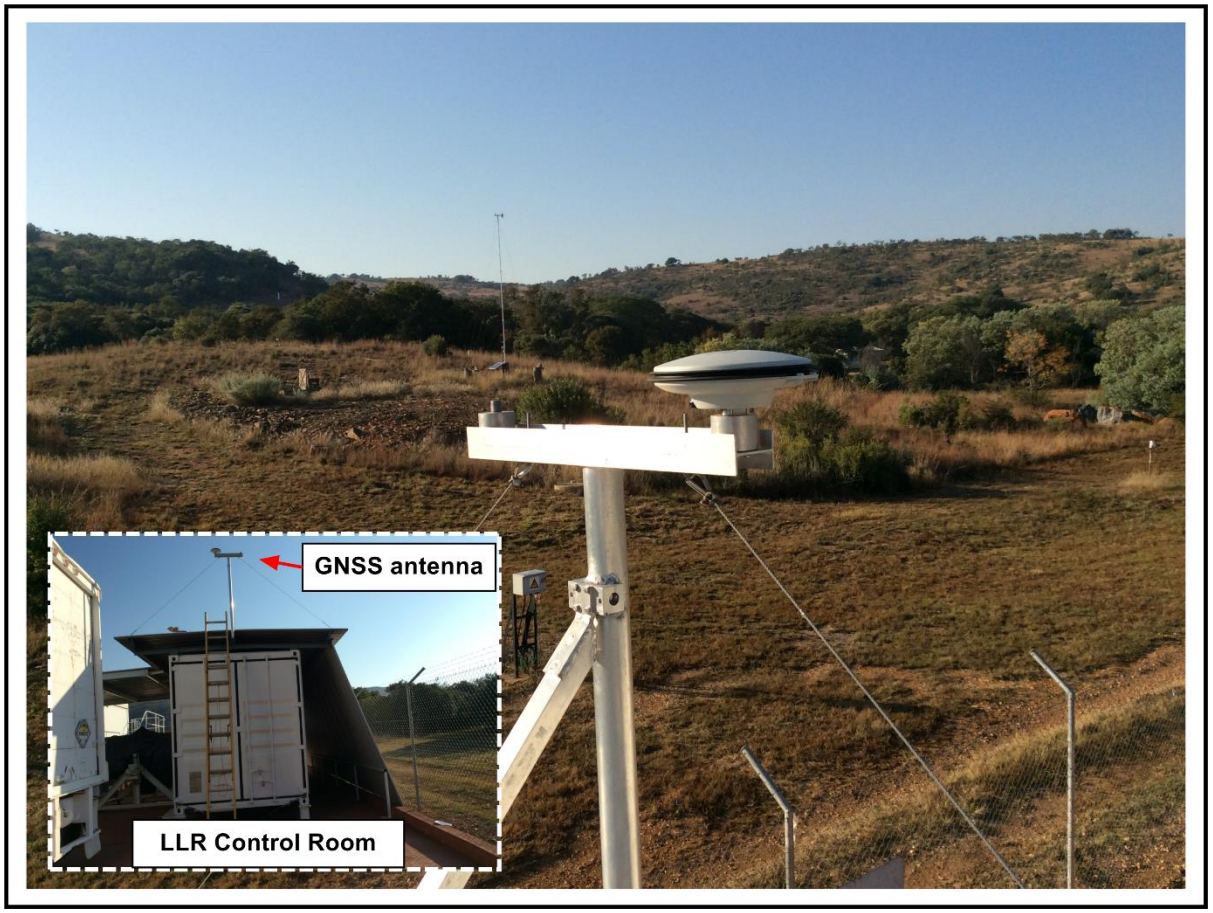

Figure 36. The GPS-702-GG Novatel dual-frequency antenna installed on top of the LLR control room. The mounting pole is custom-made to ensure position stability.

The phase noise of the clock (in decibels relative to the carrier, dBc) is -113 dBc at 1 Hz. Phase noise that is "close-in" (close to the central frequency of 10 MHz, ~within 100 Hz)

would affect the spectral resolution of the system whereas broadband noise (up to 10 kHz from the centre frequency) affects the overall system signal to noise ratio (SNR). Phase noise can also be described as the short-term random fluctuations of the frequency of the sine/square wave. The properties of this oscillator compare favourably with other timing reference systems used for SLR/LLR applications in the ILRS network (Figure 3 in Chapter 1). Therefore, some improvements on measurements are expected from the HartRAO's LLR station.

Errors introduced by temperature variations can be reduced given that the timing system will be installed in a temperature-controlled room. Transmitted photons take approximately 2.5 s to travel from Earth to the Moon and back to the receiving telescope. The time error for one photon round-trip (assuming Allan deviation of 1×10^{-13} at 1 second) is small enough to allow sub-centimetre measurement precision. However, other electronic systems must be taken into account. The long-term stability of the clock is provided by GPS, which is referenced to a ground-based network of atomic clocks (hydrogen MASERS and Cesium) (Lewandowski, 1999; Dach et al., 2002). This is achieved through a time transfer technique, where ground stations send accurate timing data to the GNSS satellites. The updated time from the GNSS satellites is then broadcasted together with navigation messages to the user anywhere in the world. It is expected that the station time (i.e., a local time generated by the local clock) will be well within 20 ns of the Coordinated Universal Time (UTC) scale when locked/slaved to GPS. Thus, the crystal oscillator provides short–term phase and frequency stability but is corrected for long-term drift and ageing by the GPS system.

The frequency noise for 10 MHz was estimated from the phase noise data (Table 8) using Equation (4.1) given in Maxim Integrated Products (2004),

$$RMS = \frac{1}{2\pi f_c 10^6}\sqrt{2\sum_{i=1}^{k-1} 10^{\frac{b_i}{10}} f_i^{\frac{-a_i}{10}} \int_{f_i}^{f_{i+1}} f^{\frac{a_i}{10}} df}\,. \qquad (4.1)$$

Where f_c is the frequency of the oscillator, b_i is the phase noise measurements $L(f_i)$ and $a_i = (L(f_{i+1}) - L(f_i))/(\log(f_{i+1}) - \log(f_i))$. Equation (4.1) converts the phase-noise spectrum in Table 8 to period jitter. The relationship between the period jitter and the phase-noise spectrum is given by

$$RMS_{jit_{per}} = \frac{1}{2\pi}\sqrt{\langle\theta^2(t)\rangle} = \frac{1}{2\pi f_c}\sqrt{2\int_0^{\infty} 10^{\frac{L(f)}{10}} df} \quad \text{and} \qquad (4.2)$$

$$Jit_{per} = \frac{\theta(t)}{2\pi f_c}, \tag{4.3}$$

where θ(t) is the phase-noise. This allows jitter to be estimated directly from the phase-noise spectrum measurements without making use of experimental setups, which can be expensive (Maxim Integrated Products, 2004).

Table 7. A list of selected stations in the ILRS network illustrating different timing systems (source: http://ilrs.gsfc.nasa.gov/). The proposed timing system for the LLR station at HartRAO has an improved Allan deviation compared to other stations.

Site Name	Frequency Standard Type	Short Term	Time Reference	Sync
Wettzel	H-MASER	0.15×10^{-12}	GPS	GPS
Riga	rubidium	20×10^{-12}	UTC (GPS)	GPS
McDonal Observatory	Oven Controlled Crystal Oscillator	$<10 \times 10^{-12}$	OCXO	manual
Matera	ceasium	0.7×10^{-12}	GPS	GPS
MOBLAS 6 HartRAO	rubidium	10×10^{-12}	GPS	GPS
Graz	Oven Controlled Crystal Oscillator	5×10^{-12}	GPS	GPS
LLR HartRAO	rubidium	6×10^{-13}	GPS	GPS

The value of *RMS* = 0.2174 ps was obtained from the 1 Hz to 100 kHz bandwidth. In particular, 1 ps equates to 0.3 mm in one-way range (0.15 up-down or two-way) and 40 ps delivers 12 mm one-way and 6 mm two-way. This value is within the specifications of the sub-centimetre regime for LLR applications.

Table 8. Phase noise parameters of the proposed 4380A oscillator for the LLR system (Source: http://www.microsemi.com).

f (Hz)	1	10	100	1000	10000	100000
L(f)(dBc)	-110	-132	-136	-141	-141	-155
b(dBc)	-110	-132	-136	-141	-141	-155
a (dBc/decade)	-22	-4	-5	0	-14	

The timing unit is designed to be accessible, monitored and controlled on-site via Ethernet/RS232. Both time and frequency will be monitored in near real-time and logged to aid in characterising system performance. Timing signals will be routed through a distribution amplifier to other subsystems. In this configuration, I would supply the Event Timer (reported in e.g., Panek et al., (2010) and Kodet and Prochazka, (2012)) with a highly stable 10 MHz directly from a 4380A oscillator timing unit to minimise additional phase distortions from the distribution amplifier. It is envisaged that the current system design and considerations will provide a cost effective method for high timing resolution for the LLR station at HartRAO.

4.6. Frequency stability of 4380A rubidium clock

To measure short-term frequency stability of 4380A Rubidium clock, I follow the method described in Munghemezulu et al., (2016c). The three oscillators, two-channel model (Chernyshev et al., 2012; Groslambert et al., 1981) was used to measure frequency instabilities of the 4380A Rubidium clock using VCH-314 frequency comparator, the two hydrogen maser clocks EFOS28 and EFOS6 were used as reference standards at a frequency of 5 MHz. According to Chernyshev et al., (2012), this method reduces errors associated with the noise of the frequency comparator. To achieve a centimetre level of accuracy from the photon detection system, a stable frequency of better than 10^{-10} is required and the measurement of the range must be accurate to 1 μs (Lu et al., 2014). Figure 37 illustrate that the 4380A can maintain frequency stability of better than picosecond level for the period of 17 minutes. Our results compares favourably with those published in the datasheet of 4380A Rubidium clock, indicating less degradation of the signal quality under operational conditions.

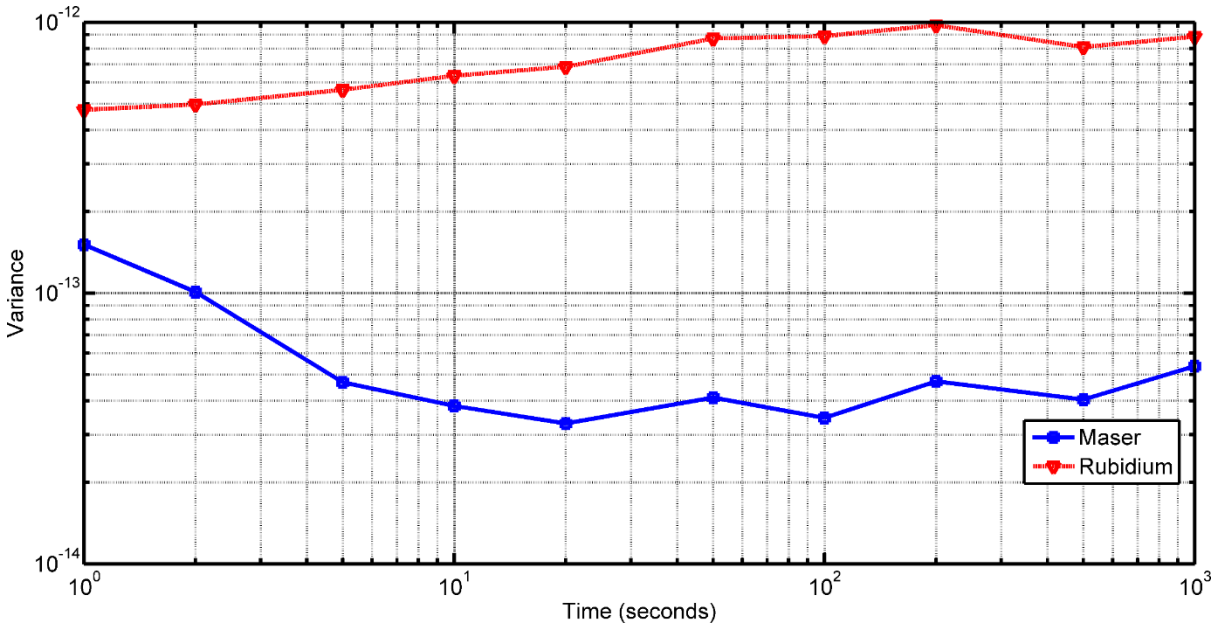

Figure 37. Short-term stability of the rubidium clock measured against hydrogen maser clock. The rubidium clock has a sub-picosecond stability over 10^3 s period.

4.7. Photon detection subsystem and signal calibration

Ranging to the Moon is a difficult task with only an average of 5 return photons per minute expected from a single pulse of laser light containing approximately 10^{19} photons for the LLR station at HartRAO. This exercise requires high accuracy and precision of the measuring devices to properly measure two-way ToF of the laser pulses. During the earlier stages of LLR development in the late 1960's, the accuracy and precision of measuring ToF was influenced by the high noise of the electronic systems of the telescope, atmospheric effects and poor understanding of the Earth-Moon dynamics (Degnan, 1993). Improvements have been made over the years, particularly in electronic systems such as photon detectors, event timers, telescope pointing model and reference timing systems (Kodet and Prochazka, 2012; Panek et al., 2010). However, the atmosphere still remains a big contributing factor in degrading the accuracy of the measured ToF (Andrews and Phillips, 2005).

The proposed optical path configuration is depicted in Figure 38. The laser pulses from the control room are transmitted through a coudé path to the telescope, where a telescope of 1-metre aperture collimates the laser beam in the direction of retro-reflectors on the surface of the Moon. The start detector located at the laser table provides a start time T_{d1}, which is registered by the event timer.

A calibration retro-reflector located inside the telescope tube at the exit point of the laser returns a fraction of light that can be used to calibrate the event timer and the internal calibration time T_{d2}. This information can then be used to provide accurate ToF between the Moon and the calibration mirror, which act as a reference point for the telescope. During the receiving stage, the return detector detects the returning photons from the Moon as T_{d3}. The ToF (time between the Moon and the calibration mirror) can be calculated by

$$ToF = [T_{d3} - T_{d1}] - [T_{d2} - T_{d1}]. \tag{4.4}$$

According to Samain et al., (1998), if the calibration mirror is located higher up the telescope tube (closer to the secondary mirror) in such a way that there is some distance between the intersections of the mechanical axis of the telescope and the calibration reflector; then Equation (4.5) can be used to calculate ToF, where c is the speed of light, η_{Air} is the air refraction index and dC_{mirr} is the distance between the calibration mirror and the reference point of the telescope (intersection of the two azimuth and elevation axis).

$$ToF = [T_{d3} - T_{d1}] - [T_{d2} - T_{d1}] + \frac{2dC_{mirr}\eta_{Air}}{c}. \tag{4.5}$$

The different electrical signal transmitting medium such as coaxial cables or fibre optics introduce time delays (see Equation (4.6)), phase shifts (ϕ) (see Equation (4.8)), phase noise and a varying velocity factor vf (as given in Equation (4.7)) due to the dielectric constant of the transmitting medium. Therefore, the delay introduced by the transmitting medium must be calibrated especially in laser ranging applications where measurements of ToF are required to be highly accurate. In the case of coaxial cable, (according to Horowitz and Hill (1989); Lorber and Duboff (1975)), the delay (D) in Equation (4.6) can be calculated given the capacitance C and inductance values L. These values are measured experimentally and depend on the type of cable used.

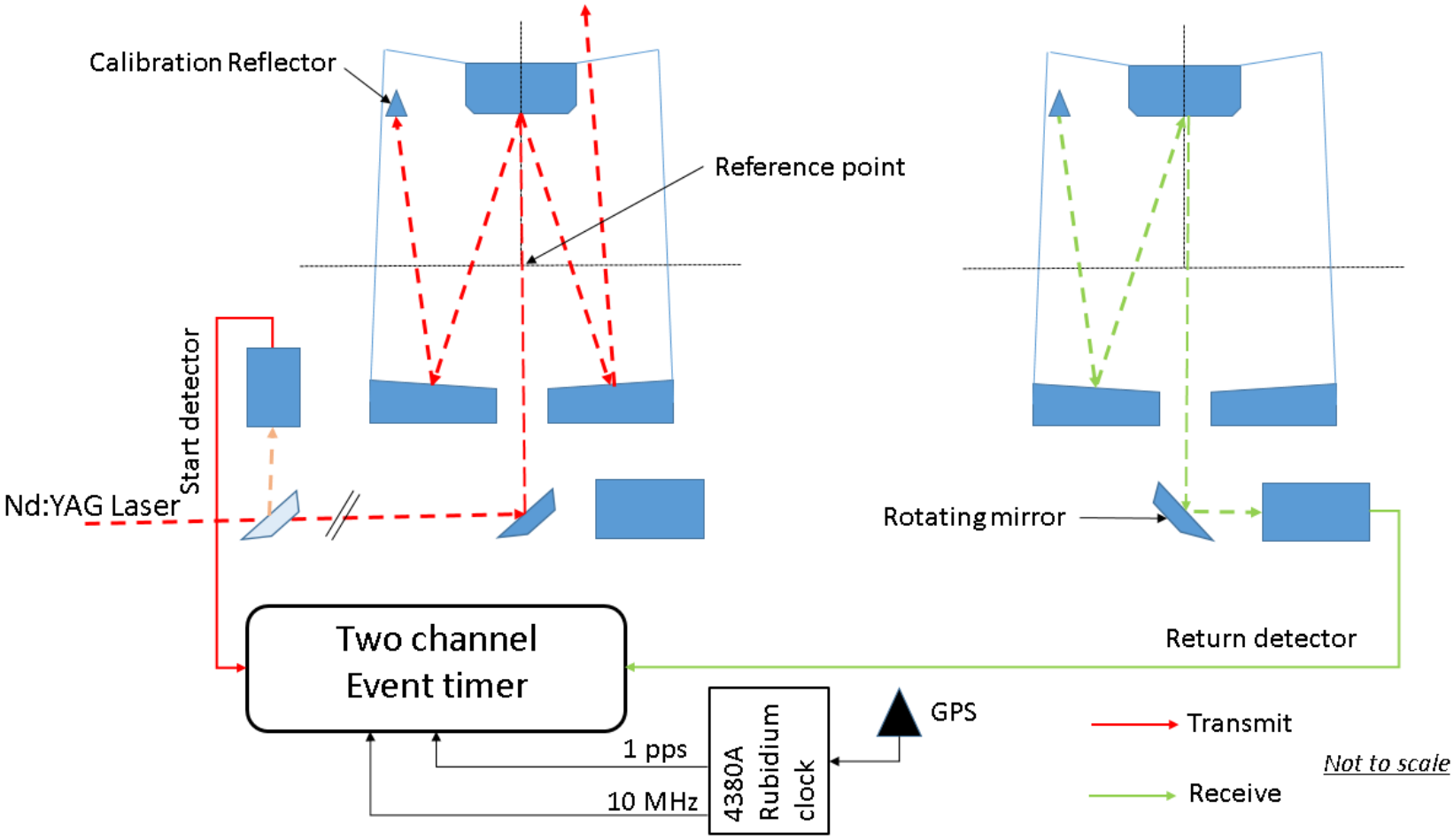

Figure 38. Simplified schematic of the transmit and receive laser coudé path for the LLR station at HartRAO. The calibration reflector also allows the station to carry out internal calibration as well as ground-based (ranging to a stable target, the figure is not to scale).

$$D = \sqrt{L \times C} \tag{4.6}$$

$$v_f = (l / D) / c \tag{4.7}$$

$$\varphi = f \times 360 \times Delay \tag{4.8}$$

In Equation (4.7), l is the length of the cable. As an example, assume we have C=31.2 pF and L=76.8 nH for a coaxial cable RG-58U. The delay of an electrical signal is estimated to be 1.55 ns, vf= 67% and a phase shift of 56°. As a result, Equation (4.4) and (4.5) are required to be modified in order to account for the delay biases introduced by the cables and the delay of the start detector and return detector electronics represented by C_{Dn}. An example of such modification is given as,

$$\begin{aligned} TOF = & [(T_{d3} - C_{d3}) - (T_{d1} - C_{d1})] \\ & - [(T_{d2} - C_{d2}) - (T_{d1} - C_{d1})] + \frac{2dC_{mirr}\eta_{Air}}{c}. \end{aligned} \tag{4.9}$$

The estimated maximum errors from the two subsystems proposed for the LLR are listed in Table 9. These errors are associated with jittering of the electronic systems that are measuring ToF values. An estimated value of about 45 mm associated with a random error of a single photon is achieved for the proposed subsystems. The noise in the electronics is mainly caused by thermal variations, energy fluctuations of laser pulses, duration of the laser pulses and white noise (Samain et al., 2010; Samain et al., 2015).

To achieve a 1 mm statistical error regardless of the electronic jitter, a higher photon return rate is required. The return rate depends on the size of the telescope and the seeing conditions of the site. I estimate on average about 5 photons per minute with seeing conditions of 1 to 3 arc seconds and using the 1 m telescope aperture. The APOLLO LLR station collects about 100 photons per minute using a 3.5 m telescope (Murphy et al., 2000), this allows the station to statistically achieve 1 mm precision (Murphy, 2013). The size of the telescope and seeing conditions affect the photon return rate, hence the APOLLO station seems to perform better compared to other existing stations at the moment. They also utilise an array of 4×4 Avalanche Photon Detectors developed by APOLLO in collaboration with the MIT Lincoln Laboratories. This gives them an advantage of detecting adequate photons for milimetre ranging precision (Strasburg, 2002; Murphy et al., 2002).

Table 9. Estimated statistical RMS errors per photon for the timing systems.

Error source	**RMS Error (ps)**	**RMS Error (mm)**
10 MHz Reference	~0.2174	~0.06522
Rubidium 1 pps	<100	<30
Start detector	<20	9
Return signal detector	<15	5
Event Timer	3	1
Total	<138	<45

4.8. Concluding remarks

The current network of space geodetic stations is weak in the Southern Hemisphere, particularly in Africa. Installation of more geodetic stations in Africa will contribute towards improving our current understanding of the Earth-Moon system. In light of this, the development of the LLR at HartRAO will improve the current network of the ILRS by adding a station in the Southern Hemisphere. This is expected to constrain geometrical errors or network dependent biases as well as contribute valuable data to be used by a variety of different scientific communities.

In terms of the LLR timing system being developed at HartRAO, the rubidium clock, which has an Allan deviation of better than a picosecond at 1 s and a very low phase noise of -110 dBc at 1 Hz is being considered. Furthermore, the photon detection subsystem in consideration has low cumulative RMS jitter errors. The maximum total estimated random error per photon contributed by the two subsystems is 45 mm. To achieve 1 mm ranging precision, a high photon return rate ought to be achieved. The estimated return rate of 5 photons per minute implies that the LLR must range for longer than 30 minutes in order to collect adequate photons to statistically achieve sub-centimetre ranging precision during calculation of the normal points. Ranging periods have been identified using meteorological data that will minimise thermal deformations of the telescope and to ensure the best performance of the electronic systems that are exposed to the ambient air. Overall, the new LLR station in the Southern Hemisphere will contribute towards better understanding of the Earth-Moon system.

Chapter 5

The performance of hydrogen maser clocks at HartRAO

Abstract

Hydrogen maser frequency standards are commonly utilised in various space geodetic techniques such as Very Long Baseline Interferometry (VLBI) as local reference clocks. The Hartebeesthoek Radio Astronomy Observatory in South Africa is currently operating two maser frequency standards i.e., an EFOS28 and an iMaser72 for the 15 m and 26 m VLBI radio telescopes respectively, an older EFOS6 is a standby spare. This study utilised the least-squares method to derive clock parameters, which are used to measure the performance levels of the masers by making use of the offset measurements obtained between hydrogen maser clock 1 pps and GNSS 1 pps for a period of 35 days. The masers were also compared using a frequency comparator (VCH-314) for a time period of 100 s. The results indicate that the performances of both Masers are relatively similar to each other, with short-term and long-term results indicating good agreement. The iMaser72 has a better standard error of 0.0039 μs compared to the standard error of 0.0059 μs for EFOS28 maser clock. In general, both masers performed at an expected level required for radio astronomy and geodetic VLBI applications. The method used in this study proved to be useful in managing local hydrogen maser clocks to ensure accurate VLBI observations are obtained.

5.1. Introduction

Most geodetic techniques rely on the accuracy and stability of their reference clocks; the clock characteristics have a direct influence on precision and accuracy of the observations. To achieve accurate observations at the sub-centimetre level, the local clocks must be accurate to sub-picoseconds (ps) level. Different timing reference standards are used to provide accurate time in geodetic and astronomical instrumentations such as Cesium, Rubidium, Oven Controlled Crystal Oscillators (OCXO) and atomic hydrogen maser clocks. For the Very Long Baseline Interferometry (VLBI) applications, hydrogen maser clocks are recommended as frequency standards (Levine and Vessot, 1970; Schuh and Böhm, 2012). Other clocks are mainly used in Satellite Laser Ranging (SLR) or Lunar Laser Ranging (LLR) applications. For example, the MOBLAS-6 SLR station at the Hartebeesthoek Radio Astronomy Observatory (HartRAO) utilises a Rubidium-disciplined crystal oscillator for local reference time (Combrinck, 2009). It is well known that clocks drift over time due to thermal instabilities, noise in the electrical circuits, etc. Hence, they need to be adjusted after some time to compensate for drifts and ageing characteristics to allow proper alignment to the Coordinated Universal Time (UTC) to within a few microseconds (Allan, 1987; Lewandowski et al., 1999).

Atomic fountain clocks with high accuracy and stability have been developed to improve the measurement of time with uncertainties of a few parts in 10^{16} (Wynands and Weyers, 2005). The National Institute of Standards and Technology (NIST) is currently operating two Ceasium Fountain Clocks (NIST-F1 and NIST-F2) to define time with supreme accuracy (Donley et al., 2004). Optical frequency standards using a spin-1/2 system has been reported to yield better accuracy than the microwave based frequency standards (Lemke et al., 2009). Ely et al., (2014) and Ely and Seubert (2015) have reported on a small mercury-ion atomic clock with Allan deviation of less than 10^{-14} per day for use in deep space applications through the Deep Space Atomic Clock (DSAC) programme of NASA. However, these clocks have not yet been employed in VLBI applications but are bound to be used in the future when these clocks become affordable.

Friedrich Robert Helmert (1843-1917) defined geodesy as the science of measurements and mapping of the Earth's surface. This definition has evolved over time due to technological advancements and is now defined as the science of determining the geometry, gravity field and rotation of the Earth and the evolution of these three pillars over time (Plag et al., 2009). Combrinck (2014), proposed a fourth pillar of geodesy i.e., space-time curvature. The General

Theory of Relativity (GRT) describes the space-time curvature and its effects on all measurements made by space geodetic techniques (Ciufolini, 1990; Combrinck, 2013). Hence, it is important to consider space-time curvature as one of the pillars of modern geodesy due to its influence on geodetic observations. For instance, clocks in orbit around the Earth run faster than those on Earth due to the weaker gravity field, this effect has to be compensated for. Space geodesy makes use of the Global Navigation Satellite Systems (GNSS), SLR, VLBI, and Doppler Orbitography and Radiopositioning Integrated by Satellite (DORIS) techniques to study the Earth system; all these techniques have very stringent clock requirements.

The VLBI technique, in particular, is important for studying positions and structural variability of astronomical radio sources (e.g., quasars) by utilising a network of radio telescopes. Even though this technique was originally developed by astronomers for radio astronomy research, it is also applied in geodesy (in an inverse sense) to study geodynamics by determining baselines and their rates between different stations (Ronnang, 1989). The technique also defines and maintains the International Celestial Reference Frame (ICRF). The Earth Orientation Parameters (EOP) are also determined with high accuracy and they include polar motion, precession-nutation and Length of Day (LOD). The technique also contributes towards the International Terrestrial Reference Frame (ITRF) by providing positions of the VLBI antennas and the reference frame scale component (Schuh and Böhm, 2012). These data products are important for a number of applications such as establishment and maintenance of reference frames and determination of orbit parameters for spacecraft and satellites.

HartRAO operates two VLBI radio telescopes (Figure 39). The telescopes function within the framework of the International VLBI Service for Astrometry and Geodesy (IVS) and participate in various international programmes. They use hydrogen maser clocks as their local reference timing systems. I evaluate and compare the performance of the two hydrogen maser clocks by using the least-squares approach to determine their clock parameters.

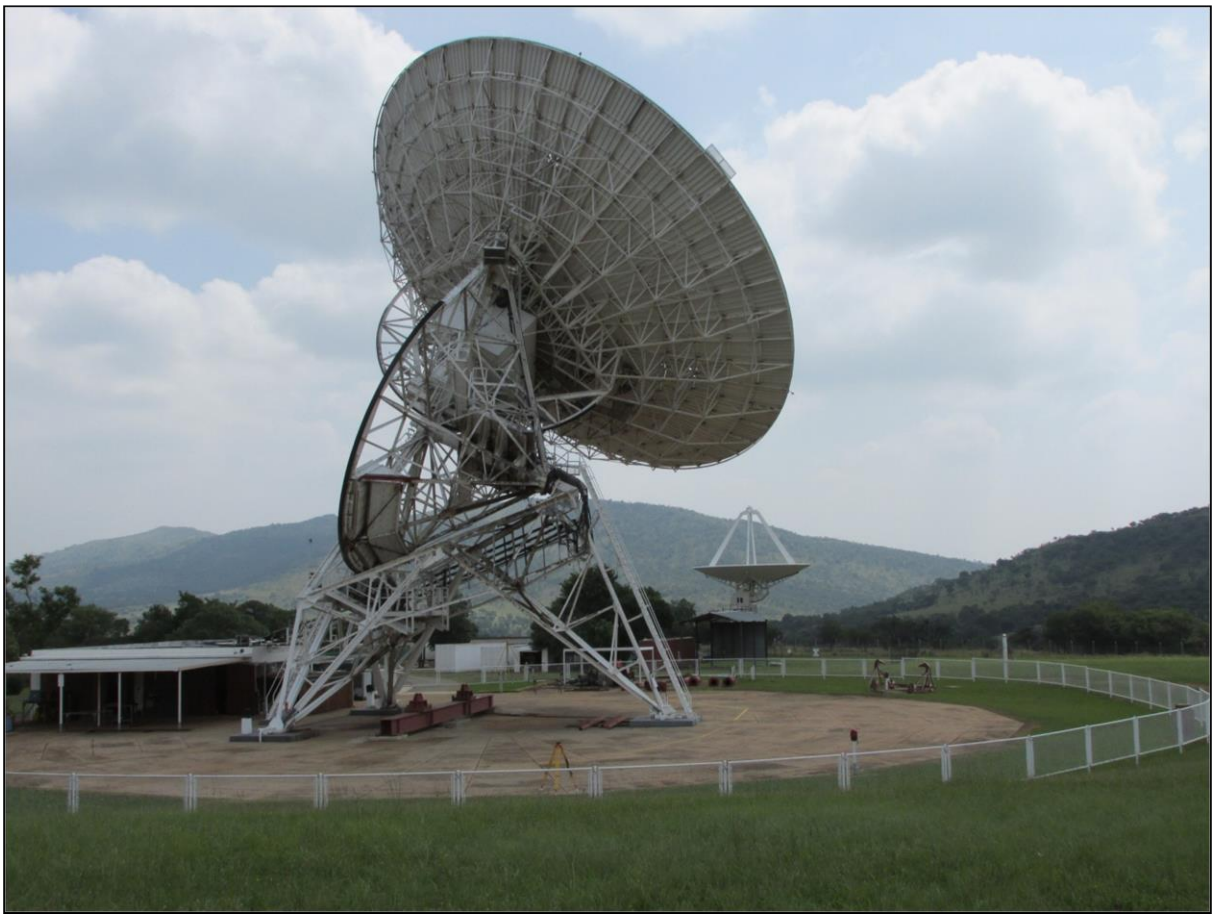

Figure 39. The VLBI radio telescopes located at HartRAO, South Africa. The 26 m antenna is located in the forefront and the 15 m antenna can be seen in the background.

5.2. Hydrogen maser clocks at HartRAO

The iMaser72, EFOS28 and EFOS6 hydrogen maser clocks used at HartRAO for VLBI applications can be seen in Figure 40. They are stored in a temperature controlled room, which is maintained at $25.7 \pm 0.5°C$. Each maser rests on an independent pillar of the floor foundation; the pillars are also designed with thermal insulators so that they do not influence the temperature stability of the maser enclosure and that of the room. The EFOS28 maser replaced the EFOS6, which in service for 18 years prior to installation of the EFOS28 maser by the Observatoire Cantonal de Neuchatel in 2003. The EFOS28 has an Allan deviation of 1.5×10^{-13} at 1 s and thermal stability of $1.9\times10^{-15}/°C$ as specified by the manufacturer. The iMaser72 was installed in 2013. Its manufacturer specifications are 1.26×10^{-13} at 1 s Allan deviation and it has a thermal stability of $3.5\times10^{-15}/°C$.

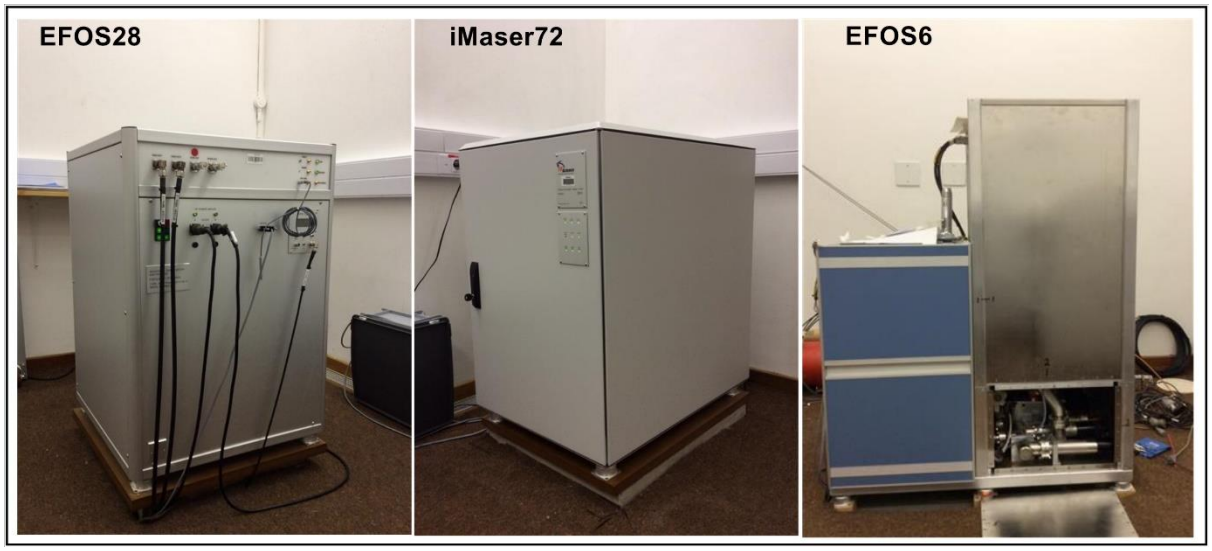

Figure 40. The EFOS28, iMaser72 and EFOS6 hydrogen Maser clocks of HartRAO. The iMaser72 and EFOS28 are utilised as frequency standards for the 26 m and 15 m VLBI telescopes respectively; the EFOS6 Maser is for backup purposes.

Hydrogen Maser clocks are based on the resonance frequency of the hydrogen atom (1420405751.68 Hz). Usually, hydrogen is supplied by heating a solid state metallic compound $(LaNi_5H)_x$, which releases the gas. The molecular hydrogen is purified and stored in the discharge bulb. The beam of hydrogen atoms are passed through a multiple magnetic pole state selector (4, 6 or 8 poles can be used).

Depending on the energy state of the hydrogen atoms, those with upper levels designated by F=1, m_f=1 and m_f=0 will be directed towards a quartz storage bulb and those with lower levels (i.e, F=0, m_f=-1, m_f=0) will be pumped off. The quartz storage bulb is coated with Teflon to minimise interaction with the hydrogen atoms. The bulb is stored in a cavity that is thermally and magnetically protected (having a typical shield factor of 10^5), and tuned to a frequency of 1420 GHz which is related to the upper energy levels of the hydrogen atoms (Vessot, 2005). Atoms in the storage bulb continuously interact and during this process, they lose energy and translate from upper level to lower level state. The photons released cause other upper-level atoms to lose energy as well. This results in a self-sustaining microwave field in the bulb. The low maser signal (about 10^{-13} W) generated in the cavity is amplified and locked to a resonance frequency of the hydrogen atom and is utilised to generate a one pulse per second (1 pps) and a standard frequency signal (typically 5 or 10 MHz) by the frequency synthesiser system. More information can be found in Lombardi, (2002); Mizuhiko, (2003);

Middelberg and Bach, (2008); Vessot, (2005); where detailed information about hydrogen maser clocks and the factors that affect their performance levels are discussed.

5.3. Basic principles of the VLBI technique

The VLBI technique is designed to study extra-galactic and radio sources (quasars). Among other applications, VLBI results are applied in determining EOP values as well as expanding and maintaining the ICRF with high angular resolution. The angular resolution of a single antenna dish can be approximated by

$$\varepsilon \approx \frac{\lambda}{d}, \tag{5.1}$$

where λ is the wavelength of a particular radio source and d is the telescope diameter. To improve the angular resolution, observations can be made through a configuration of a network of antennas that are widely distributed around the world. In this case, the size of the Earth becomes the diameter of one big single antenna dish that can reach an angular resolution of about 1 mas (milli-arcsecond) or better (Seeber, 1993; Heinkelmann and Schuh, 2010). In the early days of VLBI experiments, the telescopes observing the same source in a network were configured as a Connected Element Interferometer (CEI), where the observing telescopes were connected to a single oscillator by a fibre cable (Edwards et al., 1992). This method limits the baseline length. Today, most telescopes are equipped with atomic hydrogen maser clocks to allow inter-continental baseline lengths to be achieved.

The observation made by two or (more telescopes) is the difference in arrival time (group delay, τ_g) of a planar wave signal (S_o being the direction of the source) from quasars or an extragalactic radio source received by the two or more antennas separated by a vector b (Robertson, 1991; Figure 41). The group delay can then be defined by the scalar product of S_o and b divided by the speed of light (c),

$$\tau_g = \frac{b \times s_o}{c} = (t_1 - t_2). \tag{5.2}$$

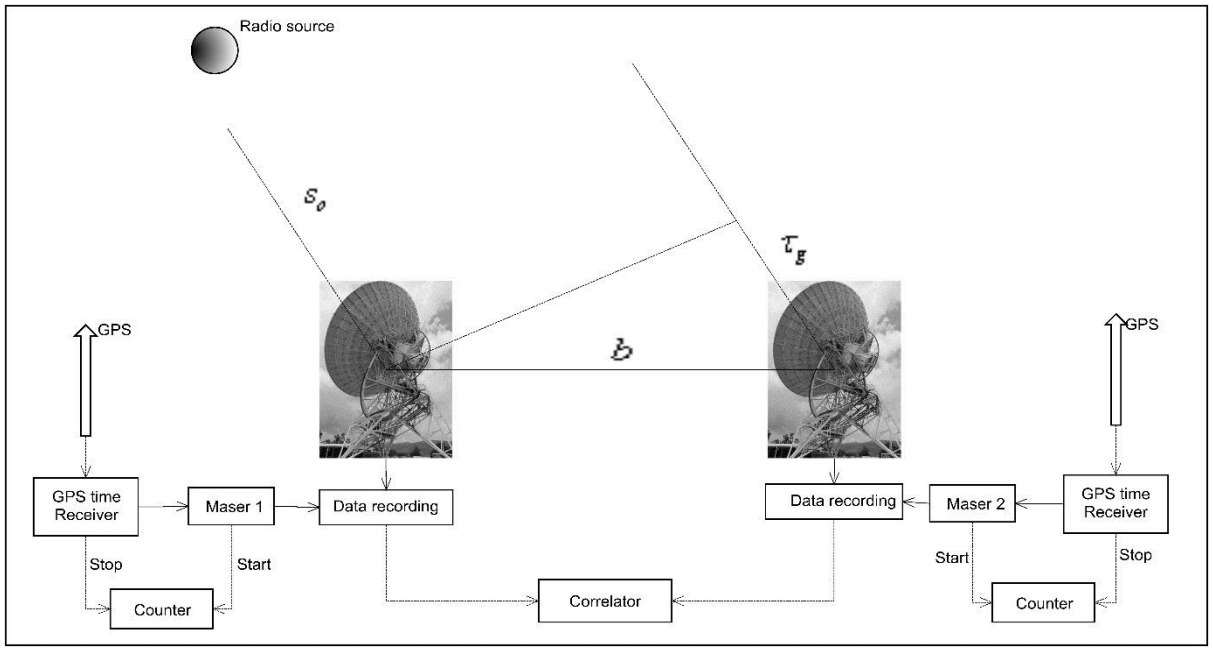

Figure 41. Basic principles of VLBI technique and measurement method for the clock offset data.

A complete observation Equation should include corrections for bias and clock drift, atmospheric refraction, special and relativistic effects, cable delay and diurnal aberration. For more details on VLBI, see Seeber, (1993); Schuh and Böhm, (2012); Schuh and Behrend, (2012). During observations, data are recorded on disc packs if the baselines are large and correlated at a later stage. If the telescopes are close to each other, they can be connected via CEI and data can be transmitted to the correlator almost instantly. In recent years, electronic VLBI (e-VLBI) has been developed to allow data correlation of longer baselines via broadband data transmission and real-time data processing.

Existing VLBI telescopes are being upgraded and new telescopes are being developed through the initiatives of the IVS with the aim of achieving 0.1 mm/yr and 1 mm accuracy in reference frame stability and station position respectively (Pet et al., 2009). The new antennas have been named "VLBI2010 Global Observing System" (VGOS) antennas. HartRAO is currently in the process of building one of the VGOS antennas, this new antenna will improve the observations and strengthen the network in the Southern Hemisphere (Mayer et al., 2014). Niell et al., (2005) identified a number of strategies to achieve 1 mm accuracy and one of them is to improve the frequency reference standards that are used at observatories. To achieve 1 mm accuracy, the frequency standard accuracy must reach a stability of few parts in 10^{-16} for averaging times longer than 1 hour. The frequency stability of about $\pm 5\times10^{-13}$ in a 24 hour period is usually required in the current operational requirements (Zhang et al., 2001).

Moran (1989) explains further the importance of accurate timing systems in geodetic VLBI and astronomy, where the Signal-to-Noise ratio (SNR) received can be written as

$$SNR = \frac{SA\sqrt{2B\tau_c}}{kT_s}. \tag{5.3}$$

In Equation (5.3), S is the source density flux, A is the geometric mean of the telescope collecting areas, B is the bandwidth, k is Boltzmann's constant, T_s is the geometric mean of the system temperature of the telescope and τ_c is the coherent integration time, which can be estimated by

$$\omega \times \tau_c \times \sigma_y(T) = 1. \tag{5.4}$$

In Equation(5.4), $\sigma_y(T)$ is the two-sample Allan variation and ω is the local oscillator frequency in radians per second. For example, to achieve a signal coherence for an observation period of 1000 s, if the local oscillator is set to 8.0 GHz, the two observing stations must maintain relative stability of ~2×10^{-14} (Combrinck, 2013). Therefore, it is important for observatories to keep track of their hydrogen maser clock performance and to make sure that the drifts and ageing characteristics are properly understood and corrected to allow accurate measurement during experiments.

5.4. Data and analysis method

5.4.1. Long-term data

Hydrogen maser clocks at VLBI sites require calibration to account for systematic drifts. This requires comparison with an external independent stable timing reference system, which is accomplished through time transfer technique by utilising GNSS technology (Lewandowski et al., 1999). Data from the network of hydrogen maser clocks (U.S Naval Observatory-USNO) are used to update the GNSS satellites with timing information, and then the satellites transmit updated time and navigation messages to the user. The transmitted information is then used to allow local timing systems to be calibrated to the USNO UTC time.

Two hydrogen maser clocks i.e., iMaser72 and EFOS28 are used for the 26 m and 15 m telescopes respectively for geodesy and astronomy observations at HartRAO. The two

masers are connected to a GNSS time receiver and high-speed counters are used to measure the offsets between 1 pps from the Maser clocks and from the GNSS UTC time receivers (Figure 41). The maser 1 pps signal is used as the start and the 1 pps signal from the GNSS receiver is used as the stop signal. The measurements are made by high-speed counter every second but averaged to a 24 hour period, later on, this is to minimise short-term noise in the GNSS due to ionospheric and tropospheric effects and taking into account the orbit period of satellites, which repeats every 24 hours (Lombardi, 2002). Data were collected simultaneously for the two maser clocks for 35 days starting from 04-15-2015 to 05-19-2015 period. The data contains daily averaged offset measurements between each maser clock and GPS UTC in μs.

The 24-hour offset data sets were analysed by using a second quadratic trend model given by Levine et al., (1999) as

$$Y_i = b_o + b_1 x_i + b_2 x_i^2. \tag{5.5}$$

The coefficients for Equation (5.5) were determined using a least-squares curve fit in Microsoft Excel. The drift parameters of the clocks were calculated by taking the first derivative of Equation (5.5) to arrive at Equation (5.6), where Δt is the range period of the observations. The units are given as microseconds per day (μs/d) for Equation (5.6). By taking the derivative of Equation (5.6), ageing parameters of the clocks can be derived in microseconds per day per day (μs/d/d) as given by Equation (5.7),

$$drift = b_1 + 2b_2 \Delta t, \tag{5.6}$$

$$Ageing = 2b_2. \tag{5.7}$$

The EFOS28 MASER clocks can be adjusted by using Equation (5.8), where f_H is the Hydrogen MASER frequency (1402405751.6893 Hz), $\pm\Delta f$ is the fractional frequency error (calculated by dividing the drift by the number of seconds in a day) and this value can be positive or negative depending on the behaviour of the MASER, and f_{synth} (this is the last value obtained when correcting the maser, in this case, I use the initial value of 5751.68267),

$$f_{adj}(EFOS28) = f_{synth} - \Delta f \times f_H. \tag{5.8}$$

The iMaser72 clock is adjusted by using Equation(5.8), where the fractional frequency error is either added or subtracted in the Direct Digital Synthesizer (DDS) value, (in this case,

the initial DDS value for the iMaser72 is 1420405750.291886) and the maser software will carry out further computations to adjust the output frequency of the maser and determine the new DDS value based on the input $\pm\Delta f$,

$$f_{adj}(iMASER72) = \pm\Delta f. \tag{5.9}$$

It is important to note that the adjustment procedure for different maser clocks will be different depending on the design and the manufacturer.

5.4.2. Short-term data

The short-term stability variations were analysed using a frequency comparator (VCH-314). The three oscillators, two-channel model (Chernyshev et al., 2012) was used to measure frequency instabilities of the iMaser72, EFOS28 and EFOS6 masers simultaneously. The EFOS6 maser was used as a reference for the other two maser clocks. This particular setup reduces systematic errors due to instabilities of the reference clock and comparator (Groslambert et al., 1981). Two 5 MHz signals from iMaser72 and EFOS28 are connected to two identical frequency comparators as f_{y1} and f_{y2} respectively. The reference signal of 5 MHz is connected to a signal splitter to produce two identical signals that are then connected to the frequency comparators as f_x.

The experiment was set to measure frequency phase differences of the signals for the time period of 100 s with an averaging number of 10. Measurements were sampled at 10 nanoseconds resolution, maximum frequency difference and variance is set at 1×10^{-08} as a limiting factor to exclude noise in the data. The Time Instance Meter (TIM) module of the frequency comparator produces two sets of phase measurements (1) as direct measurement f_{y1}, f_{y2}, *and* f_x; (2) as f_{y1x}, *and* f_{y2x}, which are calculated as

$$f_{y1x}[Hz] = 1 + \frac{k(f_{y1} - f_x)}{f_x},\ f_{y2x}[Hz] = 1 + \frac{k(f_{y2} - f_x)}{f_x}\ . \tag{5.10}$$

Where k (1×10^6) is the multiplicative factor for the frequency noise.

5.5. Results and discussion

The results for the two MASER clocks are plotted in Figure 42, and the derived parameters from the long-term data are summarised in Table 10. The raw data for the EFOS28 maser and the iMaser72 maser have a range of 0.1163 μs and 0.1945 μs respectively. In general, both maser clocks indicate smooth offset data with small fluctuations in the order of 10^{-2} μs. This might be due to noise in the GNSS signal, maser instrumentation and thermal variations among other things that result in fluctuation as explained in Allan and Weiss (1980) and Dach et al., (2002). The second quadratic trend model Equation (5.5), gives a very good coefficient of determination (R^2) of 0.9958 for iMaser72 and it yielded R^2 value of 0.9768 for EFOS25 maser clock. The coefficients of the trend models are given in Table 10. Standard errors and F values for the two masers are all very small and statistically significant, indicating good performance of the trend models.

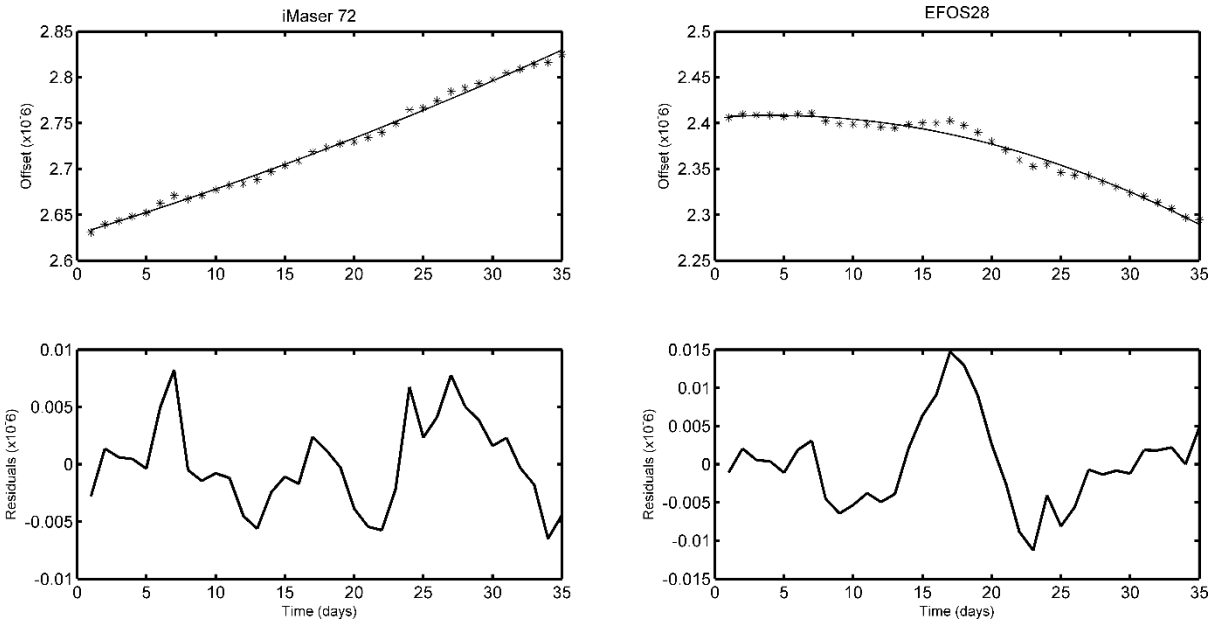

Figure 42. Time offset data for the EFOS28 and iMaser72 masers (top) and their least-squares residuals (bottom), (the units of the data in all the plots are in μs).

The residual plots in Figure 42 indicates parameters that are not modelled. The standard deviation of the iMaser72 and EFOS28 residuals are 0.0053 and 0.0060 μs, respectively with a clear pattern. This pattern could be related to a number of factors which are (1) local environment where maser clocks are stored, especially thermal variations. The microwave cavity of the maser is very sensitive to shock-vibrations, atmospheric pressure, DC magnetic

field and temperature fluctuations. A change of 1°C in the temperature of the microwave cavity can result in a frequency change of about 3.5×10^{-15} and this will result in fluctuation of the output frequency (Goujon et al., 2010). Hence, it is important to keep the storage room at a constant temperature to minimise frequency fluctuations. (3) Radio signals transmitted by the GPS satellites to the receiving station are adversely affected by ionospheric delay (Allan and Weiss, 1980), tropospheric delay (Böhm et al., 2015), multipath and satellite clock errors. A good example to illustrate the effect of ionospheric effect on GPS applications (in this case, timing applications) is given by Allan and Weiss (1980), they estimated that a Total Electron Content of about 10^{18} electrons per metre squared will result in the delay of about 54 ns at low latitude at 1.575 GHz C/A carrier frequency. This value can exceed 100 ns during periods of solar maximum. All these factors contribute towards the pattern that is evident on the residual plots.

Based on the observational data period used in this study, the calculated parameters indicate that both masers have a similar performance. The fractional frequency errors are -8.6554×10^{-14} and 7.9063×10^{-14} for the EFOS28 and iMaser72 maser respectively. An example is given to illustrate a practical use of the method described in Section 6.4. By applying Equation (5.8), a value of 5751.686454 Hz must be applied to EFOS28 to correct for the drift. The iMaser72 can be corrected by applying a value of Δf directly to the maser. If Δf is positive, a negative value of Δf must be applied to turn the clock around and the opposite applies. Note that these masers are corrected differently because they were manufactured by different companies. Differences in drift rates can be attributed to many factors, such as different oscillator properties that are used to generate the 5 MHz reference signal, thermal variations, supplied voltage fluctuations, crystal structure and impurities of the OCXO crystal or external factors that are discussed above (Prestage et al., 1995; Walsworth et al., 1990).

The individual short-term performances of the three maser clocks are depicted in Figure 43, where the iMaser72 has better performance over 1 s compared to the EFOS28 and EFOS6. Between 2 and 50 s, the reference signal (EFOS6) seems to have better performance while other clocks have similar performance within this range. The derived fractional frequency error values (Table 10), are in good agreement with the short-term results.

In general, both masers perform at an expected level required for radio astronomy and geodetic VLBI applications. The highly accurate timing systems contribute towards VLBI system integrity and the accuracy of the observations (whereas factors such as mechanical

errors, axis offset deformations due to temperature variations, etc. adversely affect system integrity) (Combrinck and Merry 1997). Hence, it is important for the observatories to keep track of their local timing systems to ensure that accurate observations are made.

Table 10. Statistical and clock parameters as determined through least squares.

Statistical Parameters	**EFOS28 (15 m)**	**iMaser72 (26 m)**
R Square	0.9768	0.9958
Standard Error (μs)	0.0059	0.0039
y-Intercept	2.4062 ± 0.0032	2.6289 ± 0.0021
b_1	0.0011 ± 0.0004	$0.00457 \pm 2.724\times10^{-4}$
b_2	$-0.0001 \pm 1.1013\times10^{-5}$	$3.3227 \pm 7.339\times10^{-6}$
Significance F-values	7.28×10^{-27}	8.98×10^{-39}
Calculated clock parameters		
Drift (s/d)	-7.4783×10^{-9}	6.8310×10^{-9}
Ageing (s/d/d)	-2.5096×10^{-10}	6.6456×10^{-11}
Fractional Frequency Error	-8.6554×10^{-14}	7.9063×10^{-14}

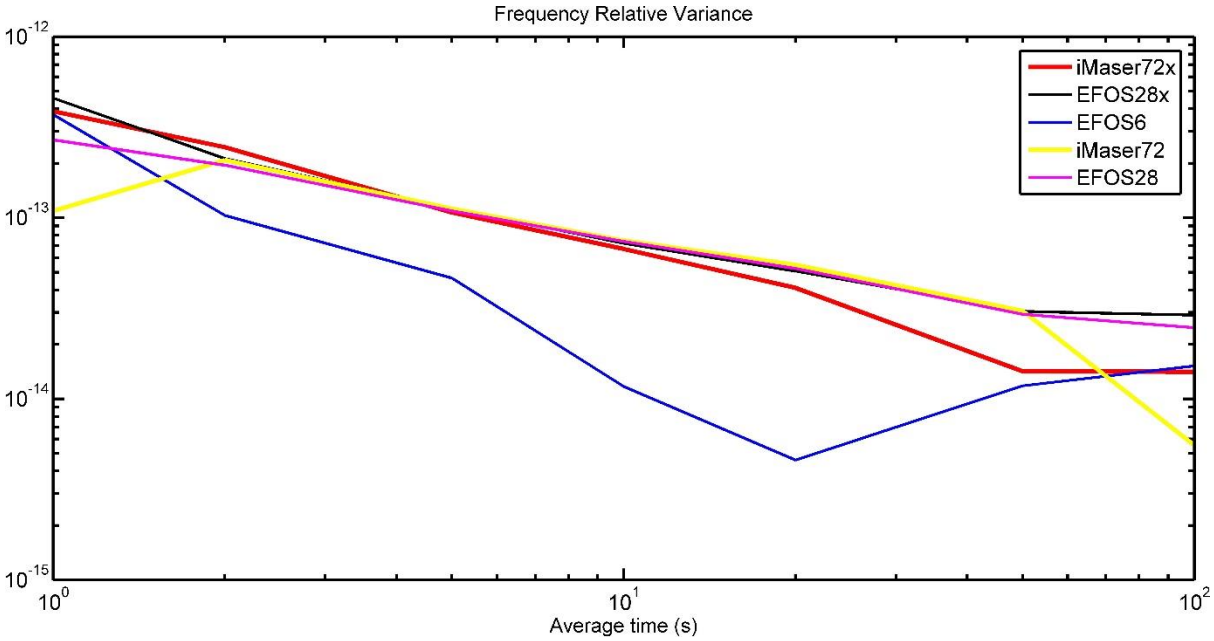

Figure 43. Individual frequency relative variance performance of each hydrogen maser clock.

5.6. Concluding remarks

The least-squares technique was used in this study to derive hydrogen maser clock parameters, enabling the management of maser clocks at HartRAO to function within predefined limits for VLBI applications. Small deviations that became apparent in the residuals require further investigations to determine the relationship between unmodeled components in the GNSS signal, which might be related to ionospheric or tropospheric effects. This could lead to the removal of the unexplained trend in the residuals. It was demonstrated that the two maser clocks currently used at HartRAO can maintain a relative stability of better than a picosecond (10^{-12}), which is important to geodetic VLBI and radio astronomy applications and our results compare favourably with the specifications by the manufacturers.

Chapter 6

A case study of the application of GPS to lunar laser ranging timing system at HartRAO

Abstract

The Hartebeesthoek Radio Astronomy Observatory is currently building a Lunar Laser Ranging station. This geodetic technique requires a good timing system to measure a round trip of laser photons from the telescope to the Moon and back to the telescope. We test the newly acquired timing system using examples of the Global Positioning System applications. Data in Receiver Independent Exchange Format was processed using GAMIT/GLOBK software. The results were compared against those derived from the Global Positioning System receivers that were integrated with a frequency standard from a hydrogen maser and a standard internal quartz. The results indicate that (i) the rubidium clock operates optimally and the clock drifted to within error margins of sub-centimetre level during the period of 2.5 seconds, (ii) the selected site for the permanent installation of the timing antenna has minimal multipath effect and (iii) we observed no improvement in Global Positioning System products derived from receivers that were integrated with different frequency standards.

6.1. Introduction

The Lunar Laser Ranging (LLR) technique provides valuable data that allows the study of Earth-Moon dynamic system. This technique involves transmitting short laser pulses (about 0.03 m) to the retro-reflectors located on the surface of the Moon. The laser pulses are reflected back to the transmitting telescope by the retro-reflectors. This allows distance between the telescope on Earth and the retro-reflector to be measured with high precision and accuracy. A detailed history on LLR can be found in Murphy (2013), modelling strategies and science contribution can be found in Hofmann et al., (2018), Hofmann and Müller (2018), Munghemezulu et al., (2016) and the references therein.

At the heart of the LLR technique, is the timing system responsible to measure time intervals of the laser pulses very precisely. A stable clock (with an accuracy of or better than 10^{-12}) is required to reduce systematic errors in the time interval measurements. The Global Positioning System (GPS) provides and guarantees a long-term frequency stability via time transfer techniques (Murphy, 2013). Other components of the LLR system that must be fully characterized include the event timer, photon detectors and internal system calibration (reference point for the telescope and cable delays). This ensures that the millimetre ranging accuracy is achieved and time bias values are reduced. For example, the Apache Point Observatory Lunar Laser Ranging Operation (APOLLO) has developed an absolute calibration system capable of improving data to the level of 2 mm. They have recently replaced the LLR reference timing system i.e., TrueTime XL-DC (GPS-disciplined) with a Cesium clock. These changes are anticipated to improve LLR data quality moving forward (Adelberger et al., 2017).

The stability of the timing system on GPS receivers is very important to ensure that accurate observations are measured. This ensures that the receiver can lock and track GPS satellites (Mannermaa et al., 1999). Clock instability can lead to a loss of tracking of satellites and this can lead into Dilution of Precision (DOP) effect, where the accuracy of the position of the receiver can be affected. The most important characteristics of the local clock is that its bias relative to the GPS–time changes smoothly, this will allow a smooth function to predict the clock very accurately over a short period of time (at a level of seconds) (Misra, 1996). Therefore, an optimal functioning clock can drift over time but the drift should be predictable over short periods and a clock not functioning optimally will be unpredictable over short intervals and it will be characterised high levels of phase noise.

On average, laser pulses take about 2.5 seconds round trip period from the Earth to the Moon and back. To achieve sub-millimetre level precision, a reference clock must maintain relative frequency stability of 10^{-12} during this period (Murphy, 2013). Since most reference timing systems for the LLR stations are steered by GPS, it is therefore important for the GPS antenna to have minimal multipath effect, be installed on a stable pier to minimise positional changes of the antenna. This is to ensure that the GPS-disciplined timing system is adjusted correctly from the algorithm that constantly steers the clock. Combrinck (2017) indicated that in the future, most geodetic techniques at the Hartebeesthoek Radio Astronomy Observatory (HartRAO) will be connected to the 5 MHz standard frequency from the hydrogen maser to ensure optimal accuracy for all subsystems. He also stated that highly accurate clocks with a fractional frequency of 10^{-18} should be installed at geodetic sites to allow for Chronometric geodesy studies, for more information readers should consult Combrinck (2017) and the reference therein on this topic.

HartRAO is currently building an LLR station based on 1 m telescope donated by the Observatoire de la Côte d' Azur (OCA) (Combrinck and Botha, 2013; Combrinck, 2011a). This new LLR station will contribute significantly to the International Laser Ranging Service (ILRS) by providing ranging measurements from a strategic location (i.e., the Southern Hemisphere in Africa) and this will constrain geometrical errors in applications such as orbit determination of the Moon. The main goal of this LLR station is to achieve ranging measurement error at sub-centimetre level and timing system plays a crucial role in ensuring accurate measurements are made.

This study aims to preliminary test the performance of the newly acquired 4380A rubidium timing system for the new LLR station at HartRAO. An experiment is designed to test the timing system if it functions optimally in a thermally controlled room. A 5 MHz sine wave signal from 4380A is tested by locking it to Leica GR10 receiver and logging Receiver Independent Exchange Format (RINEX) data. The same setup is applied, but using 5 MHz from a hydrogen maser clock to a second Leica GR10 receiver and a third Leica GR10 is allowed to run freely. To limit systematic errors, one antenna is used for the three receivers and the signal from the antenna is split into three identical signals. The RINEX data from all the receivers are logged concurrently and analysed using GAMIT/GLOBK software (Herring et al., 2010).

6.2. Data analysis

6.2.1. Experimental description

Experimental design is depicted in Figure 44, the Leica AR25 antenna was mounted on a stable pier to minimise noise in positioning determination. Signals from the antenna were divided into three identical signals using dedicated GNSS signal splitter. The resulting identical signals were connected to three identical Leica GR10 receivers. One receiver made use of internal clock and we refer to this as free-run mode (normally the internal timing system make use of quartz oscillators), the second receiver was locked to 5 MHz from the rubidium clock and the third receiver was locked to 5 MHz from the hydrogen maser (see Table 11 for manufacturer specifications of Allan deviation for the hydrogen maser and rubidium clock). The receivers are set to minimise hardware dependent biases in the observed variables by: (1) observing the same number of satellites, (2) used the same version of firmware, and (3) are kept in the same controlled environment. Temperature data in the controlled room is monitored using a temperature sensor (SEN0148) with an accuracy of ±0.5℃ and it is kept to within 2-3℃.

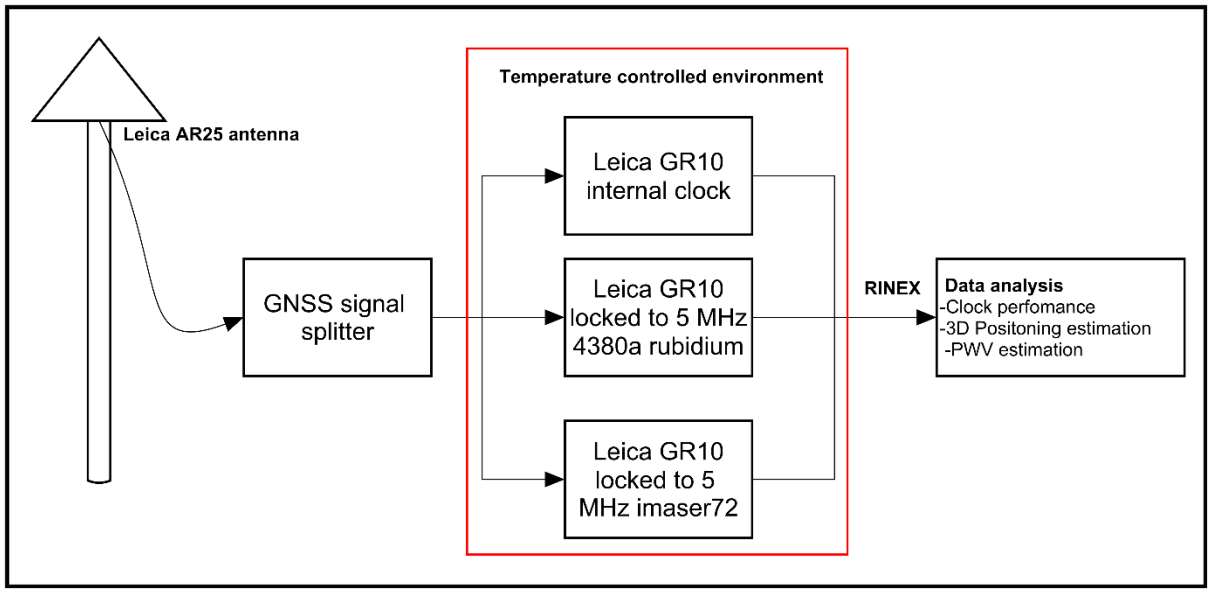

Figure 44. Experimental setup and GNSS data products derived for analysis.

Table 11. Summary of the specifications of high performing clocks used in the experiment as given by the manufactures.

Time (seconds)	iMASER7	Rubidium 4380A
	Allan deviation	Allan deviation
1	1.26×10^{-13}	6×10^{-13}
10	1.86×10^{-14}	8×10^{-13}
100	4.05×10^{-15}	8×10^{-13}
1000	1.44×10^{-15}	6×10^{-13}
10 000	2.01×10^{-15}	6×10^{-13}

6.2.2. GPS data processing

Selected stations included in the processing are depicted in Figure 45. The stations were selected based on data availability during the experiment and the fact that double differencing approach of processing the data was selected. The small network consist of permanent operating stations from the International GNSS Services (IGS) network and the National Geo-Spatial Information (NGI) Trignet network. Double differencing processing strategy as implemented by GAMIT/GLOBK 10.6 software (Herring et al., 2010) was applied to data spanning 31 days. This technique minimises errors introduced by the ionosphere compared to Precise Point Positioning (PPP) technique (Herring et al., 2010). Table 12 gives a summary of the parameters or models used in the data processing. The GAMIT software uses psuedorange and carrier phase measurements to estimate station positions, atmospheric zenith delays, station clock parameters and Earth Orientation Parameters (EOP) using a least-square approach. However, in this experiment, EOP values were not estimated. The GLOBK software used kalman filter to combine and compute station velocities within a defined reference frame (Herring et al., 2010; Banerjee and Bürgmann, 2002). The precision of station coordinates can be assessed by the weighted root mean square (WRMS) repeatability that is given by the weighted quadratic average error as (Blewitt, 1989):

$$WRMS = \left(\frac{\frac{1}{n-1}\sum_{i=1}^{n}\frac{(R_i - R_m)^2}{\sigma_i^2}}{\sum_{i=1}^{n}\frac{1}{\sigma_i^2}} \right)^{1/2} . \qquad (6.1)$$

In Equation(6.1), n is the number of occupation days, R_i is the estimated coordinate and σ_i is the formal error (standard deviation) of the coordinates for day 'i', and R_m is the weighted mean of the coordinates of station.

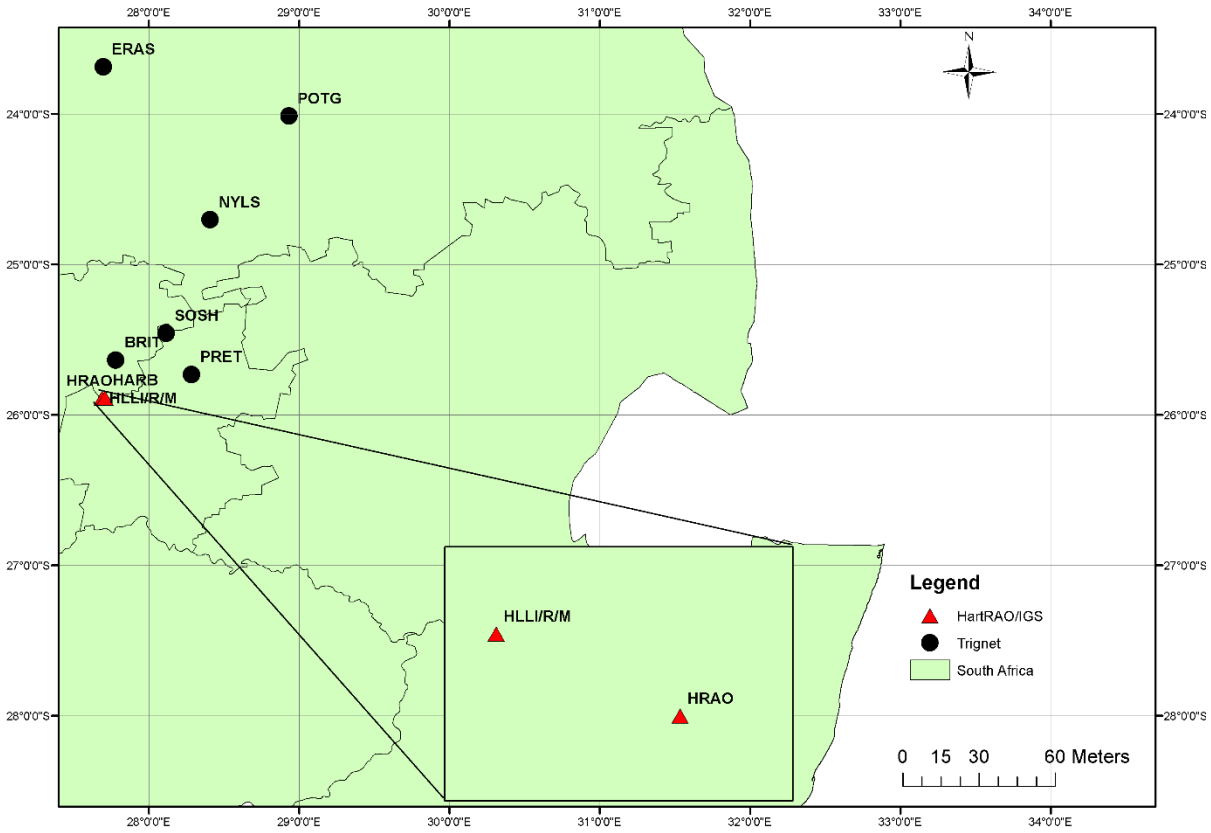

Figure 45. Map illustrating selected GNSS stations that were included in the data processing.

Table 12. Summary of the parameters used during data processing in GAMIT/GLOBK software.

Models Applied	**Description**
Reference Frame	ITRF 2014 (Altamimi et al., 2016)
Ionospheric delay	Linear combination
Multipath mitigation	Cut-off elevation angle: 10º
Mapping Function	Veinna mapping function (Böhm et al., 2006)
Ocean tide loading	FES2004 (Letellier, 2005) and CSR4 (Egbert and Ray, 2003)
Atmospheric loading	MIT
IAU nutation model	Herring et al., 2002
Ambiguity solution	Wide-Line LC
Earth Orientation Parameters	IERS2010
Epoch rate	30 second
Orbits	MIT Final

The GAMIT software also have capabilities to estimate Zenith Total Delay (ZTD) using piecewise-linear model. Onsite meteorological parameters (pressure, temperature and humidity) were measured using MET4 unit and used to correct a priori Zenith Hydrostatic Delay (ZHD) values that are initially estimated from mapping function. Zenith Wet Delay (ZWD) is determined as

$$ZWD = ZTD - ZHD, \tag{6.2}$$

and integrated PWV is calculated by converting ZWD values as in Equation (2) below. The term $\prod(T_m)$ represents a dimensionless quantity given by the mean weighted temperature of the atmosphere (Bai and Feng, 2003; Li et al., 2010).

$$PWV = \prod(T_m) ZWD. \tag{6.3}$$

6.3. Results and discussion

6.3.1. Data quality assessment

The daily one-way phase residuals root-mean-square (RMS) values derived from RINEX data are depicted in Figure 46. Higher RMS values (more than 9 mm) indicate poor tracking receiver, a high multipath environment or severe weather conditions and lower RMS (less than 9 mm) values would indicate better performing receiver with better environmental conditions (Herring et al., 2010). During severe weather conditions, the RMS values would only increase for that particular day, while errors from poor performing receiver and higher multipath environment would have a consistent RMS values over time. For example, the NGI-Trignet stations: POTG and SOSH indicate a consistent higher RMS values ranging from 10 mm to 15 mm during the period of 31 days. Figure 47 depicts RMS values as a function of elevation angle of the satellites, it is expected that observations at lower elevation would have higher RMS values and less errors at zenith. It is clear from Figure 47 that both POTG and SOSH stations are affected by high multipath environment, since the stations indicate slow decrease in RMS as a function of the elevation angle. Our experimental site station (HLLI, HLLR, HLLM) to host a permanent timing antenna for the 4380A timing system indicate less influence of multipath. The daily RMS values range between 7 and 6 mm and the elevation dependent

errors are less than 12 mm below 20º, this confirms the study done by Munghemezulu et al., (2016b).

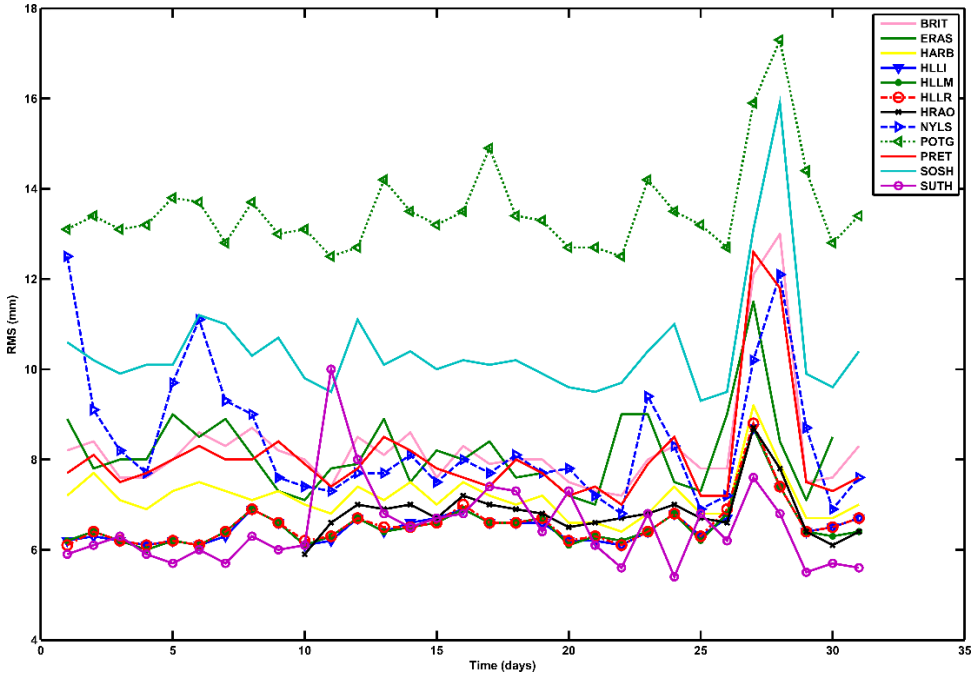

Figure 46. Daily assessment of the station performance in terms of data quality of the observations made by the receiver. The jump on day 27 could be associated with severe weather conditions.

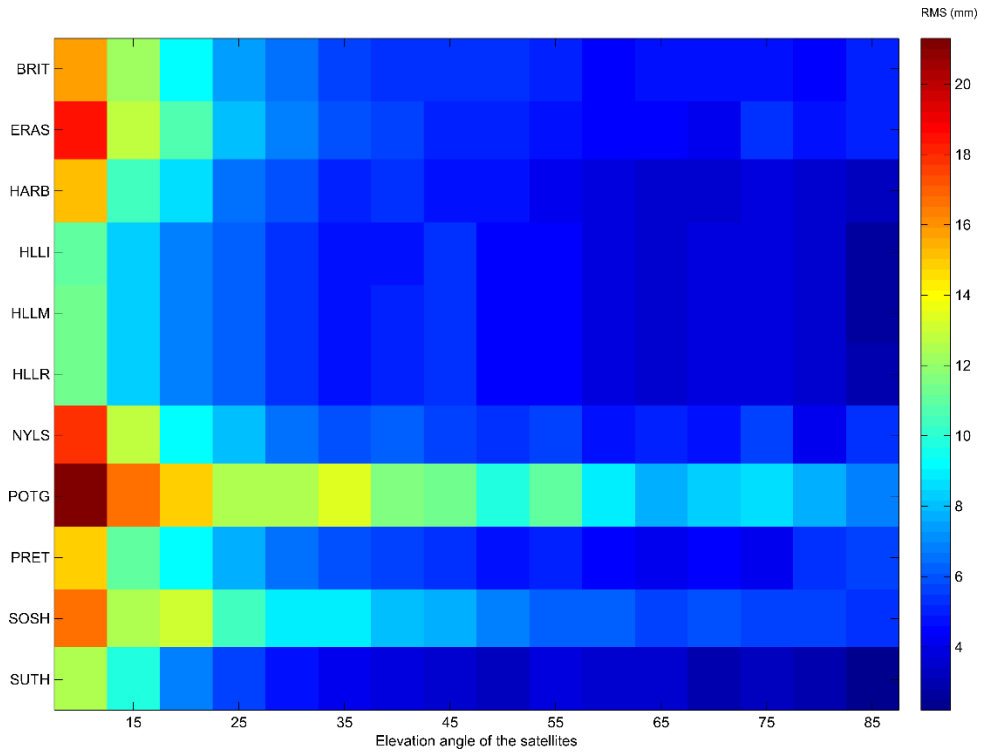

Figure 47. Elevation dependent RMS values as observed by GPS stations for day number 106 (this corresponds to day 1 in Figure 46). Stations with higher RMS values from low to high elevation angles indicate higher multipath environment.

6.3.2. Receiver clock performance

Clock offsets for the experimental stations are depicted in Figure 48. The Savitzky-Golay (S-G) filter was fitted in the data to assess the level of noise in the time series by computing standard deviation from the residuals. The S-G filter was proposed by Savitzky and Golay (1964). This method is based on a local least-squares polynomial approximation and it has been applied successfully in many applications (e.g., Chen, 2004). The S-G filter preserves the structure of the signal, while the high-frequency components are reduced to zero (Schafer, 2011). The S-G fitter signal represents an ideal signal with reduced noise; the difference between S-G filter and the actual signal indicate residual or noise in the data.

The HLLI and HLLR receivers indicate non-linear drift, which is due to the receiver adjusting itself to align it with the GPS time and maintain the deviations to within microsecond level. This is necessary to obtain millimetre accuracy in a baseline vector (Herring et al., 2010). The rubidium 4380A steering the Leica GR10 receiver (HLLR) is also steered by GPS, hence non-linear behaviour of the clock. However, the clock has better phase noise level by a factor

of 10 when compared to free-running Leica GR10 receiver (HLLI). While the maser locked Leica GR10 (HLLM) has better stability and less noise. The maser clock behaviour is very predictable over long periods, while GPS steered clocks are very difficult to predict over long periods.

Clock drift is one of the important characteristics of the clock during ranging. The ideal clock should not over drift during the period of 2.5 seconds. For example, our timing system (HLLR) in Figure 48 indicates a drift rate of 2.958×10^{-8} seconds between 6×10^{4} and 7.5×10^{4} seconds, this drift rate equates to 2.958×10^{-12} frequency error in 1×10^{4} seconds or 7.396 pico-seconds or 2.22 mm measurement error in 2.5 seconds. This proves that this timing system can achieve the overall objective of sub-centimetre accuracy measurement. The residuals for the HLLI fall well within 1 m, at 1 second this would translate to frequency error better than 1×10^{-10}. Residuals for HLLR at 0.1 m and HLLM at 0.02 m translate to frequency error better than 1×10^{-11} and 1×10^{-12} respectively at 1 second. These frequency error values compare favourably to the values listed in Table 11.

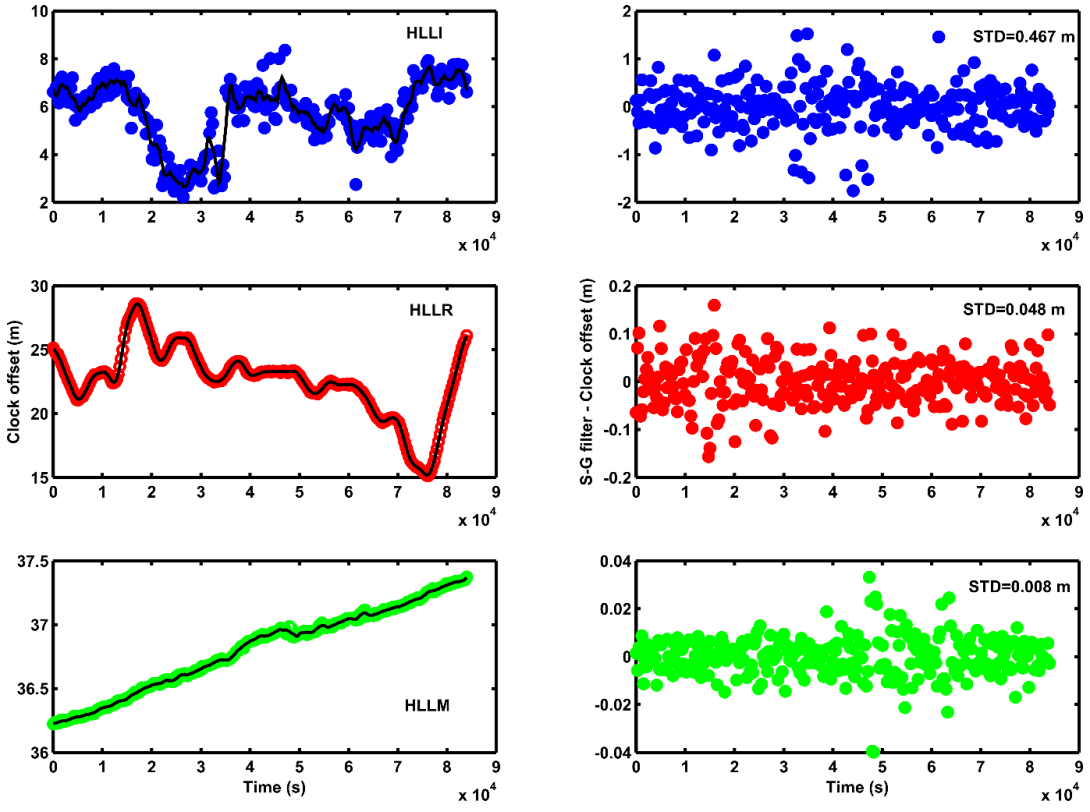

Figure 48. Variation of clock offset between GPS time and station time for day number 109. The hydrogen maser locked receiver (HLLM) indicate better performance between rubidium locked Leica GR10 receiver (HLLR) and a free running Leica GR10 receiver. Clock offsets are in meters, one microsecond (10^{-6}) equates to 300 m.

6.3.3. Positioning

The WRMS results are summarized in Table 13. All stations maintain WRMS of less than 1.1 mm in the north and east components, while the vertical component varies from 1.1 mm to 4.5 mm. The experiment site stations (HLLI, HLLR and HLLM) all maintained millimetre accuracy regardless of the accuracy of the timing system. This is mainly due to the fact that GAMIT observables are double differenced. The differences between satellites completely cancels the phase variations of the receiver clocks. However, the accuracy of the receiver to time-tag the arrival of the GNSS signals plays a crucial role in the accuracy of the position since the satellite and station positions need to be evaluated at the correct time. The range rate is 1 km/s, so a clock that has 1 µs error in the time tag will result in 1 mm error in the position. Therefore, as shown in Section 5.3.2, the timing systems used in this experiment are all better than 1 µs.

Table 13. Summary of the positioning statistics between the GPT2 and VMF1 mapping functions.

Station Code	**Repeatability (wrms-mm)** *VMF1 mapping function*			**Repeatability (wrms-mm)** *GPT2 mapping function*		
	North	**East**	**Up**	**North**	**East**	**Up**
POTG	1.1	1.1	4.0	1.2	1.1	4.0
ERAS	1.0	0.8	2.9	1.1	0.8	2.9
NYLS	0.9	0.6	3.4	0.9	0.7	3.4
BRIT	1.0	0.8	2.3	1.0	0.8	2.3
PRET	1.0	0.6	4.3	1.0	0.6	2.8
SOSH	0.9	0.7	4.5	1.0	0.7	3.6
SUTH	0.8	0.6	1.8	0.8	0.6	1.8
HRAO	0.5	0.7	1.1	0.5	0.7	1.1
HARB	0.8	0.4	1.3	0.8	0.4	1.3
HLLI	0.7	0.6	1.8	0.7	0.6	2.1
HLLR	0.7	0.6	1.9	0.7	0.6	2.1
HLLM	0.7	0.6	1.8	0.7	0.6	2.1

Stations from NGI-Trignet network indicate almost twice the noise level in the vertical component when compared to the IGS and experimental stations. This increase in noise levels

for the NGI-Trignet stations could be attributed to high multipath effect at the station, which can potentially affect station positions (King and Watson, 2010) or local instabilities at the site. Figure 49 depicts comparison of our LLR timing antenna installation with the International GNSS Services (IGS) site: HRAO, both north and the east components are similar, while the vertical component of the IGS site is very stable compared to the LLR installation (i.e., the experimental site). The differences can be attributed to the type of installations. The IGS station is installed on a pier that is mounted on the bedrock and the experimental antenna was installed on top of the LLR control room. The two stations are in close proximity of about 100 m, therefore the vertical instabilities on the LLR control room may be due to thermal expansions of the concrete bed for the LLR control room as well as the material of the control room. These differences are estimated to be within 2 mm. This could also explain high level of noise in the vertical component of NGI-Trignet stations, since most of the stations are installed on top of buildings.

The impact of a mapping function on a millimetre station position estimation can also be seen, where the VMF1 mapping function generally improves the noise in the vertical component compared to the GPT2 mapping function. This effect can be noted on the experimental stations with high accurate and stable frequencies references. However, there is no noticeable improvements in station coordinates with regard to the use of highly accurate stable frequencies from the hydrogen maser and the 4380A rubidium clocks for our experimental stations (HLLI, HLLR and HLLM).

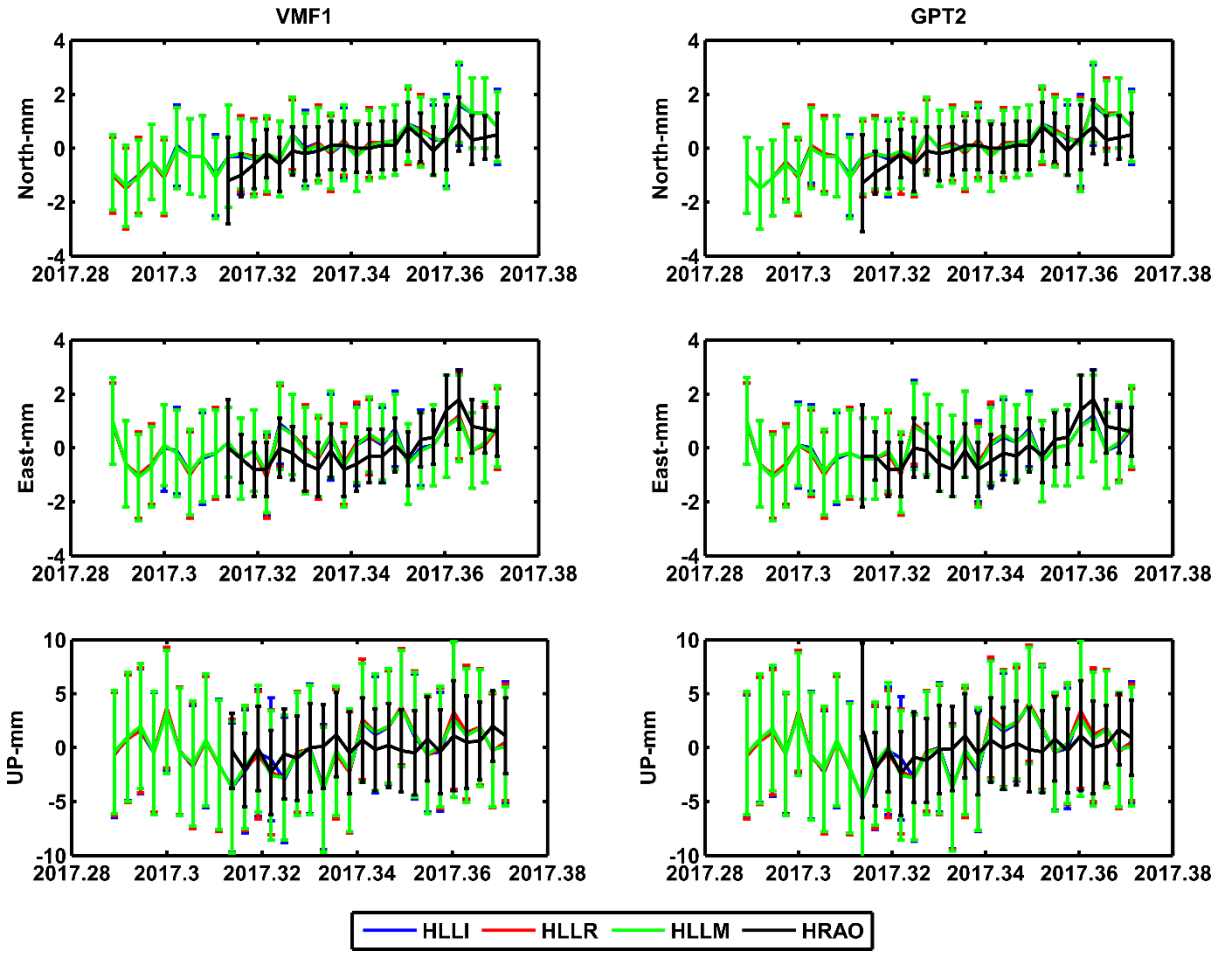

Figure 49. Comparison of station positions from our experimental results. It can be seen that Leica GR10 requires no external reference frequency since similar results are achieved when it is locked to external stable frequencies. The HRAO station indicates a stable vertical component compared to the LLR installation for this experiment.

6.3.4. Integrated Precipitable Water Vapor estimates

The Integrated Precipitable Water Vapor (IPWV) was estimated at an interval of two hours for experimental stations and IGS station: HRAO. The IGS station is within 100 m from the experimental site, the height difference between the stations is about 3 m. The results from thr experimental site indicate no significant difference between the estimated IPWV values for HLLI, HLLR and HLLM stations. This suggests that the improved frequency stability applied to the Leica GR10 receiver had no effect on IPWV estimates. However, the IGS site: HRAO indicate an over estimation of IPWV to within 1 mm when compared to the experimental site, even though the structure of the signal is preserved in both stations. Mapping function models (VMF1 and GPT2) had no effect on estimating IPWV for all stations. For

geodetic/astronomical site characterization, a high spatial resolution of GPS observations should be considered to eliminate instrumentation biases that might be related to the scaling effect as observed in Figure 50.

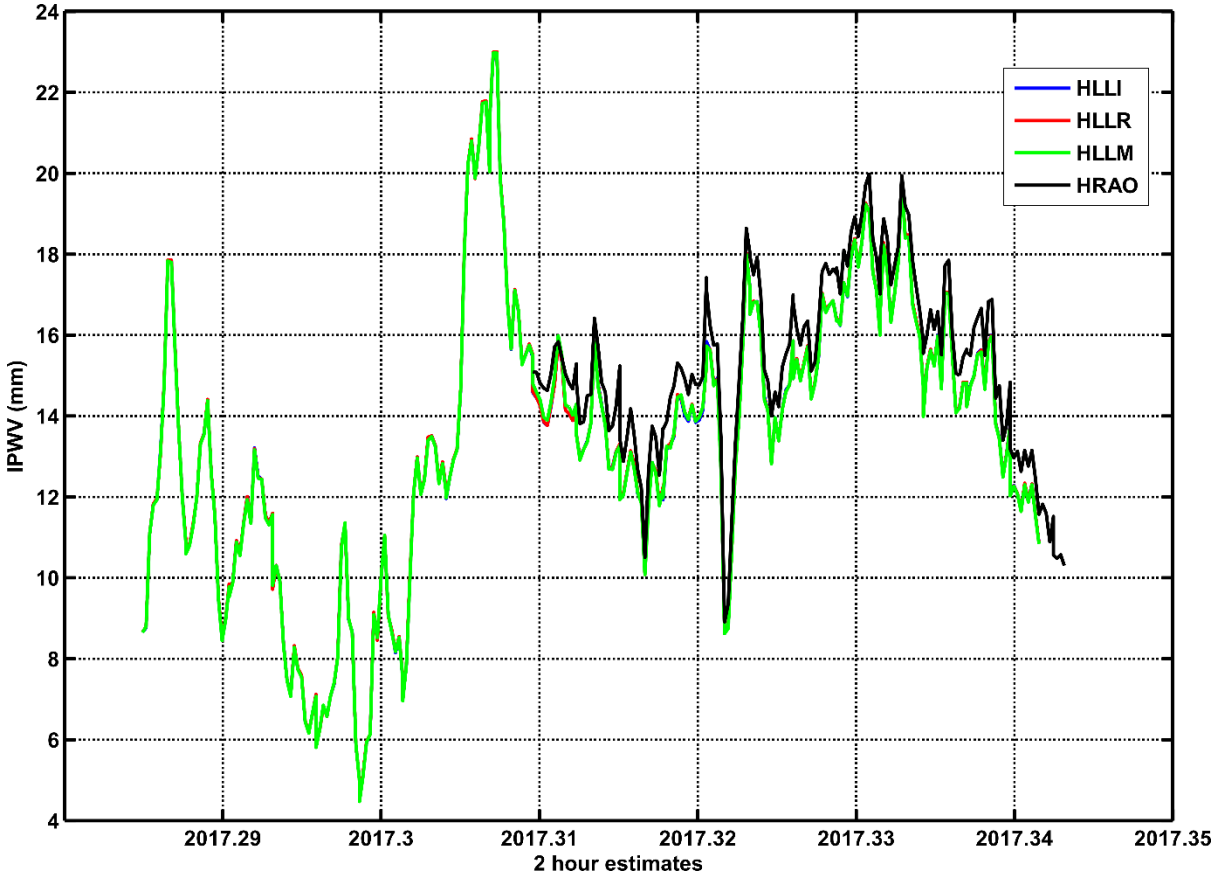

Figure 50. Estimates of IPWV for the three experimental stations, IGS station: HRAO was included as a reference station. The IGS site has an ellipsoidal height (WGS84) of 1414.152 m and the experimental site has an ellipsoidal height of about 1411.8019 m; the two sites are less than 100 m apart.

6.4. Concluding remarks

HartRAO is currently building an LLR station that will support scientific community especially the ILRS. The aim of this study was to test the newly acquired timing system for the LLR station at HartRAO. To accomplish this task, an experiment was designed, where 5 MHz from rubidium and hydrogen maser were integrated to two GNSS receivers and a third receiver made use of an internal clock. The RINEX data was processed using GAMIT/GLOBK software. The results indicate that the rubidium clock operates optimally and the clock drifted to within error margins of sub-centimetre level during the period of 2.5 seconds. The selected site for the permanent installation of the timing antenna has minimal multipath effect and it is recommended that the timing antenna be installed on a dedicated stable pier and lastly, no improvement were observed in Global Positioning System products derived from receivers that were integrated with different frequency standards.

Chapter 7

Summary

7.1. General conclusion

The new LLR station currently in development at HartRAO will be the only station in Africa to range to the retro-reflectors on the surface of the Moon once completed. It will also improve the current ILRS network by proving data that are important in improving the accuracy of the Moon's orbit parameters and reduce network dependent biases. This new LLR station will contribute to both local and global communities to meet the scientific objectives of the currently growing space science endeavours by many countries as well as supporting socio-economic developments. Data products derived from highly technical space geodetic techniques such as LLR have indirect or direct benefits to the society; hence, the LLR project at HartRAO has received local support and international support from organisations such as NASA (USA) and OCA (France). The 1.54 m Cassegrain telescope that is being utilise by HartRAO was donated by OCA. The telescope has since been refurbished but not integrated with other subsystems and the mirrors are being cleaned and awaiting recoating. There are a number of factors that must be taken into consideration during the implementation of the LLR station. One very important consideration is to ensure that highly accurate timing subsystems are implemented (sub-picosecond level) to minimise local systematic errors which is the premise of the present dissertation.

7.2. Scientific contribution

This thesis focused on the development of the timing subsystem for the new LLR station at HartRAO. The timing system is an important component of any geodetic technique and ensures that accurate observations are made. A summary of the scientific contributions based on the objectives are given below.

Objective 1

Review the LLR technique and compare the observed and calculated ToF components in order to understand the O – C residuals and their error sources.

A review of the LLR technique and the timing systems in light of the new LLR station at HartRAO was written and published to complete this objective. The difficulties associated with ranging to the Moon were highlighted and the emphasis was on factors that contribute to range bias, as these must be incorporated in the LLR analysis software.

There are a number of factors that must be taken into consideration during the implementation of the LLR analysis software. The first step is to ensure that highly accurate timing subsystems are implemented (sub-picosecond level) to minimise local systematic errors. The delay induced by the environment can be modelled with current existing algorithms to a high level of confidence.

The LLR simulator was developed and it allows simulation of different parameters such as station deformation due to Earth tides, photon delay due to the atmospheric effect at different pointing elevation angles, Moon's libration and phase angles are important factors that contribute impact on the pointing model of the telescope. Clock jitter calculations were included to estimate phase noise of the timing system being used.

Objective 2

Apply techniques to visualise and minimise the multipath effect on GPS timing antennas for the LLR station.

A technique to visualize multipath was developed and implemented on the GPS timing antenna to map spatial location of multipath and its variation over time. This is to aid in understanding the distribution of multipath before an installation for the timing antenna at HartRAO for LLR timing reference. Multipath effect can affect GPS positioning, a change in this position can affect reference time for the rubidium clock resulting in inaccurate measurements of LLR ToF. The developed technique can be applied at different times during the operation of the LLR station to characterise sources of multipath.

Objective 3

Design an integrated time/frequency for the LLR station.

In terms of the LLR timing system, the rubidium 4380A clock, which has an Allan deviation of better than a picosecond at 1 s and a very low phase noise of -110 dBc at 1 Hz was acquired and integrated in the LLR control room. Furthermore, the photon detection subsystem has low cumulative RMS jitter errors. The maximum total estimated random error per photon contributed by the two subsystems is estimated to be 45 mm. To achieve 1 mm ranging precision, a high photon return rate ought to be achieved. The estimated return rate of 5 photons per minute implies that the LLR must range for longer than 30 minutes in order to collect adequate photons to statistically achieve sub centimetre ranging precision during calculation of the normal points. Ranging periods have been identified using meteorological data that will minimise thermal deformations of the telescope and to ensure the best performance of the electronic systems that are exposed to the ambient air.

Objective 4

Evaluate the performance of the integrated time/frequency system for the LLR station.

HartRAO is currently building an LLR station that will support scientific community especially the ILRS. The aim of this study was to test the newly acquired timing system for the LLR station at HartRAO. To accomplish this task, an experiment was designed, where 5 MHz from rubidium and hydrogen maser were integrated to two GNSS receivers and a third receiver made use of an internal clock. The RINEX data was processed using GAMIT/GLOBK software. The results indicate that the rubidium clock operates optimally and the clock drifted to within error margins of sub-centimetre level during the period of 2.5 seconds. The selected site for the permanent installation of the timing antenna has minimal multipath effect and it is recommended that the timing antenna be installed on a dedicated stable pier and lastly, no improvement were observed in Global Positioning System products derived from receivers that were integrated with different frequency standards.

Objective 5

Analyse the performance of the on-site hydrogen maser clocks as they act as a crucial backup source for the LLR station and as independent calibrators of fractional frequency stability.

The performance of the hydrogen maser clocks that are available at the observatory was determined by the least-squares technique to derive hydrogen maser clock parameters. This analysis is essential as it enables the management of maser clocks at HartRAO to function within predefined limits for VLBI applications. Small deviations that became apparent in the residuals require further investigations to determine the relationship between unmodeled components in the GNSS signal, which might be related to ionospheric or tropospheric effects. This could lead to the removal of unexplained trend in the residuals. It was demonstrated that the two maser clocks currently used at HartRAO can maintain a relative stability of better than a picosecond (10^{-12}), which is important to geodetic VLBI and radio astronomy applications and our results compare favourably with the specifications by the manufacturers. As a result, the LLR timing subsystem will have the (added) opportunity to incorporate hydrogen maser clock stable frequency in case of malfunction of the 4380A rubidium timing system.

7.3. Limitation of the research

The project to develop the LLR station at HartRAO is sub-divided into sections/sub-sections. These sections include but are not limited to the timing subsystem, development of the LLR telescope steering and control software and thermal monitoring system (to be used in pointing adjustments and pointing map). These subsystems must be integrated to ensure that the telescope operate optimally. The actual performance of the telescope can only be measured if the telescope is fully integrated. In this regard, given that the telescope components have not yet been fully integrated the performance of the timing system on the range measurements (i.e., time delay measurements) can only be done if the integration is completed. Notwithstanding this limitation, the results of independent tests of the timing system reported in the thesis gives credence to robustness once all the LLR components are integrated.

7.4. Future perspectives

The LLR project at HartRAO is an important project both locally and internationally. Therefore, the completion of this project should be the main priority for the observatory. This station will have a positive impact to the scientific community and society. The strategic location of the LLR station (in the southern hemisphere), allows for the geometrical improvements in the ILRS network thereby resulting in an improved Earth-Moon physical parameters.

Further studies on the performance of the timing system should be carried out once the full integration of the telescope is completed. It is only then that the ranging accuracy of less than 1 cm that the station anticipate can be realised, evaluated and compared with other stations such as OCA and APOLLO.

The impact of this thesis is that it creates a foundation for the future development and integration of other subsystems such as photon detection subsystem. Other future projects that will be supported by this research include time transfer to satellites or space station or and stable distribution of time and frequency from a single source to other geodetic techniques. Currently, these topics remain subject of debate and they are discussed in Elisa et al., (2017).

References

Adelberger, E.G., Battat, J.B.R., Birkmeier, K.J., Colmenares, N.R., Davis, R., Hoyle, C.D., Huang, L.R., McMillan, R.J., Murphy Jr, T.W., Schlerman, E. and Skrobol, C., 2017. An absolute calibration system for millimeter-accuracy APOLLO measurements. *Classical and Quantum Gravity*, *34*(24), p.245008.

Allan, D.W., 1987. Time and frequency (time-domain) characterization, estimation, and prediction of precision clocks and oscillators. *IEEE transactions on ultrasonics, ferroelectrics, and frequency control*, *34*(6), pp.647-654.

Allan, D.W. and Weiss, M.A., 1980. *Accurate time and frequency transfer during common-view of a GPS satellite* (pp. 334-346). Electronic Industries Association.

Alley, C.O., 1983. Laser ranging to retro-reflectors on the Moon as a test of theories of gravity. In *Quantum Optics, Experimental Gravity, and Measurement Theory* (pp. 429-495). Springer US.

Altamimi, Z., Collilieux, X. and Métivier, L., 2011. ITRF2008: an improved solution of the international terrestrial reference frame. *Journal of Geodesy*, *85*(8), pp.457-473.

Altamimi, Z., Sillard, P. and Boucher, C., 2006. CATREF Software: Combination and Analysis of Terrestrial Reference Frames. Technical Manual, IGN, France. 2006. Available from: http://grgs.obs-mip.fr/en/content/download/303/2351/file/CATREF-1.pdf

Altamimi, Z., Rebischung, P., Métivier, L. and Collilieux, X., 2016. ITRF2014: A new release of the International Terrestrial Reference Frame modeling nonlinear station motions. *Journal of Geophysical Research: Solid Earth*, *121*(8), pp.6109-6131.

Andrews, L.C. and Phillips, R.L., 2005. Laser Beam Propagation through Random Media, 2nd ed., Bellingham, Washington. SPIE-The International Society for Optical Engineering Press, 9pp.

Bai, Z. and Feng, Y., 2003. GPS water vapor estimation using interpolated surface meteorological data from Australian automatic weather stations. *Journal of Global Positioning Systems*, *2*(2), pp.83-89.

Banerjee, P. and Bürgmann, R., 2002. Convergence across the northwest Himalaya from GPS measurements. *Geophysical Research Letters*, *29*(13).

Barker, E.S., Calame, O., Mulholland, J.D. and Shelus, P.J., 1975. Improved coordinates for Lunokhod 2 based on laser observations from McDonald Observatory. In *Space Research XV* (pp. 71-74).

Bastiaanssen, W.G., Molden, D.J. and Makin, I.W., 2000. Remote sensing for irrigated agriculture: examples from research and possible applications. *Agricultural water management*, *46*(2), pp.137-155.

Berquist, R.W and Collins, R, 2004. *Temperature compensation of a rubidium frequency standard*. U.S. Patent 6,710,663.

Bilich, A. and Larson, K.M., 2007. Mapping the GPS multipath environment using the signal-to-noise ratio (SNR). *Radio Science*, *42*(6).

Blewitt, G., 1989. Carrier phase ambiguity resolution for the Global Positioning System applied to geodetic baselines up to 2000 km. *Journal of Geophysical Research: Solid Earth*, *94*(B8), pp.10187-10203.

Botai, C.M., Combrinck, L. and Botai, J.O., 2015. Satellite laser ranging measurements in South Africa: Contributions to Earth system sciences. *South African Journal of Science*, *111*(3-4), pp.1-9.

Botai, M.C. and Combrinck, L., 2011. Investigating the accuracy of gravity field models using Satellite Laser Ranging data. *South African Journal of Geology*, *114*(3-4), pp.535-540.

Böhm, J., Möller, G., Schindelegger, M., Pain, G. and Weber, R., 2015. Development of an improved empirical model for slant delays in the troposphere (GPT2w). *GPS Solutions*, *19*(3), pp.433-441.

Böhm, J., Niell, A., Tregoning, P. and Schuh, H., 2006. Global Mapping Function (GMF): A new empirical mapping function based on numerical weather model data. *Geophysical Research Letters*, *33*(7).

Botteron, C., Dawes, N., Leclère, J., Skaloud, J., Weijs, S.V. and Farine, P.A., 2013. Soil moisture & snow properties determination with GNSS in alpine environments: Challenges, status, and perspectives. *Remote Sensing*, *5*(7), pp.3516-3543.

Buonsanto, M.J., 1999. Ionospheric storms—A review. *Space Science Reviews*, *88*(3-4), pp.563-601.

Chen, J., Jönsson, P., Tamura, M., Gu, Z., Matsushita, B. and Eklundh, L., 2004. A simple method for reconstructing a high-quality NDVI time-series data set based on the Savitzky–Golay filter. *Remote sensing of Environment*, *91*(3-4), pp.332-344.Chernyshev, I.N., Belyaev, A.A. and Mishagin, K.G., 2012. Error in measurement of frequency instability by method of three oscillators. *Measurement Techniques*, *55*(7), pp.792-799.

Chew, C.C., Small, E.E., Larson, K.M. and Zavorotny, V.U., 2015. Vegetation sensing using GPS-interferometric reflectometry: theoretical effects of canopy parameters on signal-to-noise ratio data. *IEEE Transactions on Geoscience and Remote Sensing*, *53*(5), pp.2755-2764.

Combrinck, L., 2017. Aspects of Time as It Relates to Space Geodesy. In *The Science of Time 2016* (pp. 243-252). Springer, Cham.

Combrinck, L., 2014, March. Space geodesy, VLBI and the fourth pillar of geodesy; spacetime curvature'. In *8th IVS General Meeting" VGOS: The New VLBI Network" Shanghai (China)* (pp. 2-7).

Combrinck, L. and Botha, R., 2014. Challenges and progress with the development of a lunar laser ranger for South Africa. International Laser Ranging Services, 11-15 November, 13-0504.

Combrinck, L., 2013. General relativity and space geodesy. In *Sciences of Geodesy-II* (pp. 53-95). Springer Berlin Heidelberg.

Combrinck, L. and Botha, R., 2013, November. Challenges and progress with the development of a Lunar Laser Ranger for South Africa. In *Proceedings of the 18th international workshop on laser ranging: pursuing ultimate accuracy and creating new synergies* (pp. 11-15).

Combrinck, L., 2012, December. A comparison of general relativity theory evaluations using VLBI and SLR: Will GGOS improve these results. In D. Behrend and K. Baver eds.,, *IVS 2012 General Meeting Proceedings* (Vol. 201, No. 2, pp. 4-9). Greenbelt^ eMD MD: International VLBI Service for Geodesy and Astrometry.

Combrinck, L., 2011a. Development of a satellite and lunar laser ranger and its future applications. In *62nd International Astronautical Congress* (pp. 03-07).

Combrinck, L., 2011b. Testing the General Relativity Theory through the estimation of PPN parameters γ and β using Satellite Laser Ranging data. *South African Journal of Geology*, *114*(3-4), pp.549-560.

Combrinck, L., 2010. Satellite laser ranging. In *Sciences of Geodesy-I* (pp. 301-338). Springer Berlin Heidelberg.

Combrinck, L., 2009, July. The MOBLAS-6 Satellite Laser Ranging station at Hartebeesthoek, South Africa; Technology and data applications. In *Geoscience and Remote Sensing Symposium, 2009 IEEE International, IGARSS 2009* (Vol. 4, pp. IV-161). IEEE.

Combrinck, L. and Suberlak, V., 2007. Earth-tide as parameter of crustal motion correction for SLR station displacement. *South African Journal of Geology*, *110*(2-3), pp.203-210.

Combrinck, L., Fourie, C.J.S., Croukamp, L. and Saunders, I., 2007. Report on preliminary geotechnical and tropospheric site investigation for a proposed space geodetic observatory near Matjiesfontein in the Great Karoo, South Africa. Journal of Geology, 110, 225-234.

Combrinck, W.L. and Merry, C.L., 1997. Very long baseline interferometry antenna axis offset and intersection determination using GPS. *Journal of Geophysical Research: Solid Earth*, *102*(B11), pp.24741-24743.

Ciufolini, I., 1990. General relativistic measurements with satellite laser ranging, lunar laser ranging and very long baseline interferometry. *Il Nuovo Cimento C*, *13*(1), pp.67-78.

Cohen, W.B. and Goward, S.N., 2004. Landsat's role in ecological applications of remote sensing. *Bioscience*, *54*(6), pp.535-545.

Crawford, M., 2009. Lunar laser ranging: 40 years of high-level science. *SPIE Newsroom, DOI*, *10*(2.2200912), p.02.

Cremers, C.J., Birkebak, R.C. and White, J.E., 1971. Lunar surface temperatures from Apollo 12. *Earth, Moon, and Planets*, *3*(3), pp.346-351.

Closas, P., Fernandez-Prades, C. and Fernandez-Rubio, J.A., 2009. A Bayesian approach to multipath mitigation in GNSS receivers. *IEEE Journal of Selected Topics in Signal Processing*, *3*(4), pp.695-706.

Dach, R., Schildknecht, T., Springer, T., Dudle, G. and Prost, L., 2002. Continuous time transfer using GPS carrier phase. *IEEE transactions on ultrasonics, ferroelectrics, and frequency control*, *49*(11), pp.1480-1490.

Degnan, J., 1993. Millimetre accuracy Satellite Laser Ranging. In: Smith, D, E and Turcotte, D.L (Editors). Contributions of Space Geodesy to Geodynamics: Crustal Dynamics, Geodynamic Series, 25, American Geophysical Union. Doi: 10.1029/GD025p0133

Dickey, J.O., Bender, P.L., Faller, J.E., Newhall, X. X., Ricklefs, R.L., Ries, J.G., Shelus, P.J., Veillet, C., Whipple, A.L., Wiant, J.R., Williams, J.G. and Yoder, C.F., 1994. Lunar Laser Ranging: a continuing legacy of the Apollo program. Science, 265,182–190.

Donley, E.A., Heavner, T.P., Tataw, M.O., Levi, F. and Jefferts, S.R., 2004. Progress towards the second-generation atomic fountain clock at NIST. In *Frequency Control Symposium and Exposition, 2004. Proceedings of the 2004 IEEE International* (pp. 82-86). IEEE.

Drewes, H. and Hornik, H., 2013. International Association of Geodesy: Travaux Reports 2011-2013. Edited for the IAG Scientific Assembly, Potsdam, Germany September 1-6, 2013; 38. Available from: http://iag.dgfi.tum.de/fileadmin/IAG-docs/Travaux_2011-2013.pdf

Eanes, R.J., Schutz, B. and Tapley, B., 1983, October. Earth and ocean tide effects on Lageos and Starlette. In *Proc. of the Ninth International Symposium on Earth Tides, Kuo, JT (ed.), E. Sckweizerbart'sche Verlagabuchhandlung, Stuttgart*.

Edwards Jr, C., Rogstad, D., Fort, D., White, L. and Iijima, B., 1992. The goldstone real-time connected element interferometer. TDA Progress Report, pp. 42 -110.

Egbert, G.D. and Ray, R.D., 2003. Semi-diurnal and diurnal tidal dissipation from TOPEX/Poseidon altimetry. *Geophysical Research Letters*, *30*(17).

Ely, T.A. and Seubert, J., 2015. One-way radiometric navigation with the deep space atomic clock. *AAS/AIAA Space Flight Mechanism, Williamsburg, United States*, pp.1-18.

Ely, T., 2014. Advancing navigation, timing, and science with the Deep Space Atomic Clock. In *SpaceOps 2014 Conference* (p. 1856).

Elisa, F. A, E.F., Combrinck, L., Gabor, P., Hohenkerk, C. and Seidelmann, P.K., (Eds)., 2017. The Science of Time 2016: Time in Astronomy & Society, Past, Present and Future. *Springer International Publishing*, 10.1007/978-3-319-59909-0

Estey, L.H. and Meertens, C.M., 1999. TEQC: the multi-purpose toolkit for GPS/GLONASS data. *GPS solutions*, *3*(1), pp.42-49.

Fienga, A., Courde, C., Torre, J.M., Manche, H., Murphy, T., Mueller, J., Laskar, J., Bouquillon, S., Biskupek, L., Hofmann, F. and Capitaine, N., 2014. Interests of a new lunar laser instrumentation on the ESO NTT Telescope. *arXiv preprint arXiv:1405.0473*.

Folkner, W.M., Williams, J.G. and Boggs, D.H., 2008. The planetary and lunar ephemeris DE 421. *IPN Progress Report*, *42*, p.178.

Giffard, R., 1999. *Estimation of GPS ionospheric delay using L1 code and carrier phase observables*. AGILENT LABORATORIES PALO ALTO CA.

Gopi, K.S., 2012. GPS-TEC Analysis Application. Institute for Scientific Research, Boston College.

Goujon, D., Rochat, P., Mosset, P., Boving, D., Perri, A., Rochat, J., Ramanan, N., Simonet, D., Vernez, X., Froidevaux, S. and Perruchoud, G., 2010, April. Development of the space active hydrogen maser for the aces mission. In *EFTF-2010 24th European Frequency and Time Forum* (pp. 1-6). IEEE.

Greene, B. and Luck, J.M., 2002. LLR developments at Mount Stromlo. In *13 International Workshop on Laser Ranging*.

Groslambert, J., Fest, D., Olivier, M. and Gagnepain, J.J., 1981, May. Characterization of frequency fluctuations by crosscorrelations and by using three or more oscillators. In *Thirty Fifth Annual Frequency Control Symposium. 1981* (pp. 458-463). IEEE.

Gross, R., Beutler, G. and Plag, H.P., 2009. Integrated scientific and societal user requirements and functional specifications for the GGOS. In *Global geodetic observing system* (pp. 209-224). Springer Berlin Heidelberg.

Gurtner, W., 2007. RINEX: The Receiver Independent Exchange Format. Version 3.00, viewed 06 February 2016, <Whttps://igscb.jpl.nasa.gov/igscb/data/format/rinex300.pdf>.

Hackman, C. and Levine, J., 2004. *Adding water vapor radiometer data to GPS carrier-phase time transfer*. National Inst of Standards and Technology Boulder Co Time and Frequency Div. Available at: http://www.dtic.mil/cgi-bin/GetTRDoc?Location=U2&doc=GetTRDoc.pdf&AD=ADA485040

Hamzah, S.Z.M. and Homam, M.J., 2015. The correlation between total electron content variations and solar activity. Available at: http://eprints.uthm.edu.my/7183/1/IC3E_2015_submission_118.pdf

Heavner, T.P., Donley, E.A., Levi, F., Costanzo, G., Parker, T.E., Shirley, J.H., Ashby, N., Barlow, S. and Jefferts, S.R., 2014. First accuracy evaluation of NIST-F2. *Metrologia*, *51*(3), p.174.

Heinkelmann, R and Schuh, H., 2010. Very long baseline interferometry: accuracy limits and relativistic tests, in Klioner SA, Seidelman PK and Soffel MH (eds.), Relativity in Fundamental Astronomy, Proceedings IAU symposium, No. 261. doi:10.1017/S1743921309990524

Hellwig, H., 1993. Time and frequency applications. *IEEE transactions on ultrasonics, ferroelectrics, and frequency control*, *40*(5), pp.538-543.

Helmert, F.R., 1884. *Die mathematischen und physikalischen theorieen der höheren geodäsie.*. [The mathematical and physical theories of higher geodesy]. (Vol. 2). BG Teubner.

Henderson, D., 2005. Essen and the National Physical Laboratory's atomic clock. *Metrologia*, *42*(3), p.S4.

Herring, T.A., King, R.W. and McClusky, S.C., 2010. Introduction to Gamit/Globk. *Massachusetts Institute of Technology, Cambridge, Massachusetts*.

Herring, T.A., Mathews, P.M. and Buffett, B.A., 2002. Modeling of nutation-precession: Very long baseline interferometry results. *Journal of Geophysical Research: Solid Earth*, *107*(B4).

Hofmann, F., Biskupek, L. and Müller, J., 2018. Contributions to reference systems from Lunar Laser Ranging using the IfE analysis model. *Journal of Geodesy*, pp.1-13.

Hofmann, F. and Müller, J., 2018. Relativistic tests with lunar laser ranging. *Classical and Quantum Gravity*, *35*(3), p.035015.

Hofmann, F., Müller, J., Biskupek, L., Mai, E. and Torre, J.M., 2013, November. Lunar laser ranging–What is it good for. In *18th International Workshop on Laser Ranging* (pp. 11-15).

Hofmann, F., Müller, J. and Biskupek, L., 2010. Lunar laser ranging test of the Nordtvedt parameter and a possible variation in the gravitational constant. A&A, 522, L5 (2010).

Hofmann, F., Müller, J. and Biskupek, L., 2010. Lunar laser ranging test of the Nordtvedt parameter and a possible variation in the gravitational constant. *Astronomy & Astrophysics*, *522*, p.L5.

Horowitz, P. and Hill, W., 1989. The art of electronics, 2nd ed., USA. Cambridge University Press, 15p.

IERS Conventions 2003, IERS Technical Note No. 32, D.D McCarthy and G. Petit (eds.), Frankfort, BKG, 2004. Source: http://www.iers.org/iers/products/conv/

International Laser Ranging Services (ILRS): LLR station log files [image on the internet]. c2009 [Updated 2015 February 04, Cited 2015 June 30]. Available from: http://ilrs.gsfc.nasa.gov/network/stations/index.html

International Laser Ranging Services (ILRS): LLR map of stations [image on the internet]. c2009 [Updated 2015 February 04, Cited 2015 May 17]. Available from: http://ilrs.gsfc.nasa.gov/science/scienceContributions/lunar.htmInternational VLBI Service for Geodesy and Astrometry: station log files. c2015 [Updated 2015 June 30, Cited 2015 June 30]. Available from: http://ivscc.gsfc.nasa.gov/about/org/components/ns-list.html

Jackson, T.J., Schmugge, J. and Engman, E.T., 1996. Remote sensing applications to hydrology: soil moisture. *Hydrological Sciences Journal*, *41*(4), pp.517-530.

Jefferts, S.R., Weiss, M.A., Levine, J., Dilla, S., Bell, E.W. and Parker, T.E., 1997. Two-way time and frequency transfer using optical fibers. *IEEE transactions on instrumentation and measurement*, *46*(2), pp.209-211.

Kerr, J.T. and Ostrovsky, M., 2003. From space to species: ecological applications for remote sensing. *Trends in Ecology & Evolution*, *18*(6), pp.299-305.

Kodet, J. and Prochazka, I., 2012. Note: Optical trigger device with sub-pico-second timing jitter and stability. Review of scientific instruments, 83, 036101.

Kunimori, H., Takahashi, F., Itabe, T. and Yamamoto, A., 1993. Laser ranging application to time transfer using geodetic satellite and to other Japanese space programs.

Larden, D.R., 1983. Monitoring the Earth's rotation by Lunar Laser Ranging. Report from school of surveying, The University of New South Wales.

Larson, K.M., Braun, J.J., Small, E.E., Zavorotny, V.U., Gutmann, E.D. and Bilich, A.L., 2010. GPS multipath and its relation to near-surface soil moisture content. *IEEE Journal of Selected Topics in Applied Earth Observations and Remote Sensing*, *3*(1), pp.91-99.

Lazzara, M.A., Coletti, A. and Diedrich, B.L., 2011. The possibilities of polar meteorology, environmental remote sensing, communications and space weather applications from Artificial Lagrange Orbit. *Advances in Space Research*, *48*(11), pp.1880-1889.

Lemke, N.D., Ludlow, A.D., Barber, Z.W., Fortier, T.M., Diddams, S.A., Jiang, Y., Jefferts, S.R., Heavner, T.P., Parker, T.E. and Oates, C.W., 2009. Spin-1/2 optical lattice clock. *Physical Review Letters*, *103*(6), p.063001.

Levine, D.M., Berenson, M.L. and Stephan, D., 1999. *Statistics for managers using Microsoft Excel* (Vol. 660). Upper Saddle River, NJ: Prentice Hall.

Levine, J., 2008. A review of time and frequency transfer methods. *Metrologia*, *45*(6), p.S162.

Levine, M.W. and Vessot, R.F., 1970. Hydrogen-maser time and frequency standard at Agassiz Observatory. *Radio Science*, *5*(10), pp.1287-1292.

Letellier, T., 2005. *Etude des ondes de marée sur les plateaux continentaux* (Doctoral dissertation, Toulouse 3).

Lewandowski, W. and Thomas, C., 1991. GPS time transfer. *Proceedings of the IEEE*, *79*(7), pp.991-1000.

Lewandowski, W., Azoubib, J. and Klepczynski, W.J., 1999. GPS: primary tool for time transfer. *Proceedings of the IEEE*, *87*(1), pp.163-172.

Lewandowski, W., Petit, G. and Thomas, C., 1993. Precision and accuracy of GPS time transfer. *IEEE transactions on instrumentation and measurement*, *42*(2), pp.474-479.

Lombardi, M.A., 2005. Fundamentals of time and frequency. In *Mechatronics: An Introduction* (pp. 10-1). CRC Press.

Lombardi M.A., 2011.The Evolution of Time Measurement, Part 2: Quartz Clocks, IEEE Instrumentation and Measurement Magazine, 14 (5); p. 41-48. Available from: http://dx.doi.org/10.1109/MIM.2011.604138

Lombardi M.A., 2011. The evolution of time measurements, part 3: Atomic Clocks. IEEE Instrumentation & Measurement Magazine, Available from: http://www.nist.gov/pml/div688/generalpubs.cfm

Lombardi, M.A., 2005. Fundamentals of time and frequency. In *Mechatronics: An Introduction* (pp. 10-1). CRC Press.

Lombardi, M.A., 2005. Bishop, R.H (ed.), Fundamentals of Time and Frequency, In: *Mechatronics: an introduction*. CRC Press.

Lorber, H. and Duboff, I., 1975. Magnetically enhanced coaxial cable with improved time delay characteristics. United States Patent, US4017344.

Lu, Z., Qu, Y. and Qiao, S., 2014. *Geodesy*. Springer Berlin Heidelberg.

Madry, S., 2015. *Space systems for disaster warning, response, and recovery*. New York: Springer.

Mannermaa, J., Kalliomaki, K., Manstén, T. and Turunen, S., 1999. Timing performance of various GPS receivers. In *Frequency and Time Forum, 1999 and the IEEE International Frequency Control Symposium, 1999., Proceedings of the 1999 Joint Meeting of the European* (Vol. 1, pp. 287-290). IEEE.

Martinez, P., 2008. Space science and technology in South Africa: An overview. *African Skies*, *12*, p.46.

Mashaba, Z.O., Combrinck, W.L., Botai, J.O., Munghemezulu, C. and Botha, R.C., 2016. Design of a web-based GNSS data management system at HartRAO: preliminary results. *South African Journal of Geology 2016*, *119*(1), pp.117-124.

Mayer, D., Böhm, J., Combrinck, L., Botai, J. and Böhm, S., 2014. Importance of the Hartebeesthoek Radio Astronomy Observatory for the VLBI network. *Acta Geodaetica et Geophysica*, *49*(3), pp.313-325.

Maxim Integrated Products, 2004. Clock (CLK) Jitter and Phase Noise Conversion. APPLICATION NOTE 3359.Copyright Maxim Integrated Products (http://www.maximintegrated.com). Used with permission. Available at: http://www.maximintegrated.com/en/app-notes/index.mvp/id/3359.

McCarthy, D.D. and Petit, G., 2004. *IERS conventions (2003)*. International Earth Rotation and Reference Systems Service (IERS) (Germany). c2013 [Updated 2004 January 01, Cited 2015 June 21]. Available from:http://www.iers.org/SharedDocs/Publikationen/EN/IERS/Publications/tn/TechnNote32/tn32.pdf?__blob=publicationFile

Meekhof, D.M., Jefferts, S.R., Stepanovic, M. and Parker, T.E., 2001. Accuracy evaluation of a cesium fountain primary frequency standard at NIST. *IEEE Transactions on Instrumentation and Measurement*, *50*(2), pp.507-509.

Mendes, V.B. and Pavlis, E.C., 2004. High-accuracy zenith delay prediction at optical wavelengths. *Geophysical Research Letters*, *31*(14).

Mendes, V.B., Prates, G., Pavlis, E.C., Pavlis, D.E. and Langley, R.B., 2002. Improved mapping functions for atmospheric refraction correction in SLR. *Geophysical Research Letters*, *29*(10).

Merkowitz, S.M., 2010. Tests of gravity using lunar laser ranging. *Living Reviews in Relativity*, *13*(1), p.7.

Métivier, L., de Viron, O., Conrad, C.P., Renault, S., Diament, M. and Patau, G., 2009. Evidence of earthquake triggering by the solid Earth tides. *Earth and Planetary Science Letters*, *278*(3), pp.370-375.

Middelberg, E. and Bach, U., 2008. High resolution radio astronomy using very long baseline interferometry. *Reports on Progress in Physics*, *71*(6), p.066901.

Mironov, V.L. and Muzalevskiy, K.V., 2012, July. The new algorithm for retrieval of soil moisture and surface roughness from GNSS reflectometry. In *Geoscience and Remote Sensing Symposium (IGARSS), 2012 IEEE International* (pp. 7530-7532). IEEE.

Misra P.N. (1996). Innovation: The Role of the Clock in a GPS Receiver. GPS world, 7(4), 60-7.

Mizuhiko, H., 2003, Atomic Frequency Standards: Basic Physics in the Atomic Frequency Standards, *Journal of the National Institute of Information and Communications Technology*, 50(1/2).

Moeketsi, D.M., 2007. *Solar cycle effects on GNSS-derived ionospheric total electron content observed over southern Africa* (Doctoral dissertation, Rhodes University).

Moran, J.M., 1989. Introduction to VLBI. In *Very Long Baseline Interferometry* (pp. 27-45). Springer Netherlands.

Mulholland, J.D. and Silverberg, E.C., 1972. Measurement of physical librations using laser retroreflectors. *Earth, Moon, and Planets*, *4*(1), pp.155-159.

Mulholland, J.D., 1972. Measures of time in astronomy. *Publications of the Astronomical Society of the Pacific*, *84*(499), p.357.

Mulholland, J.D., 1977. Mathematical Modelling of Lunar Laser Measures and their Application to Improvement of Physical Parameters. In *Scientific Applications of Lunar Laser Ranging* (pp. 9-18). Springer Netherlands.

Mulholland, J.D., 1980. Scientific achievements from ten years of lunar laser ranging. *Reviews of Geophysics*, *18*(3), pp.549-564.

Müller, J., Williams, J.G. and Turyshev, S.G., 2008. Lunar laser ranging contributions to relativity and geodesy. In *Lasers, Clocks and Drag-Free Control* (pp. 457-472). Springer Berlin Heidelberg.

Müller, J., Williams, J.G., Turyshev, S.G. and Shelus, P.J., 2007. Potential capabilities of lunar laser ranging for geodesy and relativity. In *Dynamic planet* (pp. 903-909). Springer Berlin Heidelberg.

Munghemezulu, C., Combrinck, L. and Botai, J.O., 2016. A review of the lunar laser ranging technique and contribution of timing systems. *South African Journal of Science*, *112*(3-4), pp.1-9.

Munghemezulu, C., Combrinck, L., Botai, J. and Mashaba, Z., 2016b. Mapping GPS multipath: a case study for the lunar laser ranger timing antenna at HartRAO. *South African Journal of Geomatics*, *5*(2), pp.142-155.

Munghemezulu, C., Combrinck, L., Botai, O.J. and Quick, J., 2016c. Analysis of the performance of hydrogen maser clocks at the Hartebeesthoek Radio Astronomy Observatory. *South African Journal of Geomatics*, *5*(3), pp.325-339.

Munghemezulu, C., 2013. *Determination of geodetic velocity field parameters for the African tectonic plate using the technique of Global Navigation Satellite Systems* (Masters dissertation, University of Pretoria).

Murphy, T, W., 2013. Lunar laser ranging: the millimeter challenge. *Reports on Progress in Physics*. 76, 1-21.

Murphy, T. W., Strasburg, Jr., J. D, Stubbs, C. W. Ade lberger, E. G. Angle, J. Nordtvedt, K. Williams, J. G. Dickey, J. O. and Gillespie, B. 2000. The Apache Point Observatory Lunar Laser-ranging Operation (APOLLO). 12th International Laser Ranging Workshop, Matera, Italy. Available: http://physics.ucsd.edu/~tmurphy/apollo/doc/matera.pdf

Murphy, T.W., Adelberger, Jr. E.G., Strasburg, J. D. and Stubbs, C. W., 2002. APOLLO: Multiplexed Lunar Laser Ranging. 13th International Laser Ranging workshop, Washington, DC, USA.

Murphy T., 2007. Lunar Laser Ranging: a laboratory for Gravity. SLAC Conference, Workshops & Symposiums, 2007/08/09; 2007. [Cited 2015 June 30]. Available from: http://www-conf.slac.stanford.edu

Murphy, T.W., Adelberger, E.G., Battat, J.B.R., Hoyle, C.D., McMillan, R.J., Michelsen, E.L., Samad, R.L., Stubbs, C.W. and Swanson, H.E., 2010. Long-term degradation of optical devices on the Moon. *Icarus*, *208*(1), pp.31-35.

Murphy, T., Adelberger, E., Battat, J., Colmenares, N., Crossley, D., Hoyle, C.D., Johnson, N., McMillan, R., Stubbs, C. and Swanson, E., 2014. APOLLO performance and data quality. In *19th International Workshop on Laser Ranging* (pp. 27-31).

Nez, F., Biraben, F., Felder, R. and Millerioux, Y., 1993. Optical frequency determination of the hyperfine components of the 5S12-5D32 two-photon transitions in rubidium. *Optics communications*, *102*(5-6), pp.432-438.

Ngcofe, L. and Gottschalk, K., 2013. The growth of space science in African countries for Earth observation in the 21st century. *South African Journal of Science*, *109*(1-2), pp.1-5.

Niell, A., Whitney, A., Petrachenko, W., Schluter, W., Van-denberg, N., Hase, H., Koyama, Y., Ma, C., Schuh, H. and Tuccari, G., 2007. VLBI2010: A Vision for Future Geodetic VLBI. In F. Sanso, (Editor). Dynamic Planet-Monitoring and Understanding a Dynamic Planet with geodetic and Oceanographic Tools, 130, 757-759.

Niell, A.E., Coster, A.J., Solheim, F.S., Mendes, V.B., Toor, P.C., Langley, R.B. and Upham, C.A., 2001. Comparison of measurements of atmospheric wet delay by radiosonde, water vapor radiometer, GPS, and VLBI. *Journal of Atmospheric and Oceanic Technology*, *18*(6), pp.830-850.

Nkosi, N., Combrinck, W.L. and Akombelwa, M., 2016. Optical configuration and optical tests of the HartRAO Lunar Laser Ranger. South African Journal of Geology, 119(1), pp.99-108.Perry, J., 1943. Thermal effects upon the performance of lens systems. Proceedings of the Physical Society, 55, 257.

Noda, H., Kunimori, H. and Araki, H., 2014, March. Lunar laser ranging experiment at Koganei SLR station. In *Lunar and Planetary Science Conference* (Vol. 45, p. 1638).

Ohtani, R. and Naito, I., 2000. Comparisons of GPS-derived precipitable water vapors with radiosonde observations in Japan. *Journal of geophysical research*, *105*(D22), pp.26917-26929.

Olawepo, A.O., Oladipo, O.A., Adeniyi, J.O. and Doherty, P.H., 2015. TEC response at two equatorial stations in the African sector to geomagnetic storms. *Advances in Space Research*, *56*(1), pp.19-27.

Panek, P., Prochazka, I. and Kodet, J., 2010. Time measurement device with four femtosecond stability. *Metrologia*, *47*(5), p.L13.

Panek, P., Prochanzka, I. and Kodet, J., 2010.Timing measurement device with four femotosecond stability. Metrologia, 47, L13-L16.

Pavlov, D.A., Williams, J.G. and Suvorkin, V.V., 2016. Determining parameters of Moon's orbital and rotational motion from LLR observations using GRAIL and IERS-recommended models. *Celestial Mechanics and Dynamical Astronomy*, *126*(1-3), pp.61-88.Petrov, L., 2005. Software sotid for computation of site displacements due to the solid Earth tides. Updated pdf documentation: 2005.02.11. 2005. Available from: http://gemini.gsfc.nasa.gov/sotid.

Pearlman, M.R., Degnan, J.J. and Bosworth, J.M., 2002. The international laser ranging service. *Advances in Space Research*, *30*(2), pp.135-143.

Pet, R.B., Niell, A. and Behrend, D., 2009. Design aspects of the VLBI2010 system. *IVS Annual Report, USA*, Progress report of the IVS VLB I2010 committee, Technical report, viewed 02 September 2015, <http://adsabs.harvard.edu/ abs/ 2009vlbi.rept....1P>.

Plag, H.P. and Pearlman, M. eds., 2009. *Global geodetic observing system: Meeting the requirements of a global society on a changing planet in 2020*. Springer Science & Business Media.

Plag, H, P., Altamimi, Z., Bettadpur, S., Beutler, G., Beyerle, G., Cazenve, A., Crossley, D., Donnellan, A., Forsberg, R., Gross, R., Hinderer, J., Komjathy, A., Ma, C., Mannucci, A.J., Noll, C., Nothnagel, A., Pavlis, E.C., Pearlman, M., Poli, P., Schreiber, K., Senior, K., Woodworth, P.L., Zerbini, S. and Zuffada, C., 2009. The goals, achievements, and tools of modern geodesy. In: Plag, H, -P and Pearlman, M. (Editors). Global Geodetic Observing System: Meeting the Requirements of a Global Society on a Changing Planet in 2020. Berlin Heidelberg, Springer-Verlag, 15-87.

Plag, H.P., Altamimi, Z., Bettadpur, S., Beutler, G., Beyerle, G., Cazenave, A., Crossley, D., Donnellan, A., Forsberg, R., Gross, R. and Hinderer, J., 2009. The goals, achievements, and tools of modern geodesy. In *Global Geodetic Observing System* (pp. 15-88). Springer Berlin Heidelberg.

Poultney, S. K., 1972. Single Photon Detection and Timing in the Lunar Laser Ranging Experiment.Nuclear Science, IEEE Transaction, 19, 12 -17.

Preston, A. and Merkowitz, S., 2013. Next-generation hollow retroreflectors for lunar laser ranging. *Applied optics*, *52*(36), pp.8676-8684.

Prestage, J.D., Tjoelker, R.L. and Maleki, L., 1995. Atomic clocks and variations of the fine structure constant. *Physical review letters*, *74*(18), p.3511.

Prochazka, I., Kodet, J., Blazej, J., Schreiber, U. and Cacciapuoti, L., 2010, April. Development of the European Laser Timing instrumentation for the ACES time transfer using laser pulses. In *EFTF-2010 24th European Frequency and Time Forum* (pp. 1-6). IEEE.

Pullen, S., Park, Y.S. and Enge, P., 2009. Impact and mitigation of ionospheric anomalies on ground-based augmentation of GNSS. *Radio Science*, *44*(1).

Rao, G., Kumar, G.S. and Kumar, M.N.V.S.S., 2013. GPS signal Rician fading model for precise navigation in urban environment. *89.40. Dd; 84.40. Ua; 91.10. Fc*.

Ratcliffe, J.A., 1972. Introduction to the ionosphere and magnetosphere. Cambridge University Press, Great Britain Rothacher, M., Beutler, G., Behrend, D., Donnellan, A., Hinderer, J., Ma, C., Noll, C., Oberst, J., Pearlman, M., Plag, H.P. and Richter, B., 2009. The future global geodetic observing system. In *Global Geodetic Observing System* (pp. 237-272). Springer Berlin Heidelberg.

Ray, J. and Senior, K., 2005. Geodetic techniques for time and frequency comparisons using GPS phase and code measurements. *Metrologia*, *42*(4), p.215.

Robertson, D.S., 1991. Geophysical applications of very-long-baseline interferometry. *Reviews of modern physics*, *63*(4), p.899.

Ronnang, B.O., 1989. Geodesy, Geodynamics, and Astrometry Using Very Long Baseline Interferometry. In *Very Long Baseline Interferometry* (pp. 305-317). Springer Netherlands.

Rothacher, M., 2002, November. Towards a rigorous combination of space geodetic techniques. In *Proceedings of the IERS Workshop on Combination Research and Global Geophysical Fluids* (pp. 18-21).

Rothacher, M., Beutler, G., Behrend, D., Donnellan, A., Hinderer, J., Ma, C., Noll, C., Obsert, J., Pearlman, M., Plag, H, -P., Richter, B., Schone, T., Tavernier, G. and Woodworth, P. L., 2009. The future Global Geodetic Observing System. In: Plag, H, -P and Pearlman, M. (Editors). Global Geodetic Observing System: Meeting the Requirements of a Global Society on a Changing Planet in 2020. Berlin Heidelberg, Springer-Verlag, 237-272.

Rummel, R., Beutler, G., Dehant, V., Gross, R., Ilk, K.H., Plag, H.P., Poli, P., Rothacher, M., Stein, S., Thomas, R. and Woodworth, P.L., 2009. Understanding a dynamic planet: Earth science requirements for geodesy. In *Global Geodetic Observing System* (pp. 89-133). Springer Berlin Heidelberg.

Samain, E., Mangin, J.F., Veillet, C., Torre, J.M., Fridelance, P., Chabaudie, J.E., Feraudy, D., Glentzlin, M., Pham Van, J., Furia, M., Hournet, A. and Vigouroux, G., 1998. Millimetric lunar laser ranging at OCA (Observatoire de la Côte d'Azur). Astron. Astrophys. Suppl. Ser. 130, 235-244.

Samain, E., Exertier, P., Courde, C., Fridelance, P., Guillemot, P., Laas-Bourez, M. and Torre, J.M., 2015. Time transfer by laser link: a complete analysis of the uncertainty budget. *Metrologia*, *52*(2), p.423.

Samain, E., Fridelance, P. and Guillemot, P., 2010. An ultra stable event timer designed for T2L2. *Proceedings of the EFTF/IFCS*, *9*.

Savitzky, A. and Golay, M.J., 1964. Smoothing and differentiation of data by simplified least squares procedures. *Analytical chemistry*, *36*(8), pp.1627-1639.

Shapiro, I.I., 1964. Fourth test of general relativity. *Physical Review Letters*, *13*(26), p.789.

Schafer, R.W., 2011. What is a Savitzky-Golay filter?[lecture notes]. *IEEE Signal processing*

Schuh, H. and Böhm, J., 2013. Very long baseline interferometry for geodesy and astrometry. In *Sciences of Geodesy-II* (pp. 339-376). Springer Berlin Heidelberg.

Schuh, H. and Behrend, D., 2012. VLBI: a fascinating technique for geodesy and astrometry. *Journal of Geodynamics*, *61*, pp.68-80.

Seeber, G., 1993. Satellite Geodesy: Foundations, Methods and Aplications. *New York, NY: Walter De Gruynter*.

Sinclair, A.T. Data Screening and Normal Point Formation: Re-Statement of Herstmonceux Normal Point Recommendation. 1997. [Updated 2015 February 04, Cited 2015 May 17]. Available from: http://ilrs.gsfc.nasa.gov/data_and_products/data/npt/npt_algorithm.html

Strasburg, J. D., 2002. The advantage of using Avalanche Photodiode (APD) arrays in laser ranging applications. 13th International Laser Ranging workshop, Washington, D C, USA. Available at: http://cddis.gsfc.nasa.gov/lw13/docs/presentations/detect_strasburg_1p.pdf

Torrence, C. and Compo, G.P., 1998. A practical guide to wavelet analysis. *Bulletin of the American Meteorological society*, *79*(1), pp.61-78.

Torge, W. and Müller, J., 2012. *Geodesy*. Walter de Gruyter.

Tregoning, P., Boers, R., O'Brien, D. and Hendy, M., 1998. Accuracy of absolute precipitable water vapor estimates from GPS observations. *Journal of Geophysical Research: Atmospheres*, *103*(D22), pp.28701-28710.

Tsela, P.L., Combrinck, L. and Ngcobo, B., 2016. A spatiotemporal analysis of the effect of ambient temperatures on the thermal behaviour of the Lunar Laser Ranging optical telescope at Hartebeesthoek Radio Astronomy Observatory. *South African Journal of Geomatics*, *5*(3), pp.373-392.

Tsela, P., Combrinck, L., Botha, R. and Ngcobo, B., 2015. Thermal analysis of the LLR optical telescope tube assembly based in Hartebeesthoek Radio Astronomy Observatory. *Acta Geodaetica et Geophysica*, pp.1-11.

VanDam, T.M. and Herring, T.A., 1994. Detection of atmospheric pressure loading using very long baseline interferometry measurements. *Journal of Geophysical Research: Solid Earth*, *99*(B3), pp.4505-4517.

Vasilyev, M.V., Yagudina, E.I., Torre, J.M. and Feraudy, D., 2015, August. Planned LLR station in Russia and its impact on the Lunar Ephemeris Accuracy. In *Journées 2014*.

Vasilyev, M.V., Yagudina, E.I., Torre, J.M. and Feraudy, D., 2015, August. Planned LLR

Vessot, R.F., 2005. The atomic hydrogen maser oscillator. *Metrologia*, *42*(3), p.S80.

Vokrouhlický, D., 1997. A note on the solar radiation perturbations of lunar motion. *Icarus*, *126*(2), pp.293-300.

Weinbach, U. and Schön, S., 2010, April. On the correlation of tropospheric zenith path delay and station clock estimates in geodetic GNSS frequency transfer. In *EFTF-2010 24th European Frequency and Time Forum* (pp. 1-8). IEEE.

Walsworth, R.L., Silvera, I.F., Mattison, E.M. and Vessot, R.F., 1990. Test of the linearity of quantum mechanics in an atomic system with a hydrogen maser. *Physical review letters*, *64*(22), p.2599.

Wan, W., Larson, K.M., Small, E.E., Chew, C.C. and Braun, J.J., 2015. Using geodetic GPS receivers to measure vegetation water content. *GPS solutions*, *19*(2), pp.237-248.

Williams, J. G. and Folkner, W. M., 2009. Lunar Laser Ranging: Relativistic Model and Tests of Gravitational Physics, IAU Symp. 261, BAAS, 41, 882.

William, J. G., Newhall, X. X. and Dickey, J. O., 1996. Relative parameters determined from lunar laser ranging. Physical Review, 53, 6730-6738.

Williams, J.G., Turyshev, S.G. and Boggs, D.H., 2004. Progress in lunar laser ranging tests of relativistic gravity. *Physical Review Letters*, *93*(26), p.261101.

Williams, J.G., Boggs, D.H. and Folkner, W.M., 2008. *DE421 lunar orbit, physical librations, and surface coordinates, JPL IOM 335-JW, DB*. WF-20080314-001, March 14.

Williams, J.G., Newhall, X.X. and Dickey, J.O., 1996. Relativity parameters determined from lunar laser ranging. *Physical Review D*, *53*(12), p.6730.

Wynands, R. and Weyers, S., 2005. Atomic fountain clocks. *Metrologia*, *42*(3), p.S64.

Yedukondalu, K., Sarma, A.D. and Srinivas, V.S., 2011. Estimation and mitigation of GPS multipath interference using adaptive filtering. *Progress In Electromagnetics Research M*, *21*, pp.133-148.

Ziebart, M., 2001. *High precision analytical solar radiation pressure modelling for GNSS spacecraft* (Doctoral dissertation, University of East London).

Zhang, W.Q., Lin, C.F., Yu, S.L., Wang, G.Z., Zhang, Y.P., Yang, P.H. and Zhang, J., 2001. A study and performance evaluation of hydrogen maser user in Chinese mobile VLBI stations. *Chinese Astronomy and Astrophysics*, *25*(3), pp.390-397.